EVOLUTION OF AN OLIGOCENE CANYON SYSTEM ON THE EASTERN SCOTIAN MARGIN

by

Virginia I. Brake

Submitted in partial fulfillment of the requirements
for the degree of Master of Science

at

Dalhousie University
Halifax, Nova Scotia
March 2009

DALHOUSIE UNIVERSITY

DEPARTMENT OF EARTH SCIENCES

The undersigned hereby certify that they have read and recommend to the Faculty of Graduate Studies for acceptance a thesis entitled "EVOLUTION OF AN OLIGOCENE CANYON SYSTEM ON THE EASTERN SCOTIAN MARGIN" by Virginia I. Brake in partial fulfillment of the requirements for the degree of Master of Science.

Dated: March 31, 2000

Supervisor:

Readers:

Departmental Representative:

DALHOUSIE UNIVERSITY

DATE: March 31, 2009

AUTHOR: Virginia I. Brake

TITLE: Evolution of an Oligocene canyon system on the eastern Scotian margin

DEPARTMENT OR SCHOOL: Department of Earth Sciences

DEGREE: M.Sc. CONVOCATION: October YEAR: 2009

Permission is herewith granted to Dalhousie University to circulate and to have copied for non-commercial purposes, at its discretion, the above title upon the request of individuals or institutions.

Signature of Author

TABLE OF CONTENTS

LIST OF FIGURES

ABSTRACT

Deciphering margin evolution requires understanding continental margin sedimentary processes. Seismic reflection data were used to investigate the Cenozoic section of the outer shelf and upper slope region of the eastern Scotian Slope. This section is largely progradational with marked periods of erosion and canyon incision. A widespread Oligocene unconformity includes an extensive 6-15 km-wide, 1 km-deep U-shaped canyon system that breaches the paleo-shelf break and extends >150 km to the basin floor. The history of canyon incision and infill suggests at least two cycles of major relative sea level fall and rise involved in its formation; one in the Early Oligocene and another in the Middle Oligocene. This major canyon system is indicative of margin processes that potentially supply vast quantities of sediment from shallow to deep water through a slope by-pass system; critical information for understanding and predicting margin evolution and developing hydrocarbon exploration models along passive margins.

LIST OF ABBREVIATIONS USED

GSC-A	Geological Survey of Canada – Atlantic
SMT	Seismic Micro Technology
CMP	Common Mid Point
PSTM	Prestack Time Migration
PSDM	Prestack Depth Migration
TWTT	Two Way Travel Time
CRP	Common Reflection Point
UWI	Unique Well Identifier
DGPS	Differential Global Positioning Systems
mbsl	metres below sea level

ACKNOWLEDGEMENTS

I extend my utmost thanks to my supervisors Dr. David Mosher (Geological Survey of Canada-Atlantic (GSC-A)) and Dr. Grant Wach (Dalhousie University) for planning the Stonehouse project, and for the many critical discussions, challenges and encouragement throughout the project.

Thanks are also extended to the remainder of my committee Dr. Mark Deptuck (Canada - Nova Scotia Offshore Petroleum Board) and Dr. David Piper (GSCA), for responding to my many queries, and answering quick questions that opened the door to new possibilities and providing genuine enthusiasm and encouragement.

The support of my family and friends played a motivating role through their constant encouragement. I have enjoyed being a part of "the team", Calvin with his new discoveries and ideas, my sidekick Shawn and his corel draw and animation skills, and Giles for providing the support I needed to complete this project. It is through our many discussions, suggestions, arguments and meetings that our best work is attained.

Research for this thesis was funded by the Nova Scotian Offshore Energy Technical Research Association grant No. 51834 to Drs. G. Wach and D. Mosher, as well as the Pengrowth-Nova Scotia Petroleum Innovation Grant. The three-dimensional Stonehouse dataset (time and depth migrated volumes) were donated by Encana to the Geological Survey of Canada-Atlantic (GSC-A). Two-dimensional seismic reflection data (Parex and TGS NOPEC) and workstation facilities were available through GSC-A with SMT Kingdom Suite educational licence for seismic interpretation supplied by Seismic Micro Technologies Inc.

Chapter 1. Introduction

Passive continental margin sedimentation responds to sediment influx and first order forcing mechanisms such as tectonics and sea level fluctuations in addition to reworking and transportation by ocean currents. As a result, margin sedimentary sequences experience periods of progradation, aggradation and erosion, leading to development of stratigraphic sequences. The modern seafloor of the Scotian Slope, for example, appears highly eroded with deeply incised canyons that were probably generated in response to lower sea level stands and high sediment input rates during Quaternary glacial and particularly de-glacial periods (Mosher et al. 2004). The following study investigates Cenozoic to recent strata on the eastern Scotian continental margin. Within this interval there is an unconformity of presumed Oligocene-age exhibiting a canyon system comparable to other canyons on the modern eastern Scotian Slope. Its formation, however, cannot be the result of the advance and retreat of shelf-crossing glaciations, as presumed for the modern surface since major continental ice sheets were not present in the Oligocene in the northern hemisphere (Clarke et al. 1999; DeConto et al. 2008). Its presence, therefore relates to a fundamental aspect of continental slope sedimentation processes. Understanding these processes will aid in understanding continental margin development.

1.1 Objectives

It is the purpose of this study to determine shelf to slope sedimentation processes and patterns on the eastern Scotian Slope, particularly with respect to the influence of development and occupation of the Oligocene canyon system. This will be accomplished

using seismic facies, seismic stratigraphic and seismic geomorphologic analysis. The "Oligocene unconformity" is investigated to determine the morphology of the surface and to better constrain its age. The character of large erosional features, such as canyon systems associated with the unconformity, are investigated to determine their formation and influence on sedimentation along the margin**.** The study aims to better constrain the potential roles of eustatic sea level fluctuations, tectonic uplift, and sediment delivery systems in the formation of the "Oligocene unconformity".

1.2 Study Area

The Scotian Slope trends northeast – southwest, parallel to the modern coastline of Nova Scotia and seaward of the Scotian Shelf on the passive continental margin of the western North Atlantic Ocean (Fig. 1.1). The study area spans modern outer shelf and upper slope terrain on the eastern Scotian Slope between The Gully and the Laurentian Channel in water depths of approximately 65 m – 2500 m, with a regional slope of 2.5˚ to 4˚. The seafloor is deeply incised by numerous canyons.

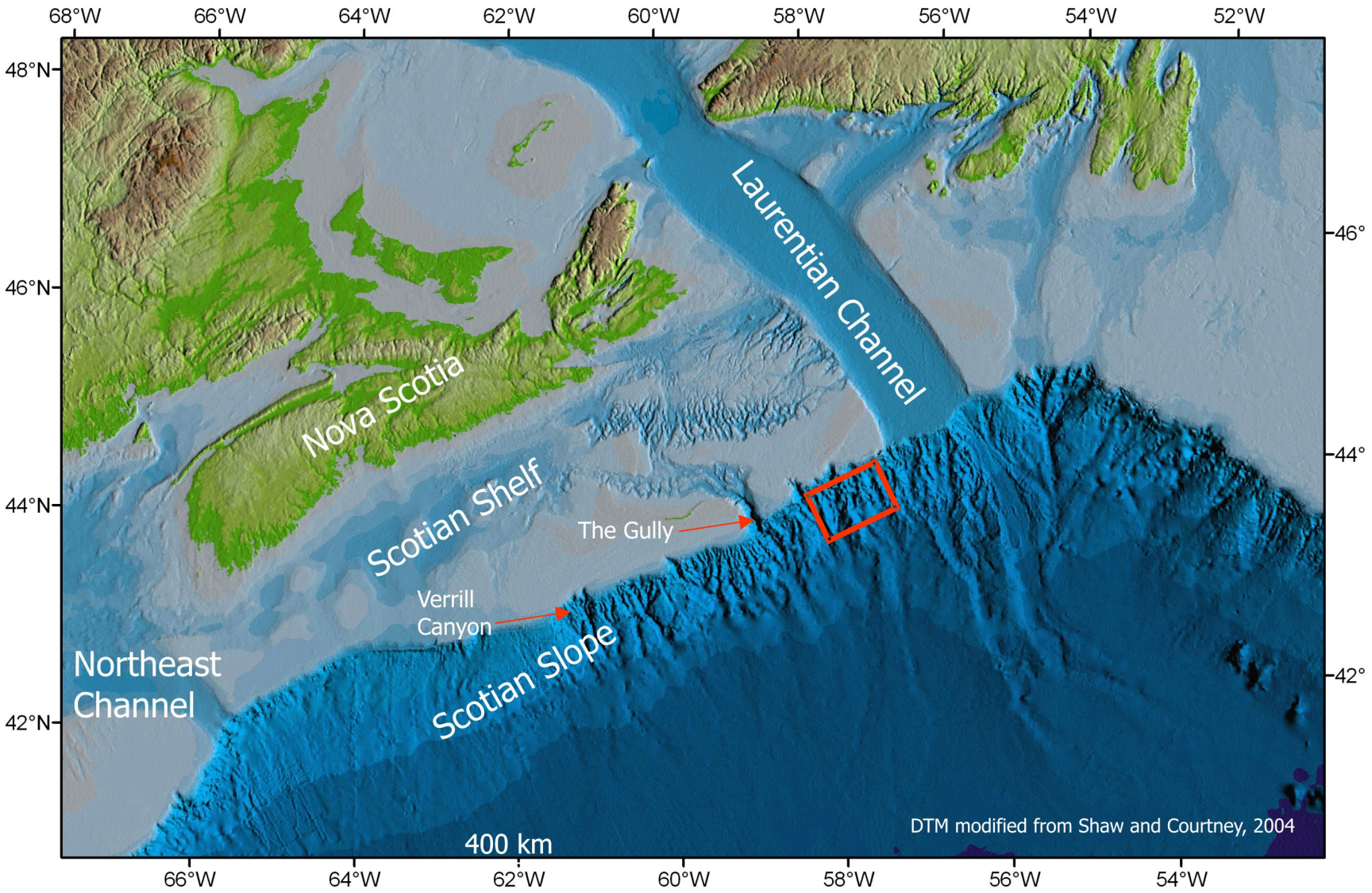

Figure 1.1: Location map of study area spanning modern outer shelf and upper slope terrain of the heavily incised eastern Scotian Slope between The Gully and the Laurentian Channel.

1.3 Geologic Setting

The Scotian Slope is part of the Scotian basin, a passive margin sequence that developed after North America rifted from the African continent in the Late Triassic to Early Jurassic. The rift phase was characterized by deposition of continental clastic sediment and evaporites, while the drift phase was characterized by clastic progradation with periods of carbonate deposition (Wade and Maclean 1990). The Abenaki carbonate platform developed in the western part of the basin during the Late Jurassic with limited extent in the east due to the presence of a major clastic deltaic depocentre near Sable Island. Transgression continued throughout the Late Cretaceous and Cenozoic punctuated by major sea level lowstand sequences (Wade and MacLean 1990; Kidston et al. 2002).

The modern Scotian Slope extends approximately 1000 km from the Laurentian Channel in the northeast to the Northeast Channel in the Southwest (Fig. 1.1). The Scotian Slope is broadly divided into two distinct morphological provinces (Uchupi and Swift 1992; Campbell et al. 2004). West of Verrill Canyon, the regional slope is 1.5° to 3° and the seabed is relatively smooth. From multibeam bathymetry, shallow submarine channels and linear escarpments tens of kilometres long and tens of metres high are observed superimposed on the smooth seabed. East of the Verrill Canyon the regional slope is steeper, 2.5° to 4°, and the seabed is deeply incised by submarine canyons, several of which cut back tens of kilometres into the continental shelf edge (Mosher et al. 2004).

On the eastern Scotian Slope, the numerous canyons are interpreted to be the continuation of subglacial meltwater channels (tunnel valleys) (Flynn 2000; Piper et al. 2007). Since the retreat of ice sheets to the present shoreline by about 12 ka, and with subsequent sea-level rise, continental slope sedimentation has been slow, dominated by pelagic and hemipelagic deposition (Mosher et al. 1994).

1.4 Basin Evolution

1.4.1 Structure

Structurally, the East Coast of Canada is divided into three distinct regions: The Scotian margin in the south, the Newfoundland margin in the centre and east, and the Labrador margin in the north (Louden 2002). The Scotian margin developed as a result of the break-up of the Pangean supercontinent in the Middle Triassic when North America and Africa rifted to form separate continents. Rifting occurred throughout the Late Triassic to Early Jurassic (~230-190 Ma) (Wade and McLean 1990), during which time the landmass comprising Nova Scotia occupied a near equatorial position adjacent to Morocco (Schenk 1973, 1981, 1997).

The final separation of North America and Africa is marked by the Break-up Unconformity (BU). The BU is manifested by complex faulting and erosion of Late Triassic and Early Jurassic rock as well as the creation of oceanic crust by volcanism with the opening of the proto-Atlantic Ocean (Keen and Beaumont 1990). The resultant Scotian basin consisted of a complex terrain of grabens and basement highs defined by the landward extensions of oceanic fracture zones onto continental curst (Welsink et al.

1990). From southwest to northeast the platforms and depocentres along the Scotian margin include the Georges Bank/Shelburne Basin, La Have Platform, Sable and Abenaki Subbasins, Banquereau Platform and the Orpheus Graben/ Laurentian subbasin.

Periods of basement subsidence during the Jurassic, Cretaceous and Cenozoic, (likely due to subsequent rifting events on the Grand Banks (Louden 2002)), deepened the interconnected subbasins, resulting in the accumulation of strata 12 km or greater in thickness (Wade and MacLean 1990). The distribution of salt suggests that the subbasins were initially the loci of evaporate deposition. Large synsedimentary faults are a prominent feature of the sedimentary section in Abenaki and Sable Subbasins resulting mainly from salt movement at depth. Many faults extend upward, well into the Cenozoic section, indicating long-term subsidence in the basin (Wade et al. 1995).

Strike-slip motion along the Cobequid – Chedabucto - Southwest Grand Banks fault system during the Cretaceous and Early Cenozoic was influential in shaping the landforms and depositional patterns on the Scotian margin; including rapid subsidence of the eastern Scotian basin in the mid-Cretaceous. Tilting of the Scotian Shelf during the Early Cenozoic led to erosion and reworking of Cretaceous inner shelf facies and deposition of deep water facies beneath the outer shelf (Wade et al. 1989) and possible Oligocene uplift of the eastern Scotian Shelf (Pe-Piper and Piper 2004).

1.4.2 Stratigraphy

Lithostratigraphic and structural evolution of the Scotian margin was first proposed by McIver (1972) and subsequently modified by Jansa and Wade (1975), Wade and

MacLean (1990), Wade et al. (1995) and Kidston et al. (2002; 2007), through the study of Scotian Shelf wells and seismic data.

Mesozoic, and in part, Cenozoic sedimentary rocks of the Scotian basin overlie a crystalline basement consisting of Paleozoic metasedimentary rocks and granites (Fig. 1.2). Restricted shallow marine conditions led to the deposition of continental redbeds of the Eurydice Formation in many of the deeper grabens, overlain and interfingered with evaporites of the Argo Formation (McIver 1972). The accumulation of extensive evaporate (salt and anhydrite) deposits perhaps up to 1-2 km in thickness, continued into the Early Jurassic as marine transgression covered the basin with a shallow sea (Wade and MacLean 1990; Kidston et al. 2002; Ings and Shimeld 2006).

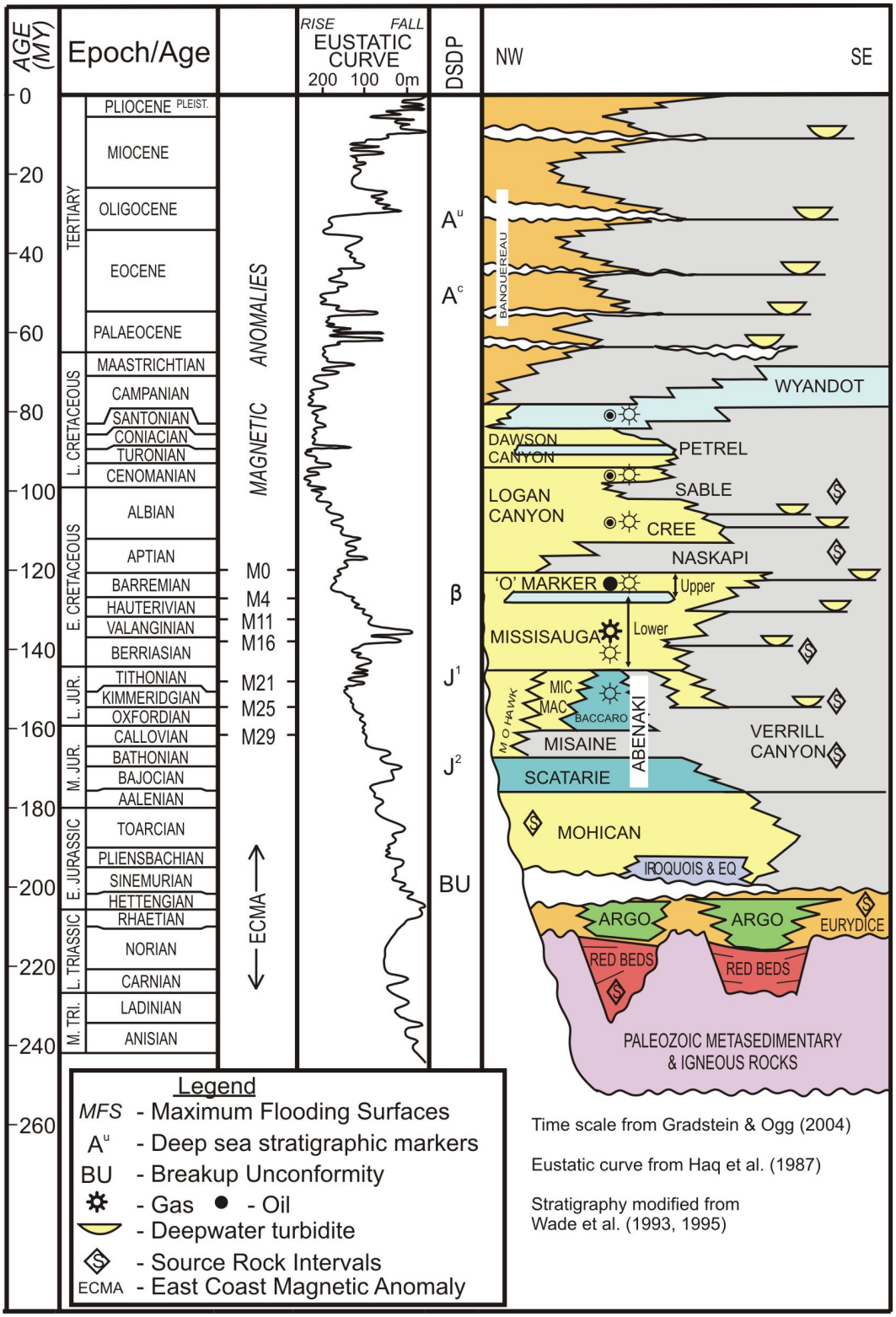

Figure 1.2: Generalized stratigraphic column for the Scotian Basin denoting major unconformities and magnetic anomalies; image from Canada Nova Scotia Offshore Petroleum Board (CNSOPB) call for bids 2008-2009, NS08-2, after Kidston et al. (2002), Wade et al. (1995), MacLean and Wade (1993).

Restricted shallow water to tidally influenced marine conditions in the Early Jurassic led to deposition of continental clastic and evaporitic dolostones of the Iroquois and Mohican formations (Given 1977), unconformably overlying the Argo and Eurydice formations (Jansa and Wade 1975; Wade and MacLean 1990; Kidston et al. 2002). The dolomite sequence was followed by a thick succession of coeval fluvial sandstone and shale of the Mohican Formation, which completed the process of filling the rift grabens and onlapped basement highs along the post-breakup surface (Wade and MacLean 1990).

Normal marine conditions were established across the basin during the Middle and Upper Jurassic, represented by continental clastics of the Mohawk Formation (McIver 1972), shallow marine sandstones, shales and limestones of the MicMac Formation (McIver 1972), a shelf carbonate facies, the Abenaki Formation (McIver 1972; Eliuk 1978) and a basinal shale facies, the Verrill Canyon Formation (Wade and MacLean 1990). Continuous sediment loading during this period initiated the mobilization of deeply buried Jurassic salt causing the vertical and lateral intrusion of overlying sediment that continues to the present day (Ings and Shimeld 2006).

The Early Cretaceous was characterized by deposition of fluvial-deltaic Missisauga and Logan Canyon formations. The Missisauga Formation (McIver 1972) consists of a series of thick deltaic packages of sand-rich sediment with broad alluvial plain, adjacent delta and prodelta facies. The deltaic facies are best known in the Sable Island area but likely occur in parts of the Laurentian and South Whale subbasins (Wade and MacLean 1990; Kidston et al. 2002). Deposition of deltaic sediment ceased following a late Early

Cretaceous marine transgression. The result of marine transgression was the accumulation of shales of the Logan Canyon Formation and transgressive marine shales and minor limestones of the Dawson Canyon Formation.

Late Cretaceous sea level rise and basin subsidence resulted in deposition of marine marls and chalky mudstones of the Wyandot Formation (McIver 1972; Wade and MacLean 1990; Kidston et al. 2002). Cretaceous sediments and the entire Cenozoic sedimentary succession above the Wyandot are designated the Banquereau Formation (McIver 1972). Marine shelf mudstones, sands and conglomerates of the Banquereau Formation were influenced throughout the Cenozoic by several major unconformities related to sea level fall (Fig. 1.2). Unconformities are noted during the Paleocene, Oligocene and Miocene intervals where fluvial and deep water currents eroded largely unconsolidated sediments, subsequently depositing them on the abyssal plain (Wade and MacLean 1990; Kidston et al. 2002). Winnowing and reworking of deep-water sediment by bottom currents began in the Oligocene (Gradstein et al. 1990; Piper 2005), providing the earliest evidence of thermohaline circulation. Sediment distribution of Miocene successions were strongly influenced by the Western Boundary Undercurrent with periods of intensified bottom current activity also occurring in the Late Pliocene (Myers and Piper 1988; Piper 2005), followed by widespread gully cutting in the Early Pleistocene. During the Quaternary to recent, several hundred metres of glacial and marine sediment were deposited on the outer shelf and slope (Piper et al. 1987; Mosher et al., 1994; Kidston et al. 2002).

On the Scotian Shelf and Grand Banks the widespread hiatus eroding either the upper part or all of the Oligocene is marked by a regional unconformity; the nature of which includes canyon formation. Canyon incision at the shelf edge initiated during the Eocene and was extensive by the Oligocene (Fensome et al. 2008). Pe-Piper and Piper (2004) noted that although Oligocene strata are absent on the Scotian Shelf and Grand Banks, they are present both on the Labrador Shelf (Balkwill and McMillan 1990) and on the New Jersey margin where small hiatuses are correlated with the global eustatic sea-level curve of Haq (1987) (Miller et al. 1985; Mountain and Tucholke 1985; Tucholke and Mountain 1986). Wade et al. (1995) attributed the missing Oligocene strata on the eastern Scotian Shelf to a broad southeasterly trending canyon associated with a sea level lowstand. This canyon system and related surface is the subject of the present study.

Chapter 2. Methods

The primary method of investigation for this study of the eastern Scotian Slope is interpretation of multi-channel seismic reflection data. The main data set is a 50 km x 60 km 3D seismic volume, known as Stonehouse, donated by Encana Ltd. Seismic interpretation began with a time-migrated volume of the Stonehouse dataset with a reprocessed, depth-migrated volume later becoming the primary dataset for the study. Regional 2D seismic lines extend interpretations from the study area to the Scotian Shelf and the abyssal plain (Fig. 2.1), while nearby well data were incorporated into the study using synthetic seismograms. Integration of reflection seismic, well data, and the application of stratigraphic concepts allows linkage of the regional stratigraphic framework of the Scotian Shelf and Slope to the Stonehouse data volume.

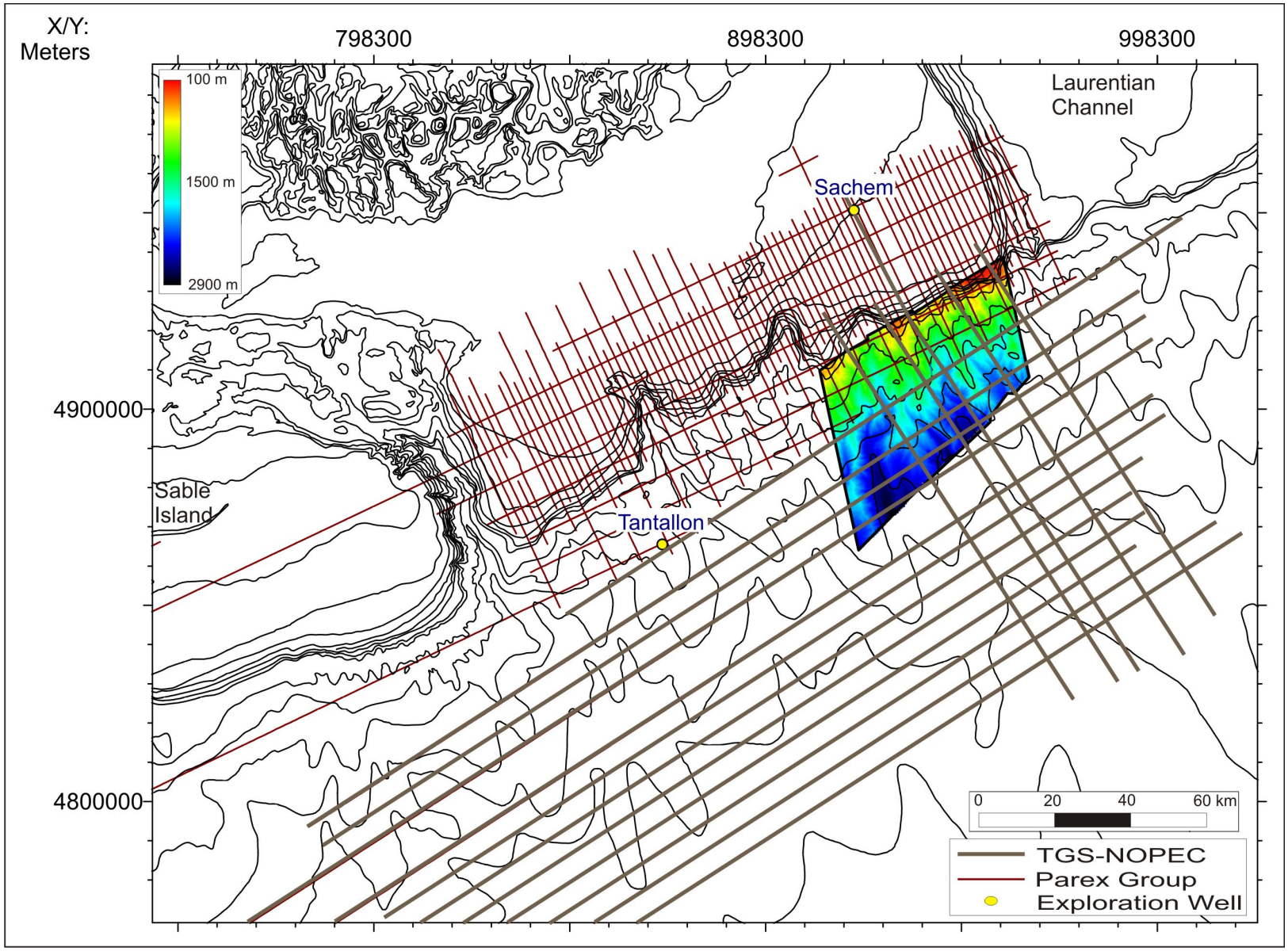

Figure 2.1: Data investigated during this study of the eastern Scotian Slope included the Stonehouse 3D volume (colors indicate distance below sea level), a series of 2D seismic reflection lines from the Parex Group and TGS-NOPEC and exploration well information for the Sachem and Tantallon wells.

2.1 Seismic reflection data

The physics and practical application of marine seismic reflection technology is the subject of numerous texts (for example: Yilmaz 1987, Telford et al., 1990, Kearey and Brooks 1991, Sheriff and Geldart 1995, Brown 1999, Yilmaz 2001, Sheriff 2002, Veeken, 2007) and will not be discussed further here except to address specifics of the data sets used in this investigation.

2.1.1 Two-dimensional seismic reflection data

A regional grid of 2D seismic reflection data is available for much of the Scotian Slope. 2D lines were collected by the Parex Group and TGS-NOPEC at a grid spacing of ~6 km. Seismic lines relevant to the development of the Cenozoic stratigraphic framework and the understanding of canyon evolution were selected and interpreted as part of this study. These data provide a means to correlate the regional stratigraphic framework into the 3D seismic volume and correlate interpretations beyond the volume (Fig. 2.1).

Approximately 9000 line-km of regional 2D seismic data were collected by Soquip Exploration in 1983 (Parex, 8620-S014-006E) along the Scotian Shelf and upper Slope. Covering an area of approximately 15,000 km^2, the regional grid of seismic data consists of strike lines oriented parallel to the present-day shelf break (ENE–WSW), evenly spaced at ~ 8 km, and dip lines trending NNW–SSE at a line spacing varying from 2 to 8 km.

Approximately 25,000 km^2 of 2D seismic data were collected in 1999 (TGS-NOPEC NS24-G026-001P) over the Scotian Slope. Strike and dip lines form a regional grid spaced at 6 km x 6 km on the Scotian Slope. Strike lines trend ENE-WSW parallel to the present-day shelf break, while perpendicular dip lines trend NNW-SSE, similar to the Parex data set.

Data for both the TGS-NOPEC and Parex datasets were processed prior to becoming available to the Geological Survey of Canada – Atlantic (GSC-A). Selected 2D seismic lines were imported into Seismic Micro Technology's™ (SMT) Kingdom suite 8.2 (64-bit) software to extend interpretations from the Stonehouse prospect onto the shelf and further along the slope.

2.1.2 Three-dimensional seismic reflection data

Approximately 1765 km^2 of three-dimensional (3D) seismic data were acquired in 2003 by CGG Canada Services Ltd, onboard the vessel M/V Geco Triton for EnCana Oil and Gas Corporation. Multisource, multisteamer 3D configurations were used to acquire up to 60 fold data. Recording configurations consisted of 8 streamers, with 25 m group intervals, 240 channels per streamer and 100m streamer separations with streamer depths of 8 $\pm$ 1m. Survey orientations ranged from NE to SW along strike of regional seafloor slope to NE-SW, perpendicular to the regional slope.

Two arrays of pneumatic air guns with total volumes of 5085 in^3 were fired alternatively (flip/flop mode) for shot point intervals of 50 m effective per common mid point (CMP)

line. Traces were binned at 25 x 25 m and sampled at an interval of 2 ms with a 3 Hz -18 db/Oct low cut filter and 200 Hz - 406 db/Oct high cut filter.

3D seimic data were time-migrated using a prestack kirchhoff time migration (PSTM), filtered and equalized, subsampled at 4 ms by EnCana in 2004. The upper 2 s of time data were donated to the GSC-A at the Bedford Institute of Oceanography for scientific research in 2006. Survey data were later reprocessed and prestack depth-migrated (PSDM) using a hybrid layer-based global gridded tomography sampled at a 10 m interval to improve resolution over potential geologic targets within the prospect. This depth-migrated subset of the Stonehouse data set spanning strata from base Cenozoic to the seafloor became available to the GSC-A in July of 2007.

SEG-Y formatted files for both the time and depth-migrated volumes of the Stonehouse data set were imported into SMT's Kingdom suite software for interpretation, where seismic stratigraphic and seismic geomorphologic techniques were applied to the volume. Reflection amplitude, termination patterns, and plan-form and 3D geometry were used to distinguish key surfaces, sequence boundaries and seismic facies. On every tenth inline and crossline, prominent reflections were mapped as horizons throughout the velocity and depth-migrated data sets. These horizons were then autoccorrelated to provide 3D images of geomorphologic surfaces that provide insight on the geologic development of the region.

2.1.3 Time versus depth data

Seismic reflection data are most commonly displayed as a plot of two-way travel times (TWTT) of reflected energy along a transect of subsequent traces. Analysis of the arrival TWTT, amplitude and character of the received seismic signal provide valuable information for interpreting the subsurface. The advantage of depth migration is that the interpreter has immediate depth sections at their disposal demonstrating true geometric relationships without time distortion artefacts. Conversion of time data into the depth domain is a costly and time consuming iterative process that uses a velocity model for the layered Earth to convert arrival times into depth sections.

In the PSDM approach, the velocities are updated in Common Reflection Point (CRP) gathers, in a layer-per-layer manner, resulting in a velocity model and gather with the best imaging and event flattening retained (Veeken 2007). The use of Kirchhoff depth migration deals with the lateral velocity changes related to steeply dipping reflectors imaged in areas with variable topography (Veeken 2007).

2.2 Seismic stratigraphy

Seismic stratigraphy is a technique used in seismic interpretation that combines seismic reflection geometries and basic stratigraphic concepts to infer depositional architecture (Vail et al. 1977). Seismic reflections (often resembling layering) are generated at acoustic impedance contrasts (Z); impedance being the product of changes in the bulk rock properties of velocity and density. Assuming normal incidence, seismic reflections are explained through the Zoeppritz equation, which reduces to the familiar equation for

the normal reflection coefficient (Equation 2.1). The equation states that the reflection amplitude, compared with the incident amplitude, varies directly as the change in acoustic impedance (Sheriff & Geldart 1995).

$$R = \frac{Z_{\text{layer 2}} - Z_{\text{layer 1}}}{Z_{\text{layer 2}} + Z_{\text{layer 1}}} \qquad (2.1)$$

Zoeppritz Equation (Zoeppritz 1919)

A reflection coefficient is generated at each change in acoustic impedance and collectively the sequence of reflection coefficients are referred to as the Earth's reflection series. The source wavelet convolves with the Earth's Reflection Coefficient series to produce a series of seismic reflections. The application of seismic facies analysis and seismic stratigraphic concepts to the interpretation of these seismic reflections helps infer depositional and tectonic evolution of depositional sequences.

Applying the principles of reflection seismology, reflections defining variations in attributes are considered based on reflection character (described in terms of reflection amplitude, frequency, coherency and continuity), reflection configuration (Fig. 2.2), and external geometry (Stoker et al. 1997). Seismic reflections are grouped into seismic facies or intervals of similar reflection characteristics. Facies are further grouped into seismic units based on patterns of occurrence or associations. Both seismic facies and units are then used to interpret the distribution of sediments and environments of deposition based on internal reflection organisation, boundary relationships, external geometry and lateral changes (for example: Mitchum et al. 1977a; Mitchum et al. 1977b;

Vail et al. 1977; Vail 1987; Galloway 1989; Christie-Blick 1991; Catuneanu 2002; Veeken 2007). Seismic facies are grouped into seismic units in order to describe overall reflection character of a specified interval or succession of seismic facies.

Bounding Discontinuities

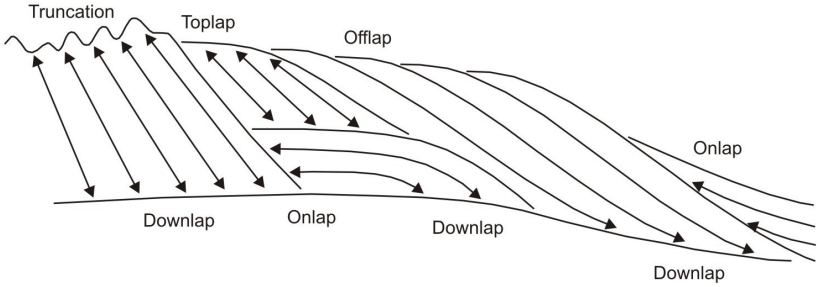

Reflection Configurations

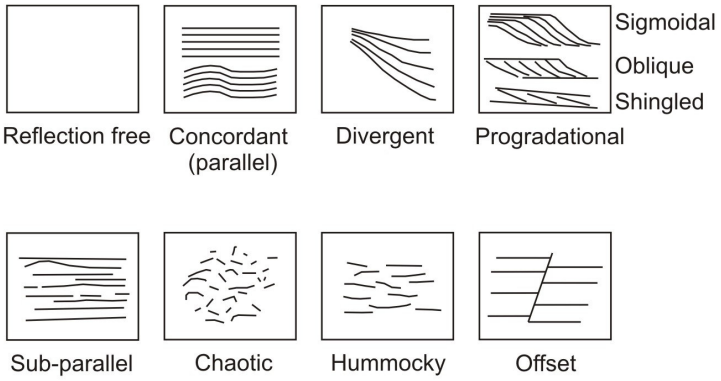

Seismic Units

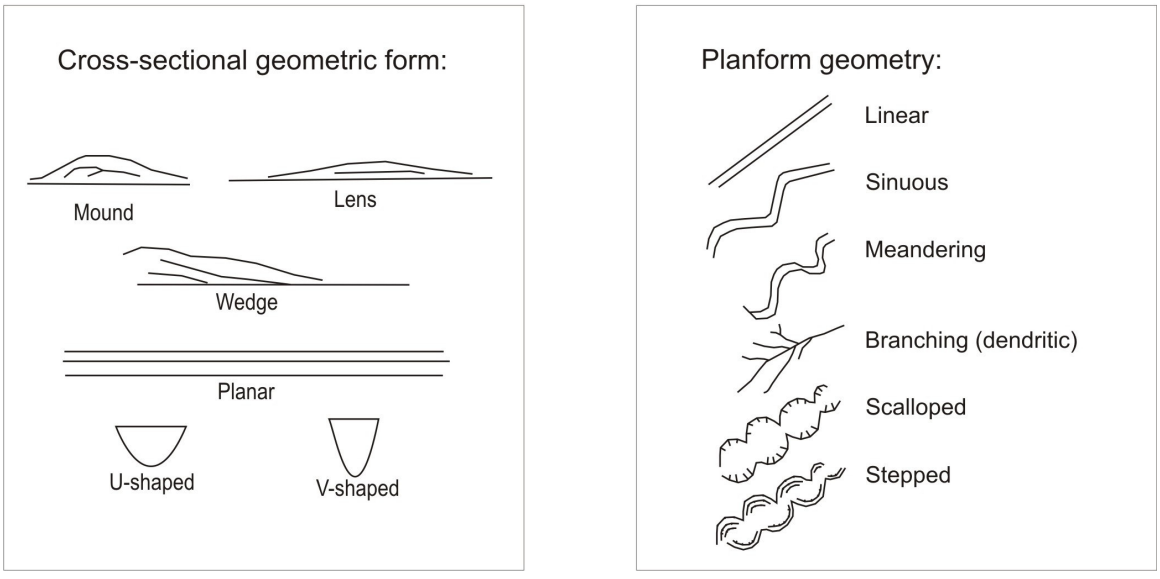

Figure 2.2: Seismic stratigraphic boundaries, configurations and geometries used to infer geologic and tectonic evolution of reflection seismic data. Bounding discontinuities modified from Sloss (1963); Mitchem et al. (1977); Vail (1987), image from Catuneanu (2002). Reflection configuration, cross-sectional and planform geometry, modified from Mitchum et al. (1977); Deptuck (2003) and MacDonald (2006).

Vertical and lateral resolution of seismic reflections is a major concern in seismic acquisition and interpretation. Issues may arise concerning the spatial resolution of 3D seismic data depending upon bin dimensions, stacking fold and errors associated with CMP positions within the bin. In most cases, bin spacing is larger than the acoustic resolution; therefore, the bin size determines the resolvable target size, minimum unaliased frequency due to dip, and lateral resolution (Mosher et al. 2006).

Spatial, or horizontal resolution of seismic reflections is described in most texts as a function of the Fresnel zone size and bin (CMP) spacing (Mosher et al. 2006). The Fresnel zone refers to the region of constructive interference surrounding the geometrically predicted reflection point. In 3D seismic migration, the Fresnel zone is collapsed in all horizontal directions, thus resolution is not limited by the Fresnel zone. The spatial resolution is therefore determined by: the frequency of the source wavelet, acoustic aperture, pattern responses and group interval, single hydrophone element spacing and spatial noise power spectrum (Mosher et al. 2006). In other words, the spatial resolution is limited by the sounding density, or bin spacing, which is 25 m x 25 m in the case of the Stonehouse volume (Fig. 2.3).

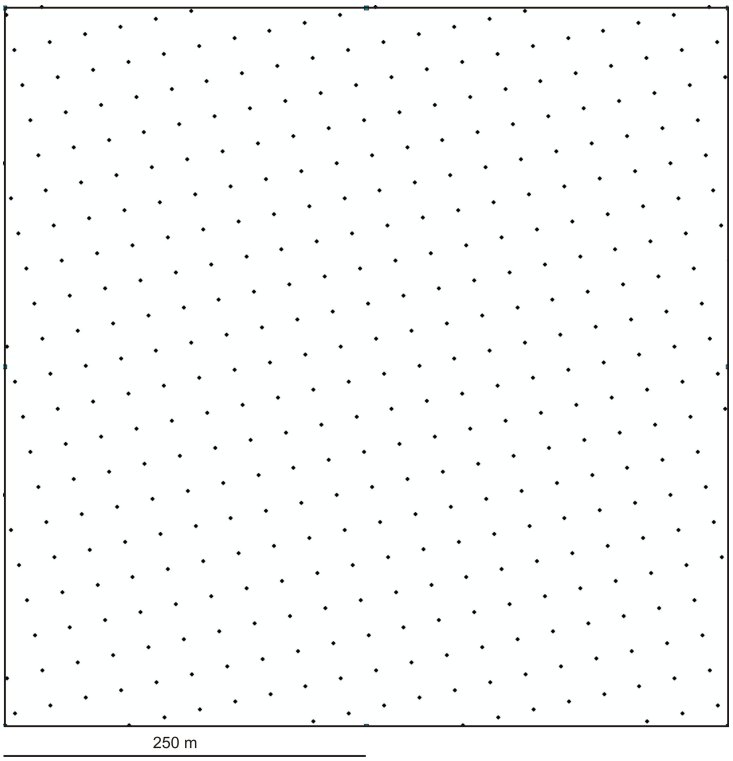

Figure 2.3: Sample density determined from the Stonehouse survey as demonstrated for an area 500 x 500 m. The 25 x 25m bin spacing results in a sounding density of 1600 soundings/km^2.

The temporal, or vertical resolution for seismic reflection data is a function of its frequency bandwidth. In general, the broader the bandwidth, the better the subsurface will be imaged. The maximum resolution (smallest resolvable target) is approximated by the Rayleigh criteria- a 1/4 λ of the highest frequency in the data. For the Encana Stonehouse volume, a power spectral density plot of the data shows its frequency bandwidth is ~10-44Hz. At 44 Hz the Rayleigh criteria indicates the smallest resolvable vertical interval is 22.7ms/4 $\simeq$ 5.68ms. At water velocity of 1500m/s that is equivalent to 8.5 m. Any interval less than 8.5 m is not distinguished by results in an interference composite with adjacent wavelets.

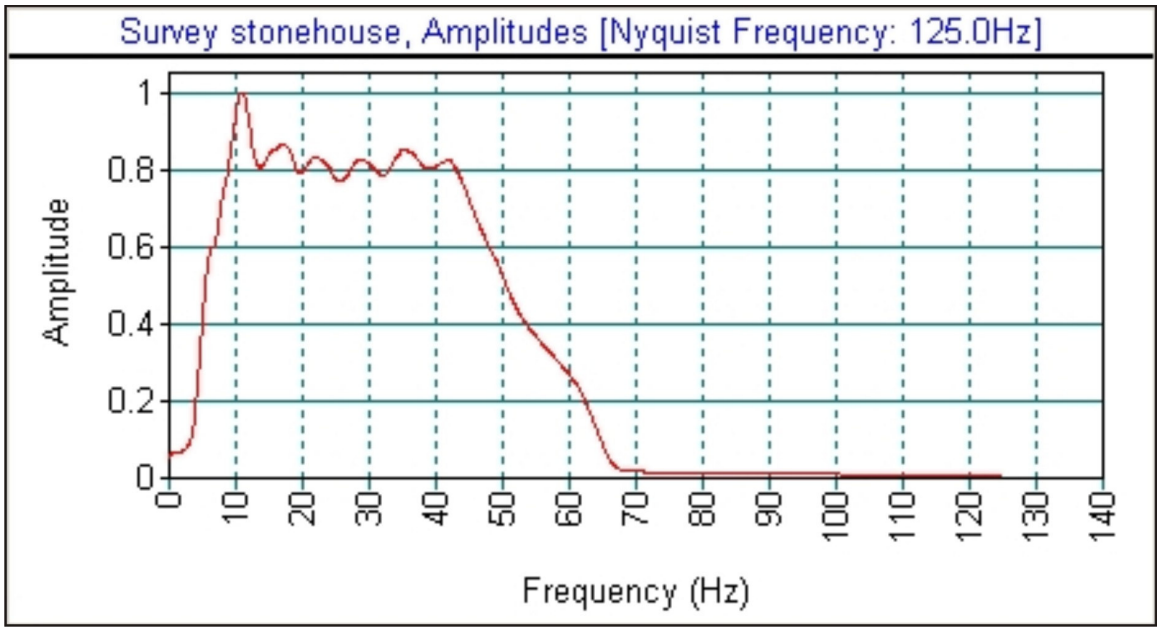

Figure 2.4: Survey spectrum for the Stonehouse dataset. The peak frequency for the spectrum is 44 Hz.

2.3 Synthetic seismograms

Synthetic seismograms are a model of the seismic response by mathematical convolution of an idealized seismic source and a calculated Earth reflection coefficient series. Synthetic seismograms for this study were generated as a means to verify the correlation between well information and seismic data. The simulated seismic response computed from velocity and density well data is used to relate geologic events and lithologies/ages recognized in wells to seismic traces. The match of the simulated seismic response to the seismic profile determines the quality of correlation and confirms velocities used for depth conversion.

Synthetic seismograms for the Stonehouse project were generated in Kingdom Suite using the SynPAK module. In order to generate a synthetic seismogram, velocity and

density data are required in addition to a model of the source wavelet. Acoustic impedance and reflection coefficients are calculated and then convolved with the source wavelet to generate a synthetic seismogram. The synthetic seismogram, therefore, represents the reflection response at the well.

Synthetic seismograms were created for two wells: Sachem D-76 (unique well identifier (UWI) 300 D76 44400 57300) which is 30 km from the study area, and Tantallon M-41 (UWI 300 M41 44000 58150), 50 km from the study area. Sachem D-76 is an exploratory well drilled by Mobil – Texaco in 1975. The Sachem well was drilled in a water depth of 58.5 m to a total depth of 4818.6 m that penetrated strata from the Banquereau Formation through to the Baccaro Member of the Abenaki Formation. The log suite includes gamma ray, neutron porosity, bulk density, acoustic and deep induction log information (Mobil-Texaco 1976). Tantallon M-41 is an exploratory well drilled by Shell in 1986 in 1516.0 m water depth to a total depth of 5602.0 m. The well penetrated strata from the Banquereau Formation through to the Missisauga Formation; gamma ray, neutron porosity, bulk density, acoustic, medium induction and deep induction log information were recorded (Shell Canada Resources 1986). Although these wells are 30 to 50 km from the Stonehouse volume (Figure 2.1) they represent the closest available well control.

2.4 Seismic attribute analysis

Seismic attributes are quantifiable derivatives of the seismic reflection measurement (time and amplitude) displayed to assist the interpreter in studies of structure, stratigraphy

and rock properties (Brown, 2003). Seismic attributes derived from the time-migrated Stonehouse 3D volume included the geometric similarity and smoothed dip of maximum similarity. Both attributes are computed by scanning adjacent traces in a user-defined range of dips as indicated from the time window. Areas of high geometric similarity values indicate a high degree of lateral signal similarity interpreted as a similar depositional environment, whereas smoothed dip of maximum similarity detects local anomalous dip variation and structural discontinuities. Data are viewed in profile to identify changes in dip, thickness, and fault offset. Data may also be viewed as time slice or horizon to assess lateral as well as vertical attribute changes. A similarity time window of 0.04 s and a variance time window of 0.12 s were used to generate 2, 3D similarity volumes.

2.5 Error Analysis

Sources of error in seismic interpretation arise from limitations in acquisition and processing artefacts, depth conversion and ability to pick and correlate horizons. The capabilities of modern Differential Global Positioning Systems (DGPS) have minimized navigational errors to a point of negligible concern in seismic acquisition. A minor correction is made however to account for tidal range, which in the study area is ~1.5 m; below seismic resolution as shown above.

Data were processed and depth migrated prior to becoming available to the GSC-A. The main quantifiable source of error for the study is therefore related to the ability to pick and correlate horizons. Mapping of seismic reflectors on both inlines and crosslines

created intersecting and/or seed points that were autocorrelated to generate a geomorphologic render of a surface (horizon). Autocorrelation began in the direction where the fewest seed points exist; running for three iterations, following which a smoothing operator of 3 x 3 was run on the surface.

In order to determine the quality of autocorrelation, the difference between the autocorrelated picks versus manual picks for the depth migrated data were investigated for a portion of the modern seafloor. A difference map was generated for an area 10 x 10 km in the central region of the dataset in order to avoid edge effects. The resultant map for the autocorrelated horizon versus manual picks was zero when the autocorrelated surface had undergone the smoothing operator function, thereby indicating anomalous values were removed.

The use of an unsmoothed autocorrelated picks versus manual picks difference map indicates areas with the greatest potential for error (Fig. 2.5). The analysis investigated 209800 numeric cells, with an average difference value of 1.85E-2 m and a standard deviation of 3.24 m.

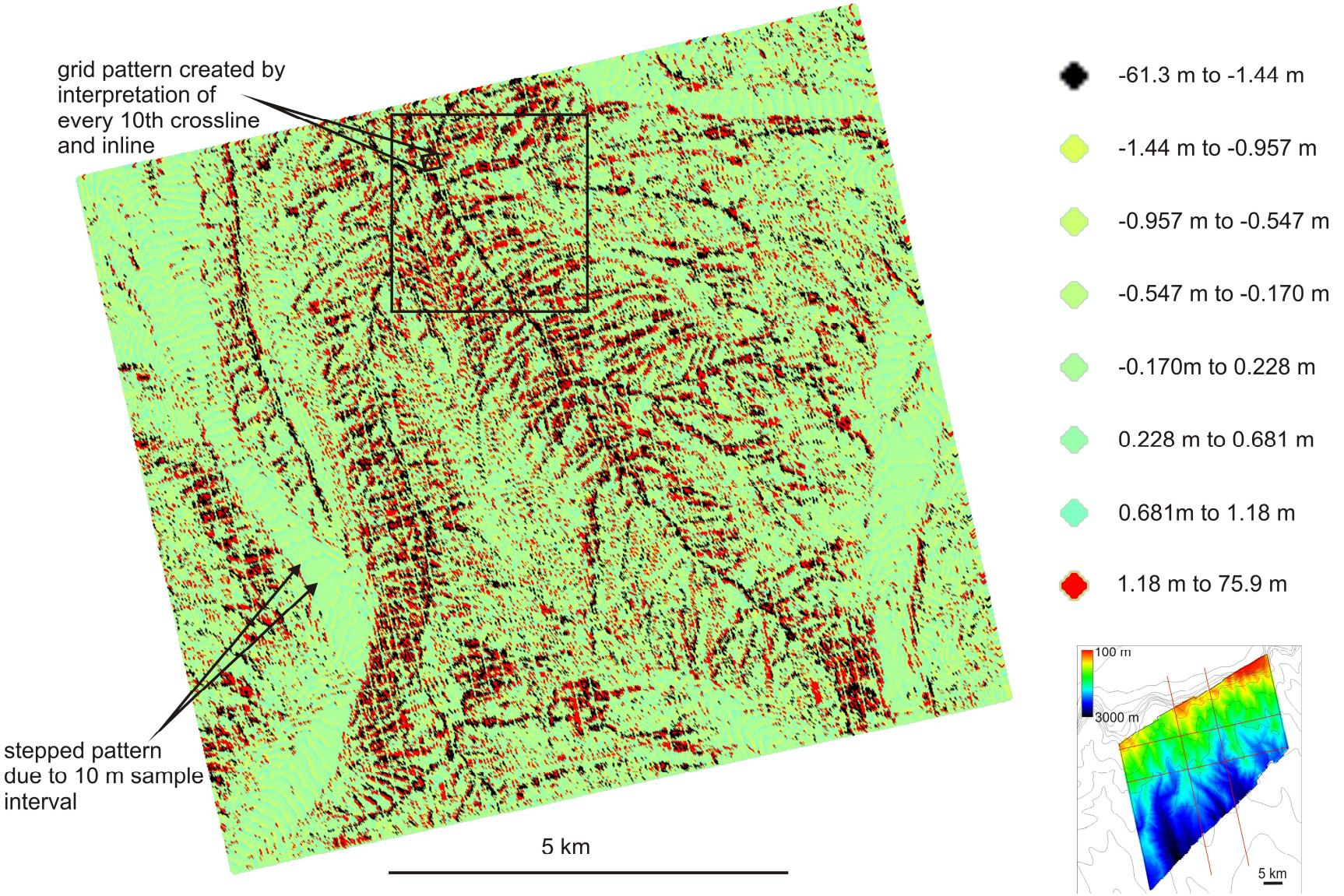

Figure 2.5: Difference map for a 10 x 10 km area of the seafloor horizon of the 3D Stonehouse dataset. The selected area is located in the central part of the data set in order to minimize edge effects.

The difference map of Figure 2.5 indicates the fit between raw picks and autocorrelated picks on the seafloor horizon, with difference values ranging from -61 m to 75.9 m. Minimum differences occur in areas of canyon floors, and gullies on canyon walls. Black areas indicate negative values ranging from 1.44 to 61.3 m (negative spike on seismic profile), which typically occur on canyon ridges. Red areas indicate positive difference values ranging from 1.18 to 75.9 m (positive spike on seismic profile) occurring along gullied canyon walls. Overall the map displays a grid pattern of zero error where the surface was picked manually. Also, the map has a stepped appearance where data were sampled at a 10 m interval during depth migration.

The largest potential for error is noted in regions with the greatest change in topography. The modern seafloor demonstrates the most variable topography within the Cenozoic section, providing the largest margin for error. Use of the smoothing operator function greatly reduces error potential, yet errors may still occur depending upon the number of seed points and the quality of initial interpretation. With few exceptions, most errors due to picking are within the vertical resolution of these seismic data and within the depth-migratation step function.

Chapter 3. Seismic Stratigraphic Framework

Seismic stratigraphy combines acoustic characteristics, seismic reflection geometries and basic stratigraphic concepts, to infer depositional architecture. Correlation of dominant reflections to stratal terminations affords the opportunity to infer sediment transport, deposition and erosion mechanisms. During the Cenozoic, sediments on the eastern Scotian Slope were deposited under variable current, sea level, and depositional regimes influenced by sediment supply and seafloor morphology (e.g., Jansa and Wade 1975; Wade and MacLean 1990; Wade et al. 1995; Kidston et al. 2002, 2007). The application of seismic stratigraphic concepts to the Cenozoic section of the Stonehouse 3D seismic data facilitates understanding of slope evolution and its response to sedimentary, tectonic, and oceanographic processes, including relative and eustatic sea level change.

3.1 Key Reflections

A number of key reflections were identified and correlated across the study area (Fig. 3.1). Reflections were given both a letter and a number to denote reflection name. The letter was arbitrarily chosen while the number indicates the position of the reflection within the sequence. The deepest reflection identified is given the number 100, the modern sea floor is reflection number 1, all other numbers define the relative position within the sequence.

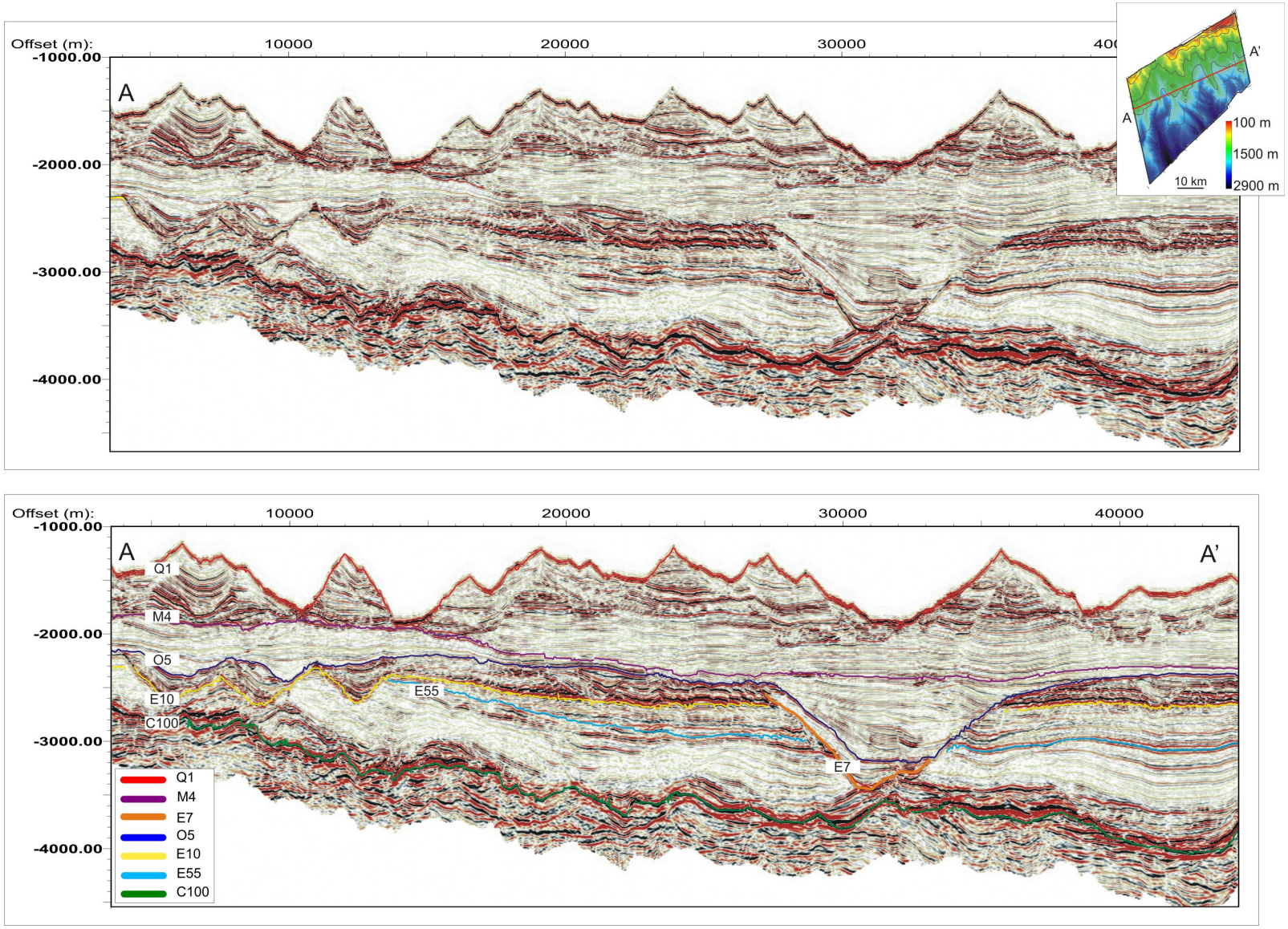

Figure 3.1: Key seismic reflections mapped across the Stonehouse dataset, which aid in separating the Cenozoic section into seismic units.

The deepest reflection described is **C100**. It is a high amplitude continuous peak periodically offset by 20 to 80 m due to faulting. The reflection is widely distributed and readily recognized based on its distinctive character bordered by high amplitude troughs above and below its peak amplitude. Interpretation becomes problematic at the top west corner of the dataset near The Gully due to the bifurcation of the reflection into as many as three major horizons.

The C100 surface displays a series of broad southeast orientated gullies 12 to 28 km in length incising to depths of ~150 to 300 m as well as two dome structures (5 km and 7 km in diameter) (Fig. 3.2). These gullies are flat-floored, with scalloped-walls and incise a gently graded slope (Fig. 3.2A). A 12 km-long semi-linear escarpment, with relief of approximately 80 m (Fig. 3.2B), is also noted in the northern region of the surface incised by a channel system that eroded through the escarpment. Dome structures (Fig. 3.2C) located near the base of slope are surrounded by radial fault patterns, indicating late stage deformation by salt diapers.

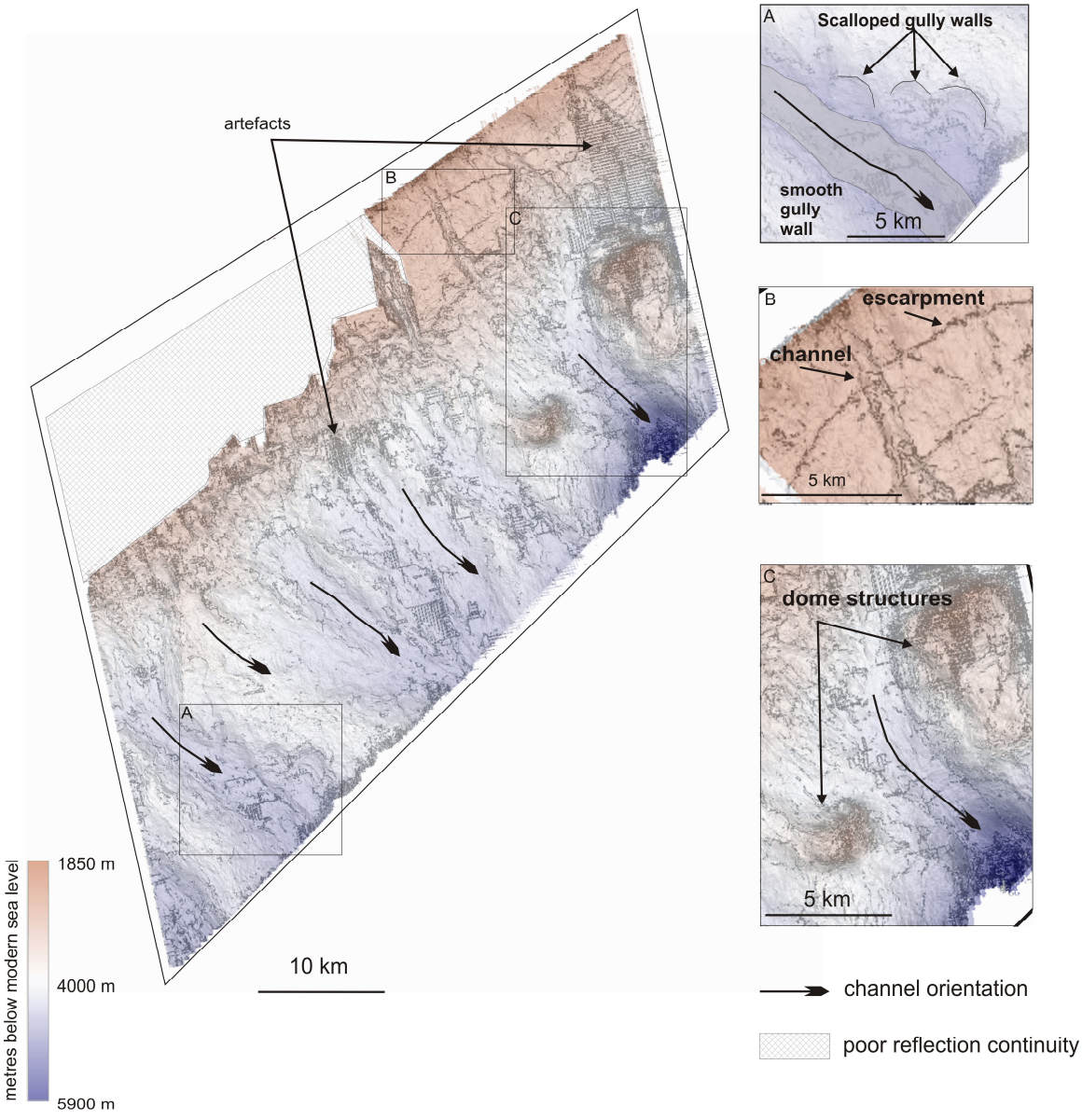

Figure 3.2: Dip map of reflection **C100** draped with colour-coded depth displaying several southeast oriented gullies and two dome structures. A) Smooth and scalloped gully wall morphology. B) A fault-controlled escarpment intersected by a seaward trending channel. C) Southeast oriented channel located between two dome structures with radial faults.

Reflection **E55** is a distinctive peak of variable amplitude that is moderately continuous across the dataset except where it is truncated along the path of several younger canyons. The reflection is of high amplitude in the seaward regions of the dataset, whereas amplitude of the reflection is moderate to low amplitude toward the shelf. Reflection E55 merges with reflection E10, an overlying reflector, from the shelf to approximately mid slope on the western part of the dataset, yet E55 and E10 are not merged to the east.

The E55 surface is at first glance similar to C100 but with much smoother topography (Fig. 3.3). Channels, 16 to 18 km in length, are oriented north-north-west to south-south east and ridges separating channels are smooth and/or pinnate. This surface in the northern region is smooth but with a system of growth faults with tens of metres of offset (Fig. 3.3A). A single dome structure that is 4 km in diameter (radial faults not imaged) is observed in a location similar to the smaller salt dome previously described (Fig. 3.3B).

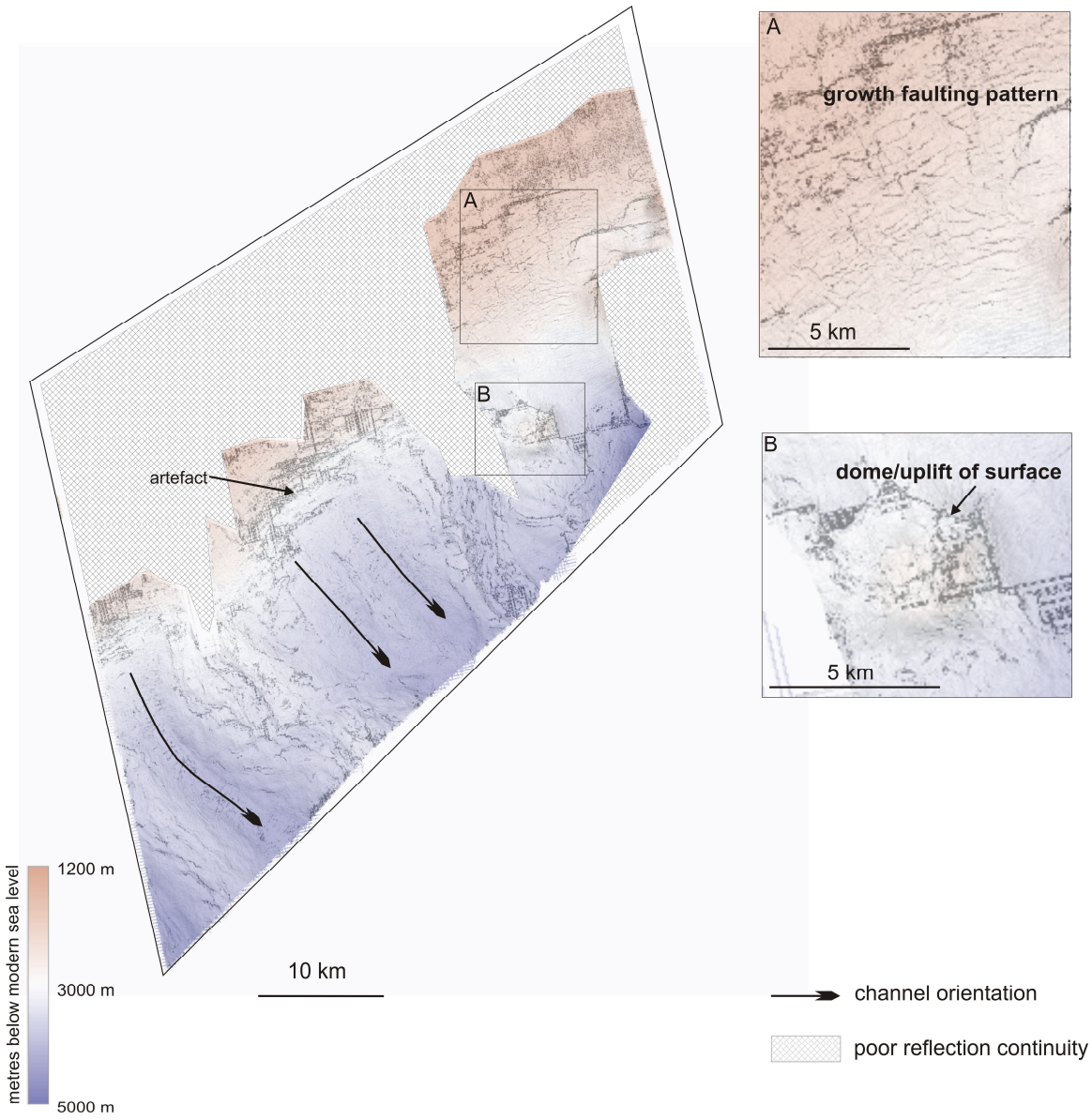

Figure 3.3: The 3D dip geometry of reflection **E55** draped with colour coded depth indicates gently sloping channel systems with a north-north-west to south-south east orientation. A) A network of growth faults are observed above the location of a fault-bounded escarpment described lower in the unit. B) The effects of salt deformation are observed in approximately the same location as the deeper surface. Reflections were autocorrelated only where confidence in interpretation exists, edge geometries therefore are not a function of depositional architecture.

Reflection **E10** is a peak of low to moderate amplitude with poor coherency due to fault offsets. The reflection is heavily faulted in the southern parts of the dataset, with minor fault offset in the upslope region. The reflection is present across the majority of the dataset, but is absent due to erosion in a few specific regions.

The E10 surface displays four canyon systems that are between 12 to 25 km long with a northwest to southeast orientation; two of which merge to form a single canyon (Fig. 3.4). Canyons incise 200 to 370 m, and were in part incised by later canyon incision in the most seaward region of the surface. The reflection is absent in a large part of the study area due to later erosion.

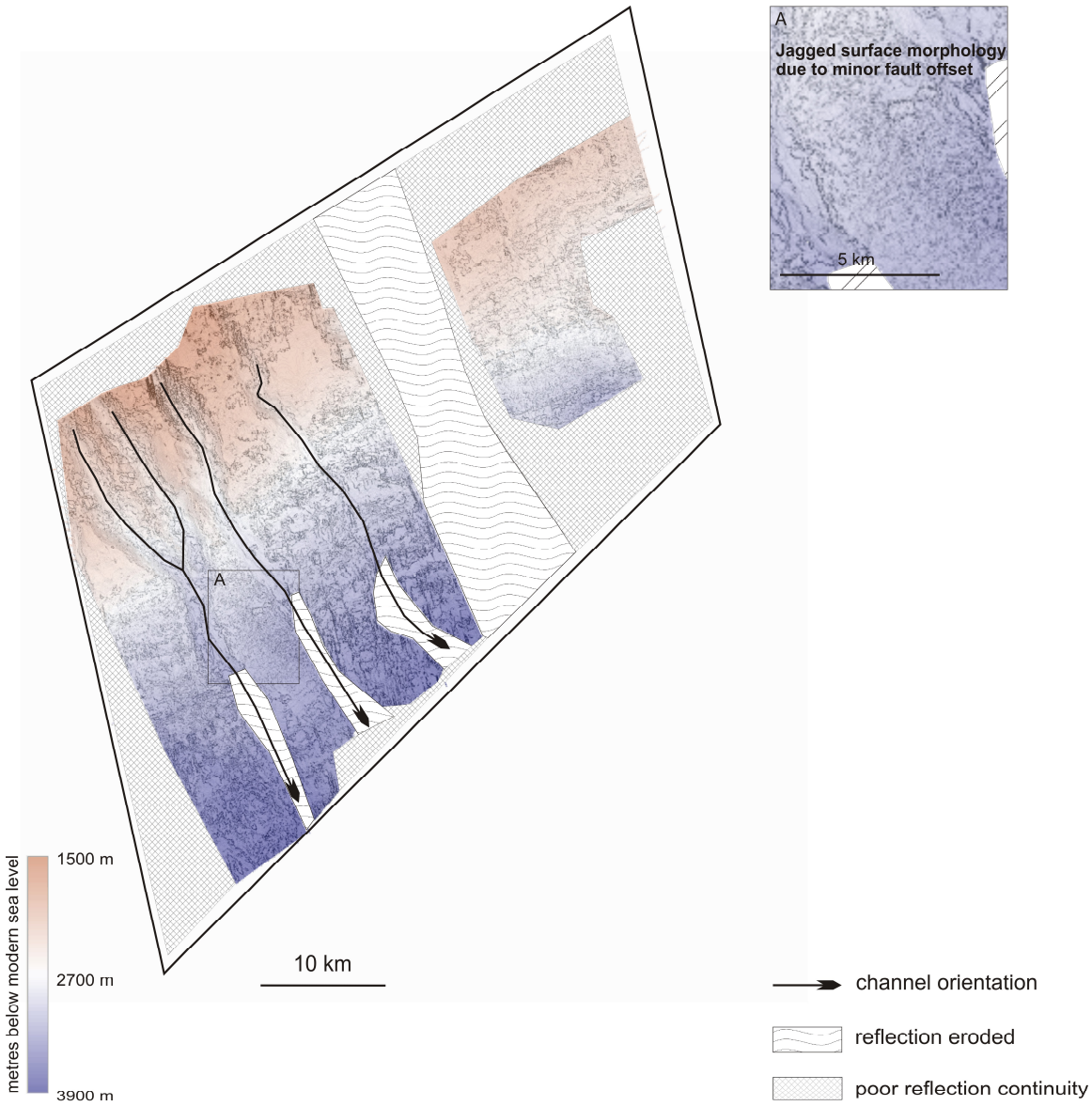

Figure 3.4: The dip map of reflection **E10** draped with a colour-coded depth scale, demonstrates a series of canyons; two of which merge to form a single canyon. The surface is partially removed by later erosion and cannot be correlated across the entire dataset. Edge geometries are a function of autocorrelation not depositional architecture.

Reflection **E7** is a high amplitude continuous reflection that incises reflections E55 and E10, marking a regional unconformity surface that includes canyon incision. The surface is somewhat limited in its extent due to later erosion and will be investigated in detail in Chapter 4.

Reflection **O5** is a low amplitude, moderately continuous peak present across the entire dataset. Recognized by its distinctive reflection character, it denotes a major regional unconformity. The moderate continuity of the reflection is due to faulting with 10 to 20 m offset that gives the reflection a jagged character.

Surface O5 is widespread and displays a major southeast trending canyon 30 km in length and 9 km in width, as well as several small-scale canyons, many of which originate midway on the slope (Fig.3.5A). The sloping surface is influenced by a single dome structure 2.5 km in diameter exhibiting a radial fault pattern (Fig.3.5B). The smoothed dip of maximum similarity attribute extracted for the O5 surface further demonstrates the jagged nature of the horizon as was noted on seismic profile (Fig. 3.5.C). Canyon walls are steep, with smooth morphology. The floor of the largest canyon appears smooth with slight narrowing on its approach to the abyssal plain. Sinuosity of the large canyon system is not observed; however, the eastern canyon wall is steeper than the western wall.

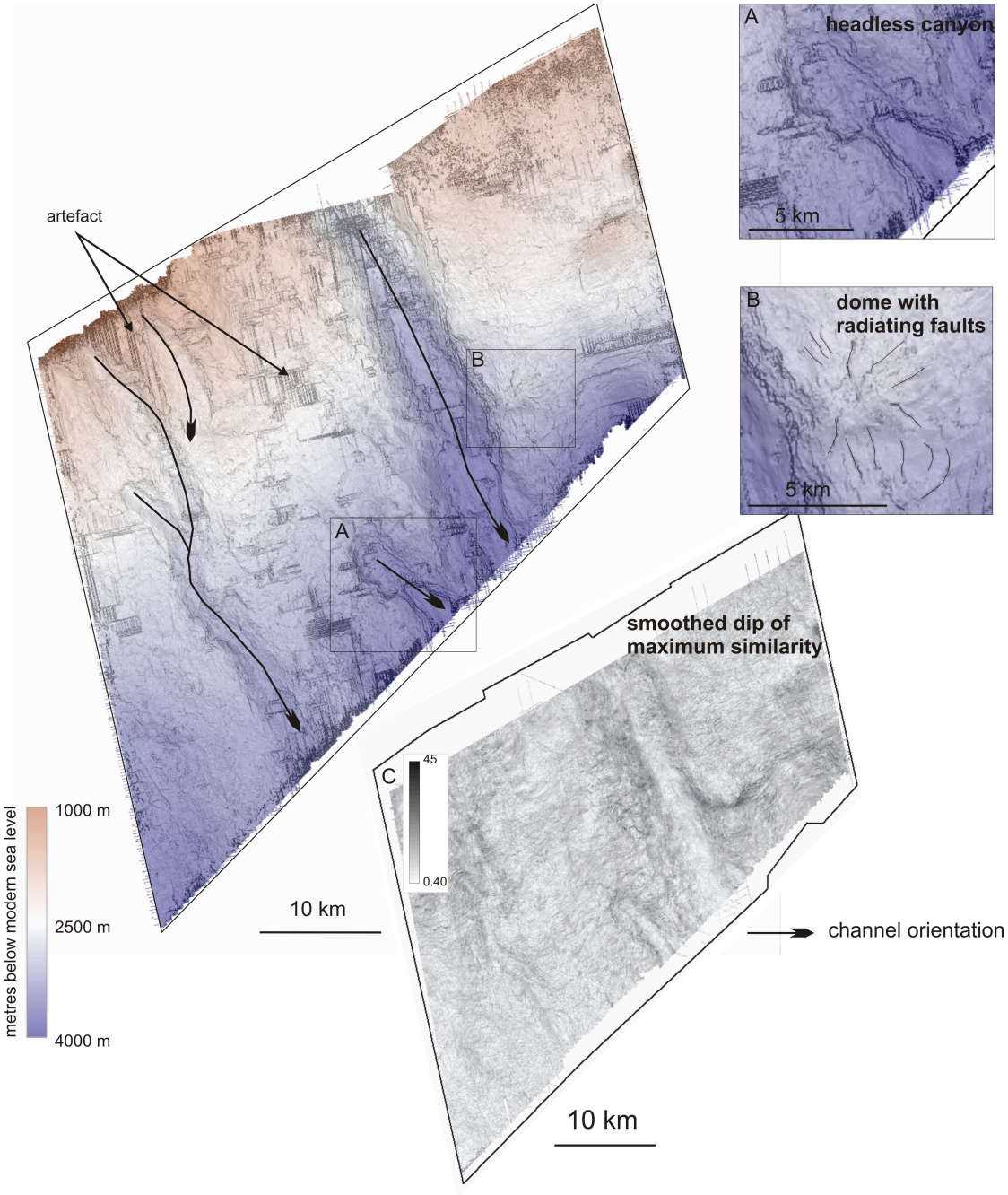

Figure 3.5: Dip map with colour-coded depth overlain, demonstrating the morphology of reflector **O5** and smoothed dip of maximum similarity surface indicate the presence of a major canyon system as well as several smaller scale canyons. A) Headless canyon in the most seaward section of the dataset. B) Salt dome with radiating faults. C) Smoothed dip of maximum similarity attribute extracted for the O5 horizon that demonstrates the irregular nature of the surface.

Reflection **M4** is low amplitude, continuous, and present across the majority of the dataset. It is close to the modern seafloor and is the shallowest reflection investigated in detail. M4 onlaps reflection O5 in the northeast corner of the dataset, and is absent on a portion of the western side.

The M4 surface is widespread across the dataset, although the reflection is disrupted by later incision (Fig. 3.6). Overall the surface is smooth but the effects of salt doming (dome approximately 2.5 km across) and radial faulting are observed in the same location as the previous surface (Fig. 3.6A). Minor channels are noted; one of which meanders over a distance of 8.6 km (Fig. 3.7B), and all of which originate midway across the surface, or in the mid-slope position and cannot be traced onto the shelf.

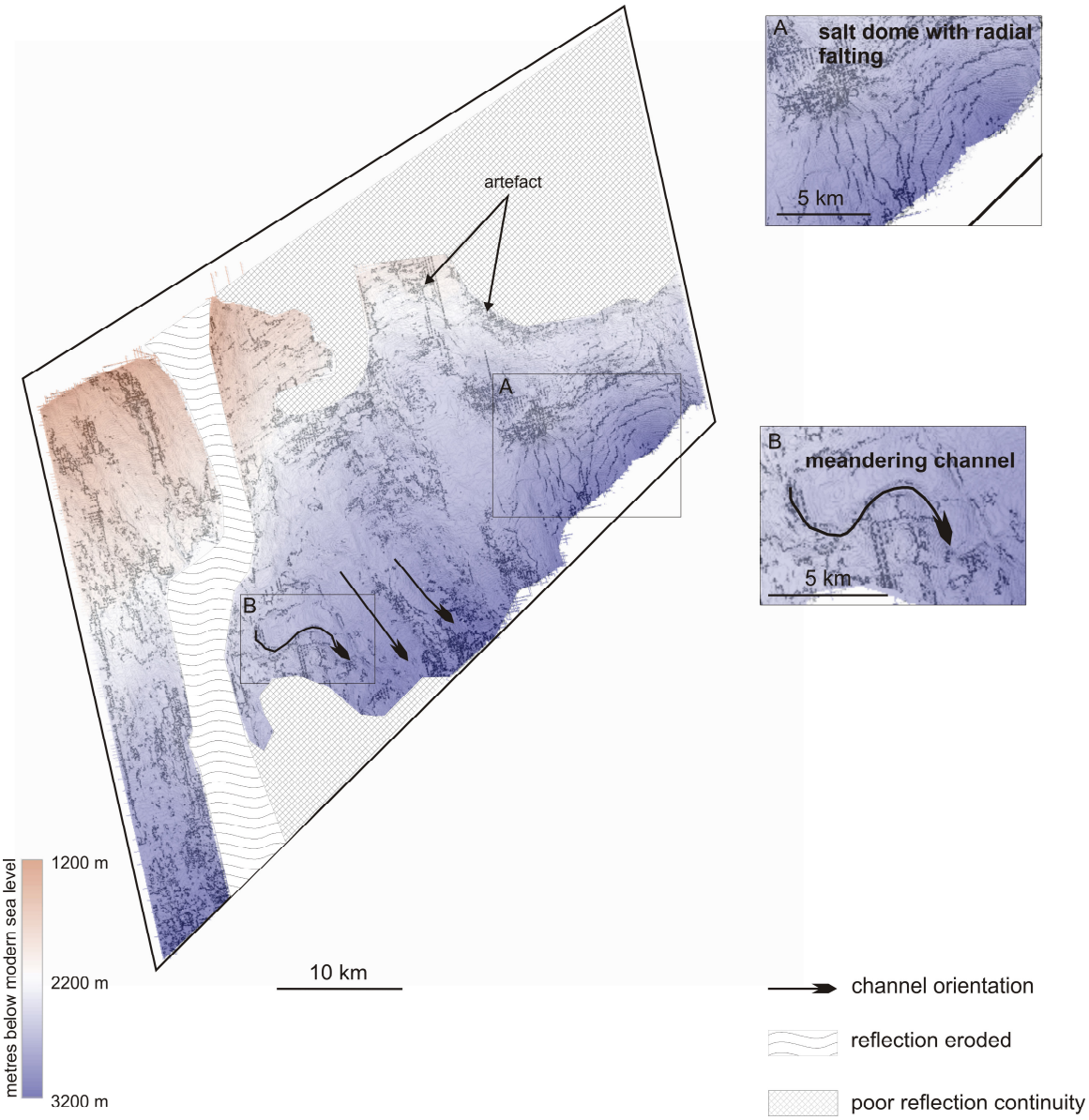

Figure 3.6: The dip map of reflection **M4** illustrates a fairly smooth surface with minor channel incision. A) Salt doming with radial faulting pattern are preserved in the southeast corner of the surface. B) Meandering canyon observed in the midslope position. Color bar indicates metres below modern sea level. Reflections were autocorrelated only where confidence in interpretation exists, edge geometries are not a function of depositional architecture.

The first arrival, seismic reflection **Q1**, represents the seafloor. The modern sea floor surface displays an extensive network of dendritic, branching canyons; the majority of which extend from the shelf onto the slope and beyond (Fig. 3.7). Modern canyon and tributary systems are on average 3 – 10 km across and extend up to 49 km in length within the dataset. They incise as much as 250 to 650m of section. Unlike the buried channels and canyons, the modern systems display sinuosity. Headless canyons (i.e. canyons that start on the slope and not at the shelf break) are also observed near the base of slope position (Fig. 3.7A). Canyon floors are gently graded with individual canyons separated by steep-sided pinate ridges.

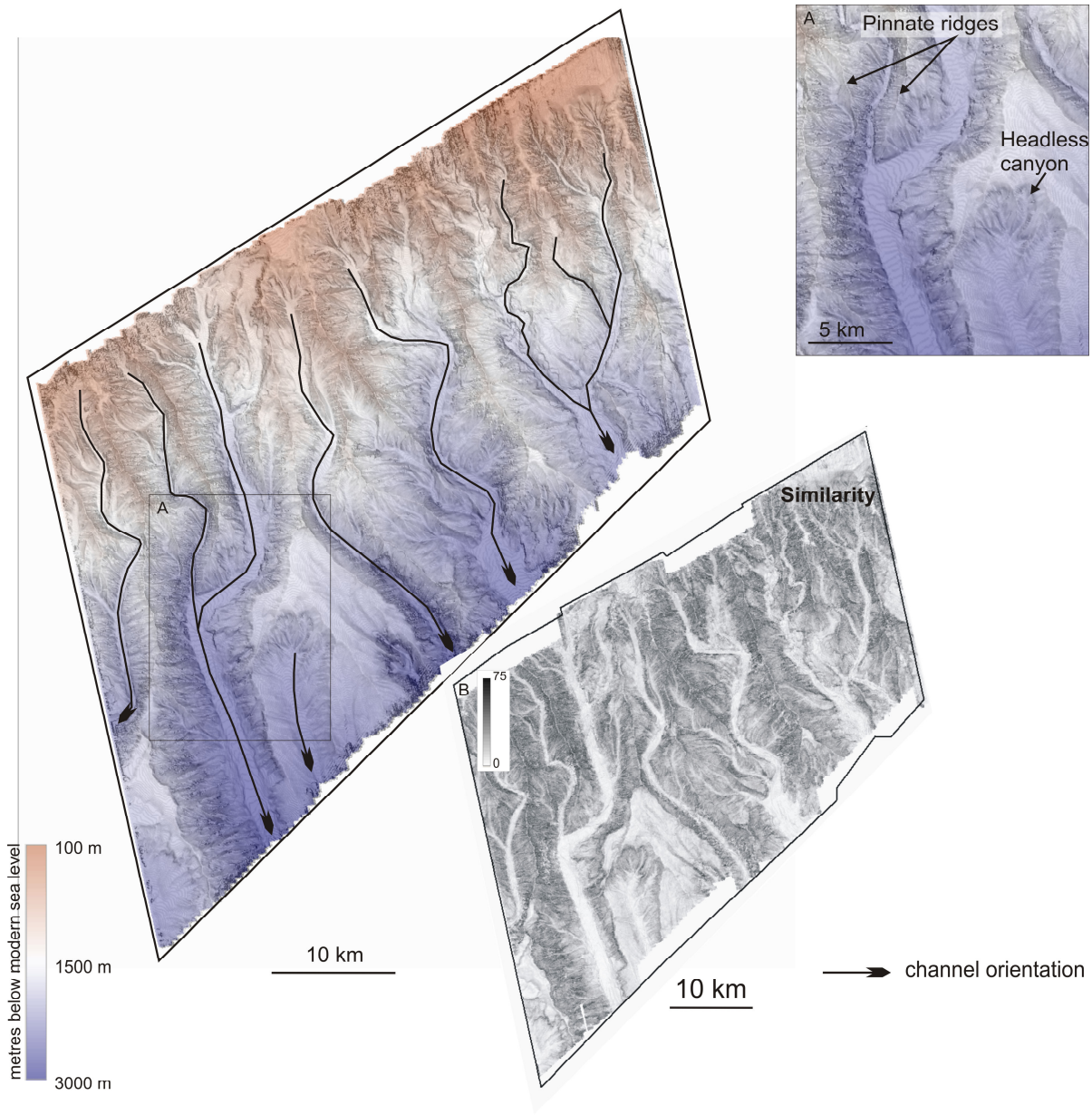

Figure 3.7: Dip map of the modern seafloor **Q1** displaying an extensive network of branching, dendritic canyons, many of which extend from the shelf break toward the abyssal plain. A) Headless canyon and pinnate ridge example near the base of slope. B) The similarity attribute for the Q1 surface displays an enhanced image of the canyon systems.

3.2 Seismic unit distribution within the Stonehouse

The distribution and thickness of seismic units within the Stonehouse survey is highly variable (Fig. 3.8 to Fig. 3.10), and changes both along strike and dip. The five main seismic units are described sequentially from oldest (deepest) to youngest (shallowest) below:

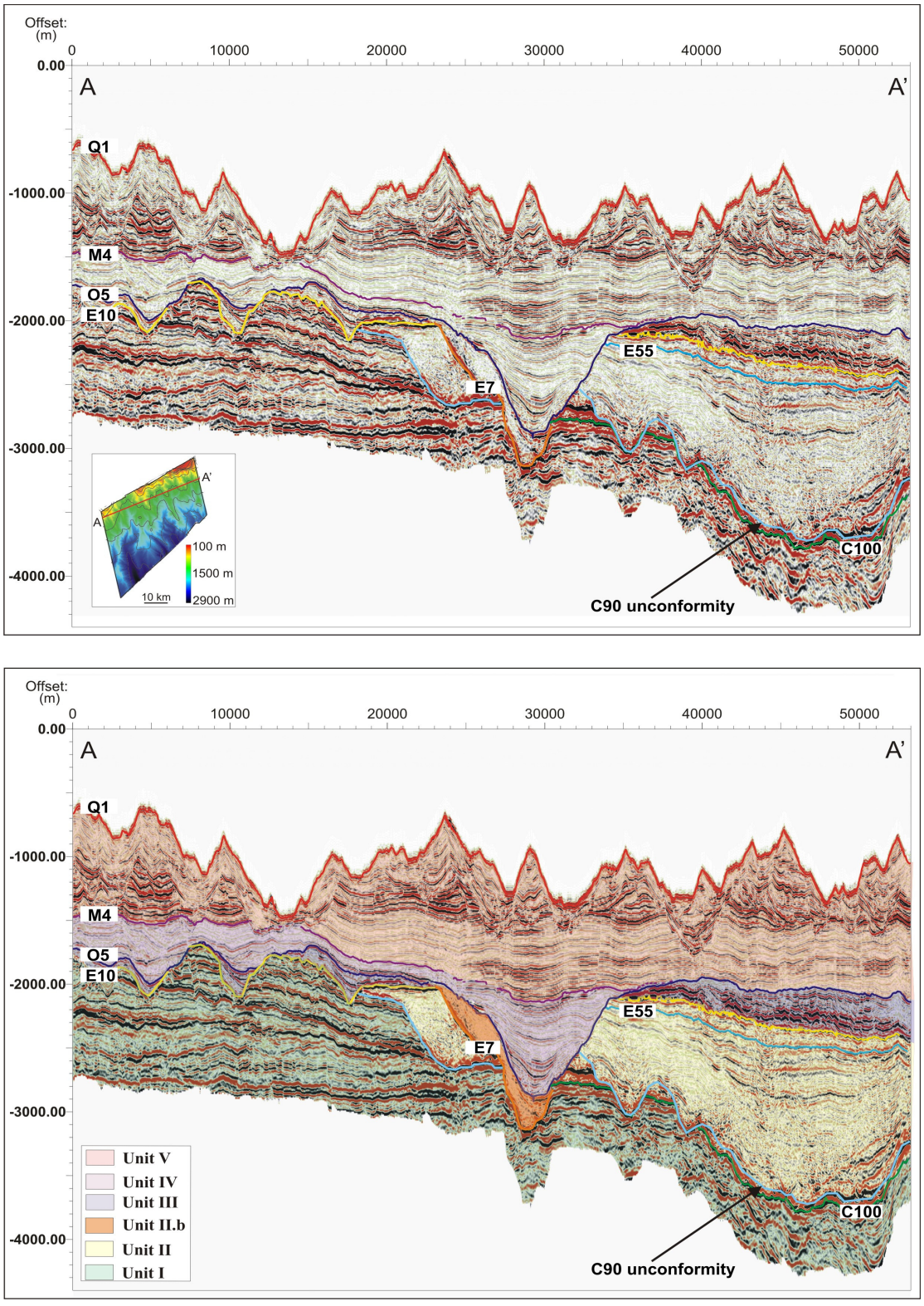

Figure 3.8: Interpretation of seismic units of the Stonehouse dataset displayed on a shelf-parallel (strike) seismic line in the upslope region of the data (see inset map for location). Note that unit thicknesses are not distributed evenly across the profile.

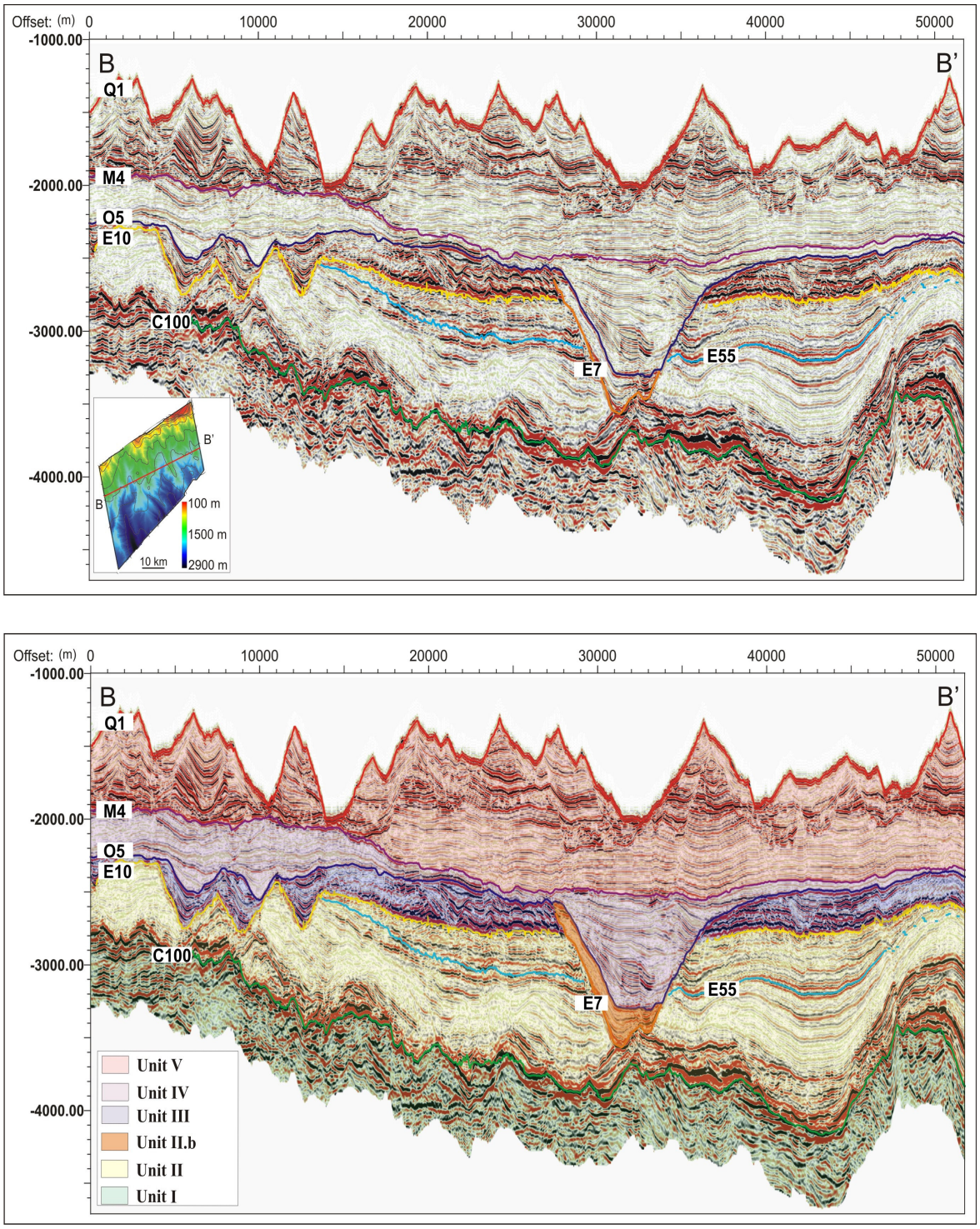

Figure 3.9: Distribution of seismic units in the midslope region of the dataset as interpreted along profile B (see inset map).

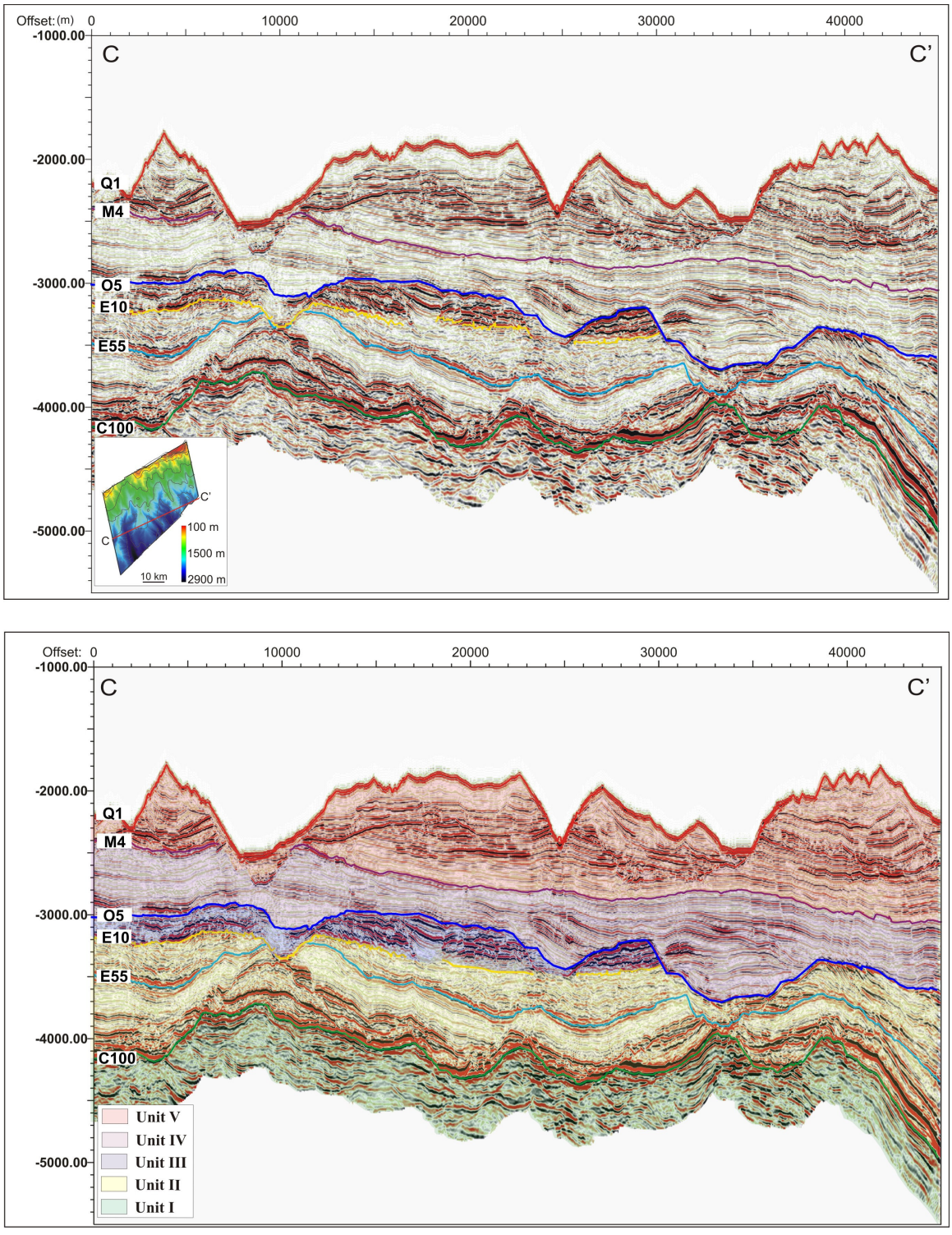

Figure 3.10: Distribution of seismic units in the most seaward section of the dataset as located along profile C (see inset map). Seismic units are evenly distributed across the profile.

The deepest of the seismic units, **Unit I**, is the section below reflector C100 to the base of the dataset. Limited data are available below the reflector due to data confidentiality; nonetheless, they display an overall chaotic arrangement of low to moderate amplitude reflections.

Unit II comprises the interval from C100 to the E10 horizon. The unit is present across most of the dataset, but absent in the northwest corner. Thickness is variable ranging from 66 to 1550 m, with the greatest thickness on the east central area of the data volume (Fig. 3.11). Outboard of the east central area the thickness is uniform.

The lower part of Unit II consists of moderate to high amplitude, fairly continuous, mounded reflections. Above the mounded reflections are a series of low amplitude continuous reflections, which switch to low amplitude, chaotic reflections near the E55 horizon and continuing up to the E10 horizon. This vertical pattern of reflection character is consistent for this sequence across the dataset.

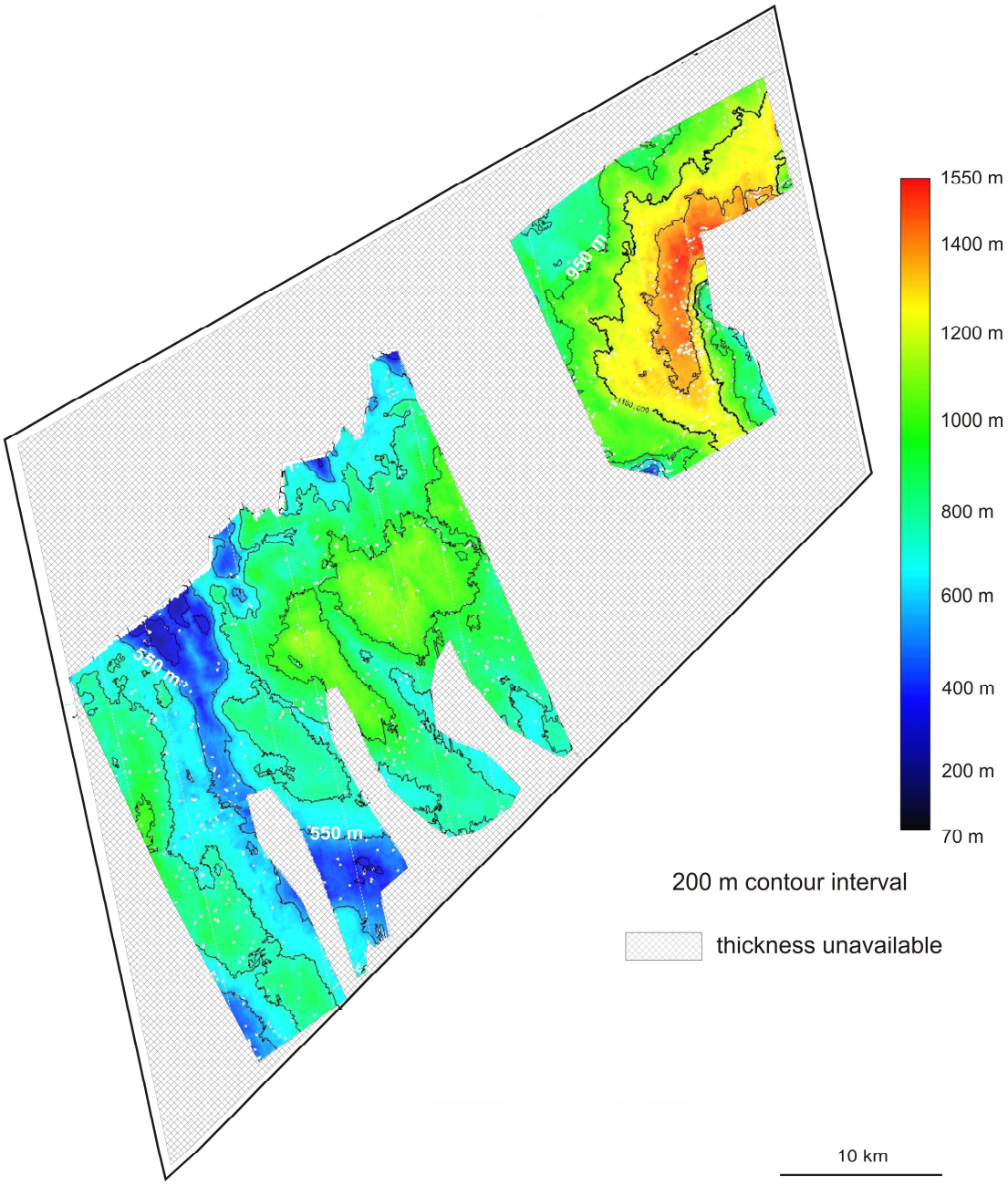

Figure 3.11: Thickness distribution of **Unit II** (interval between reflections C100 and E10). Thickness ranges from 66 to 1550 m, with greatest accumulation in the eastern portion of the dataset. Unit thickness is unavailable where the unit has been removed by subsequent erosion or autocorrelation was unreliable. Edge geometries are therefore not a function of depositional architecture.

Unit IIb is a low to moderate amplitude weakly continuous seismic unit bounded by reflection E7 at the base where the E7 horizon incises into Unit II and O5 at the top. The unit is located in the upper and mid regions of the dataset defining the canyon fill between two phases of incision. Unit IIb is limited in extent due to the re-incision yet has a maximum thickness of 250 m in the upslope region of the datset.

Unit III lies between reflection horizons E10 and O5. It is highly variable in amplitude, continuity and thickness ranging from 76 to 602 m (Fig. 3.12). It is absent in the northwest corner giving the unit an overall wedge shaped geometry. Moving seaward to the mid slope region, the chaotic nature of the unit is intermittently interrupted by stacked cuspate reflector geometry, or channel forms, that extend distally for 15 to 20 km into the deep-water section of the dataset where the unit thins to nearly absent.

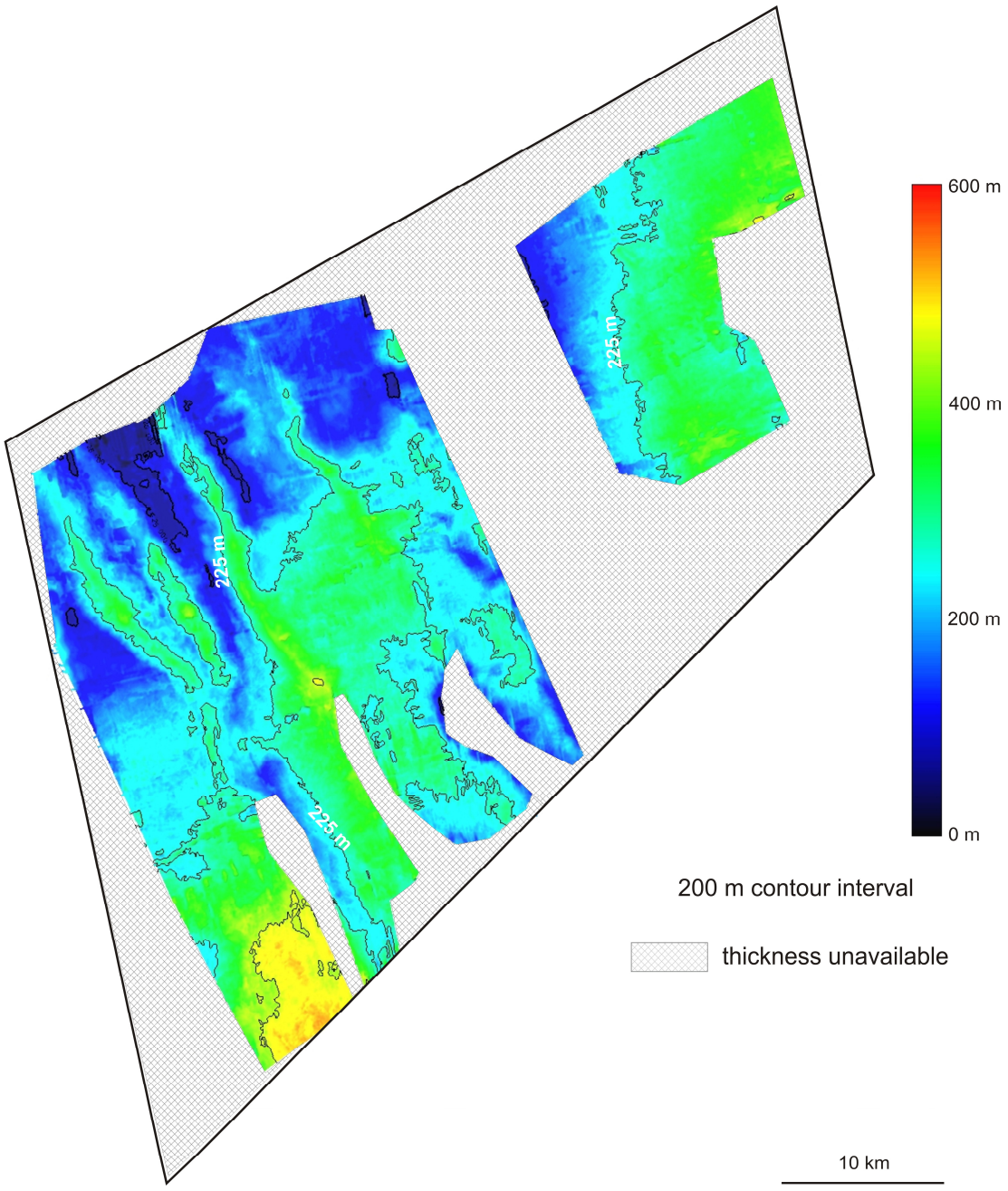

Figure 3.12: Thickness distribution of **Unit III** (interval between reflections E10 and O5). Thickness of the unit ranges from 76 to 602 m. Unit thickness is unavailable where the unit has been removed by subsequent erosion or autocorrelation was unreliable. Edge geometries are therefore not a function of depositional architecture.

Unit IV is present throughout the entire dataset, representing the interval between O5 and M4. Thickness of the unit is as much as 900 m with the thinnest areas located along the northwest side of the dataset (Fig. 3.13). Unit IV consists of low amplitude continuous reflections that infill underlying morphology. At the base of the unit, reflections locally onlap Unit III, thinning toward the west section of the dataset. Upward in the unit, reflections eventually become widespread as the morphology is smoothed. Little change in reflection character is noted throughout the dataset, yet occasionally, a low amplitude reflection will become high amplitude over a lateral distance of 200 to 800 m within the thickest sections, normally where the reflector is offset by fault motion.

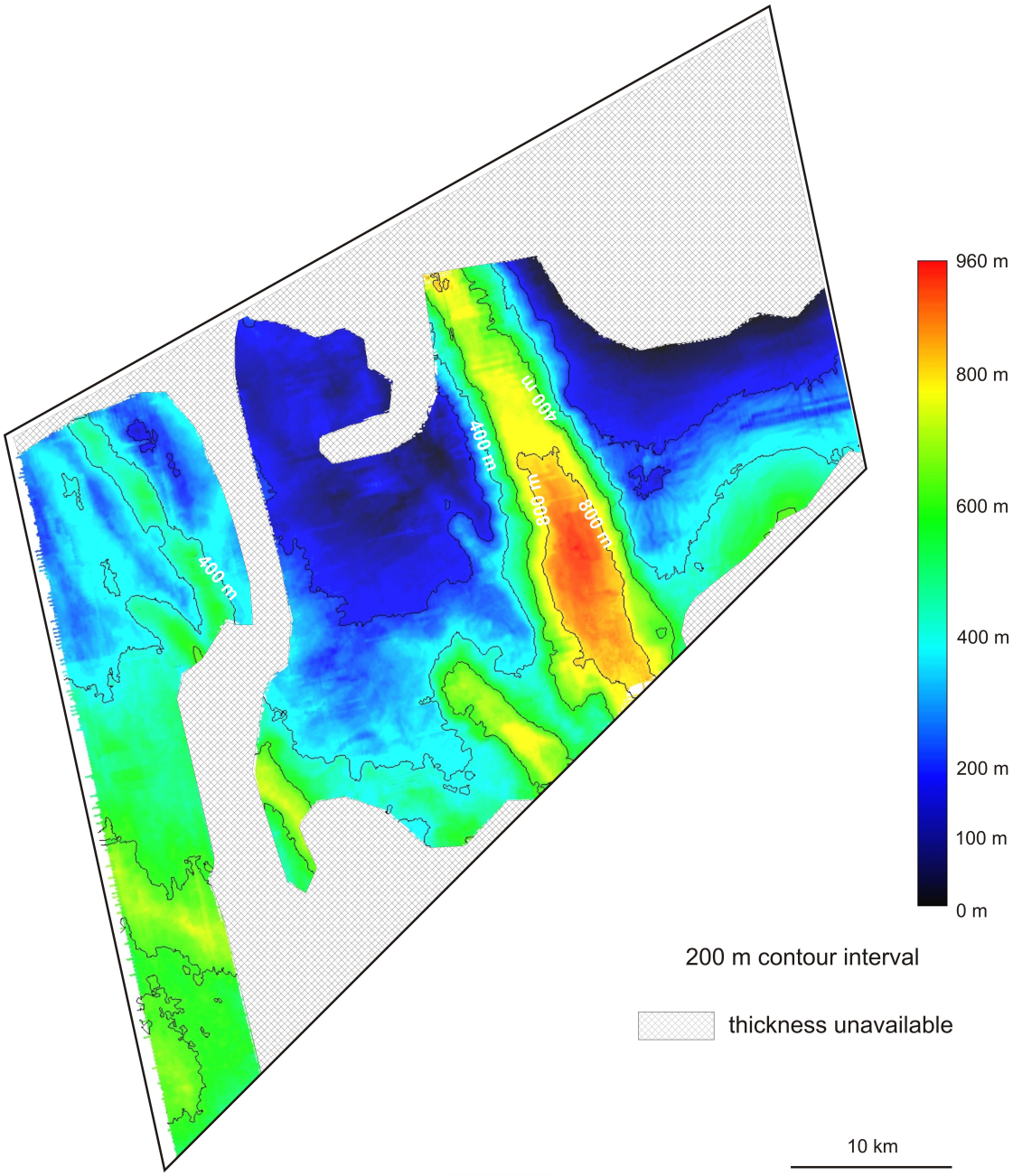

Figure 3.13: Thickness distribution of **Unit IV** (interval between reflections O5 and M4). The unit is up to 900 m thick in the central region of the dataset. Unit thickness is unavailable where the unit has been removed by subsequent erosion or autocorrelation was unreliable. Edge geometries are therefore not a function of depositional architecture.

Unit V consists of moderate to high amplitude semi-continuous reflections. Given that the top of the unit is the modern seafloor, which contains an extensive canyon network, the thickness distribution of the unit is extremely variable ranging from 0 to 1337 m (Fig.3.14), controlled principally by canyon erosion at the seafloor. Diagnostic features of Unit V includes stacked U-shaped reflections, minor offset and disruption of strata.

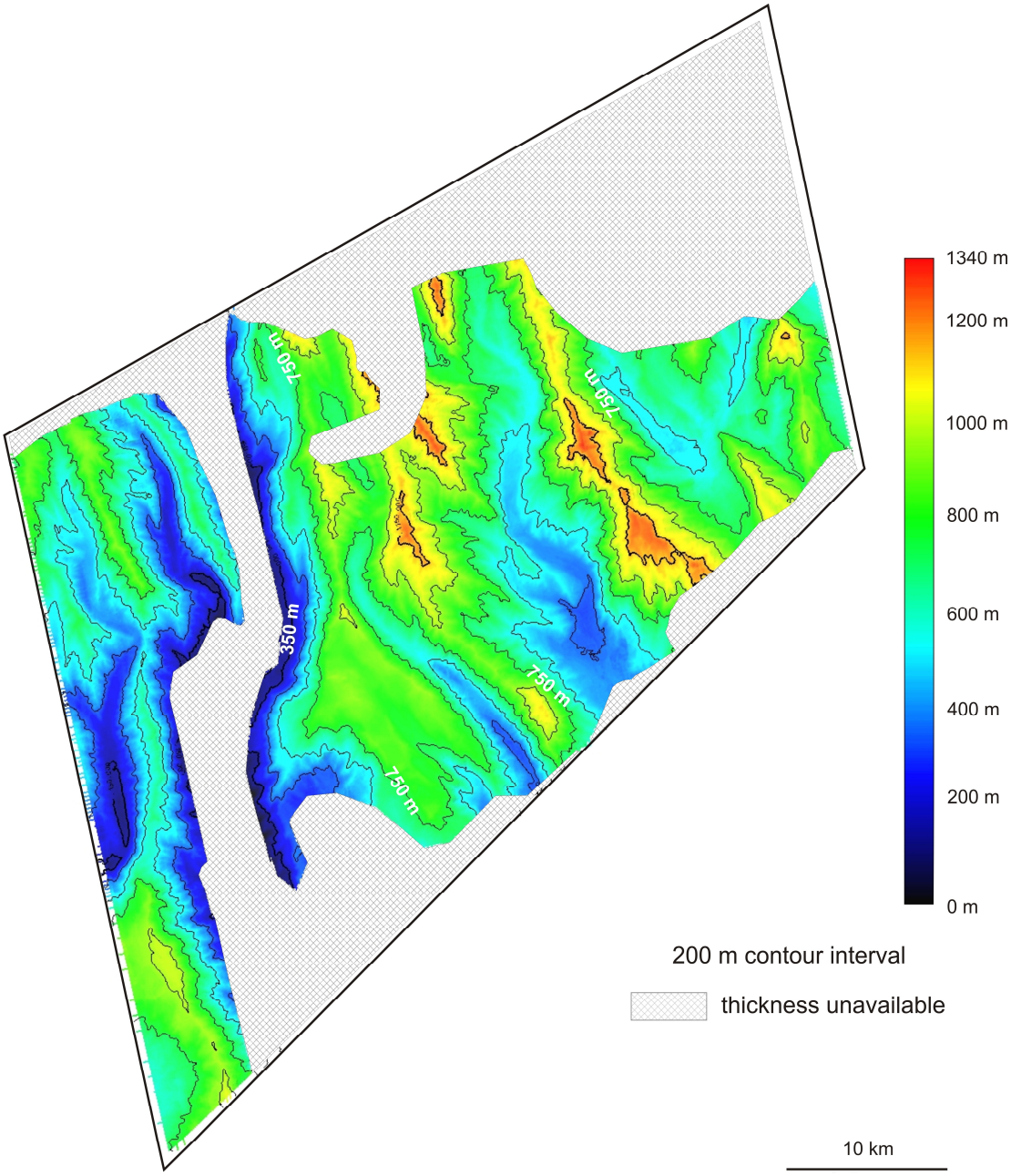

Figure 3.14: Thickness distribution of **Unit V** (interval between reflections M4 and Q1). Thickness distribution is variable, ranging from 0 to 1337 m. Unit thickness is unavailable where the unit has been removed by subsequent erosion or autocorrelation was unreliable. Edge geometries are therefore not a function of depositional architecture.

3.3 Age determination

Well data, including available age control, are correlated to seismic profiles with synthetic seismograms (Fig.3.15). Modeling allows extension of well data to a regional scale with seismic profiles. Well to seismic correlations are extended to the Stonehouse dataset by regional 2D seismic reflection profiles of the TGS-NOPEC and Parex datasets.

Correlating reflections from the continental shelf through to the slope is difficult because of multiple interference and complex geology at the shelf to slope transition zone. Along-strike correlations are typically more reliable, although episodic channel and canyon incision interrupt regional surfaces.

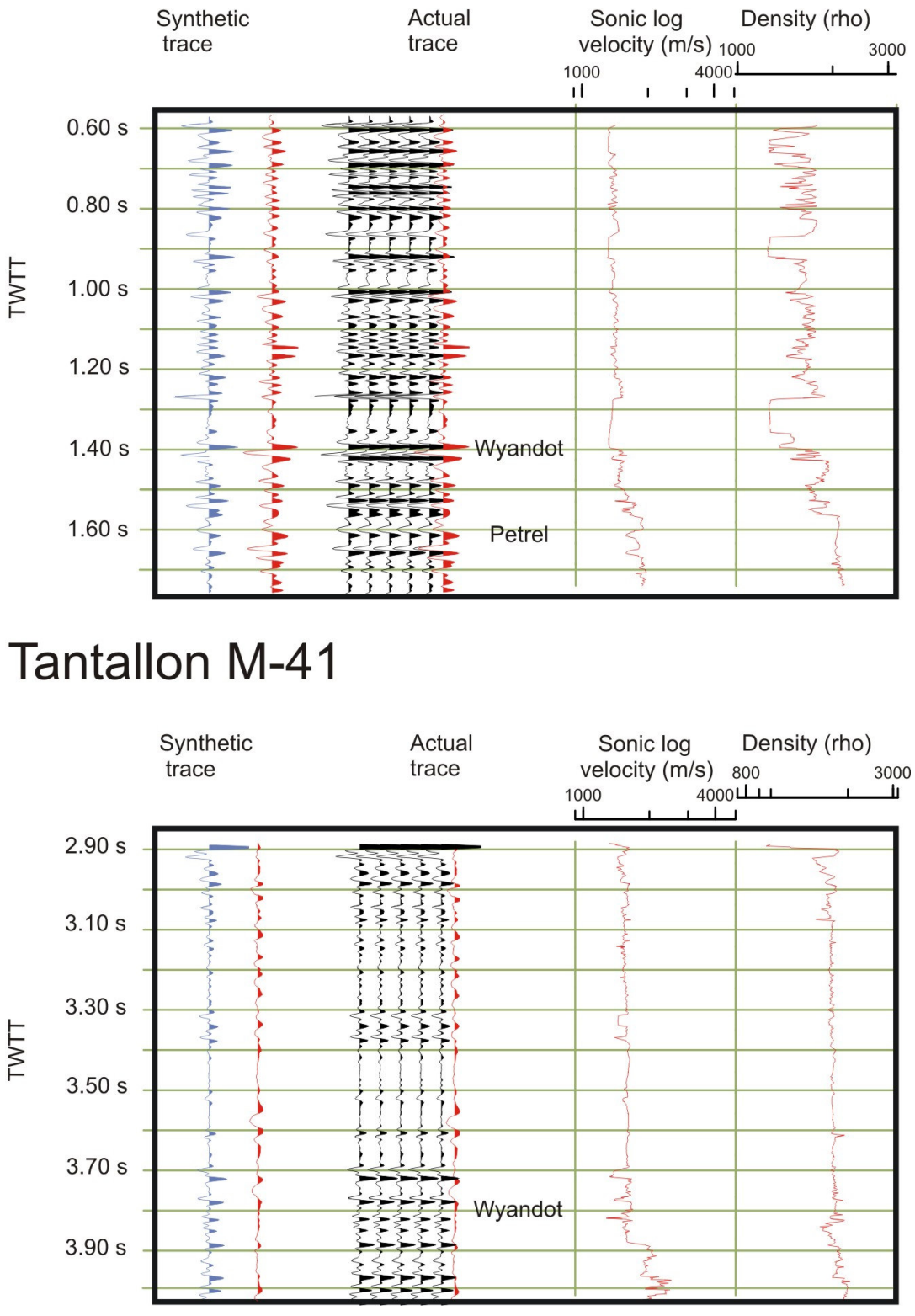

Figure 3.15: Synthetic seismograms for the Sachem D-76 and Tantallon M-41 wells calculated from Sonic and density logs. The red trace shows the actual seismic response at the well while the blue trace shows the resultant synthetic trace.

3.3.1 Sachem D-76

The Sachem well is located ~30 km shoreward of the Stonehouse volume and was correlated to the study using a composite shelf to slope seismic profile.

Biostratigraphic age control provided by micropaleontology studies provided age constraints from the Upper Jurassic through to Holocene (Fig. 3.16) (Ascoli 2005; Mobil-Texaco 1976*) and palynology (Mobil-Texaco 1976^). According to the stratigraphic column generated from sample data at Sachem, the Oligocene strata were notably absent and represent an unconformity at ~919 m (measured depth below Kelly bench). The Paleocene interval ~919 to 1372 m (measured depth below Kelly bench) consisted of alternating mudstone, sandstone, and siltstone, while the mid Miocene interval, ~809 to 919 m (MD) was dominantly mudstone. The paleoecological environments interpreted for these units are an alternation of neritic and bathyal environments (Mobil-Texaco 1976).

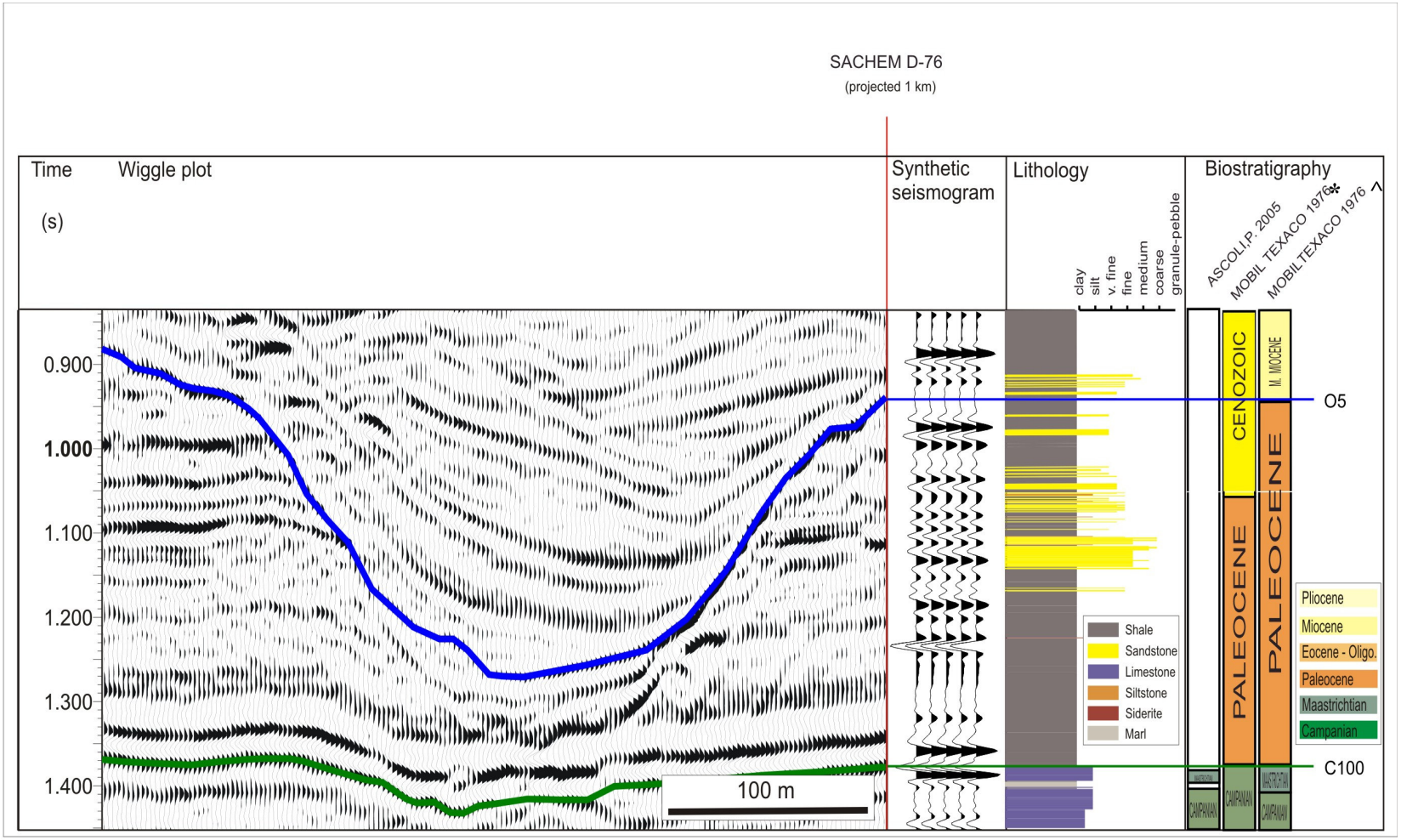

Figure 3.16: Age control diagram for the Sahem D-76 well. Seismic reflections are displayed as wiggle traces and compared to the synthetic seismogram, lithology and biostratigraphy to assign an age range to the reflections. The projected well location is represented as a vertical red line.

Two reflections identified within the Stonehouse study correlate with confidence through the shelf to slope transition zone to the Sachem well: reflections C100 and O5. The C100 reflection ranges in age from Campanian (Mobil-Texaco 1976*) to Maastrichtian (Ascoli 2005) and corresponds to the Wyandot; identified as the base of the Paleocene interval (MacLean and Wade 1993). The C100 reflection is therefore inferred to be Paleocene in age. Age constraints for the O5 marker place the reflection within the Cenozoic interval, between Middle Miocene and Paleocene (Mobil-Texaco 1976^) markers, and is tentatively given an Oligocene age. The O5 marker corresponds to the unconformity noted at ~919 m (MD) between Miocene and Paleocene strata; correlating to the margin of a southeast trending canyon.

3.3.2 Tantallon M-41

The Tantallon well is located ~50 km west of the Stonehouse volume on the eastern Scotian Slope. Data from the Tantallon well were correlated to the study through the use of along-strike seismic reflection profiles located on the slope.

Palynological (Williams 1992; Shell Canada Resources 1986) and micropaleontological (Thomas 1991; Ascoli 1989; Shell Canada Resources 1986) summaries for Tantallon M-41 provide age dates from the Lower Cretaceous through to Pliocene. Paleoecological interpretations for this interval indicate an outer neritic to bathyal environment (Shell Canada Resources 1986). Lithology of the Cenozoic section is interpreted as alternating siltstone and mudstone with glauconitic sandstone intervals within the Late Miocene and Oligocene periods (Shell Canada Resources 1986). Seismic correlation between the Tantallon well, located ~50 southwest of the Stonehouse volume, provided age constraints for the Paleocene, Eocene, Oligocene, Miocene and Pliocene markers (Fig. 3.17).

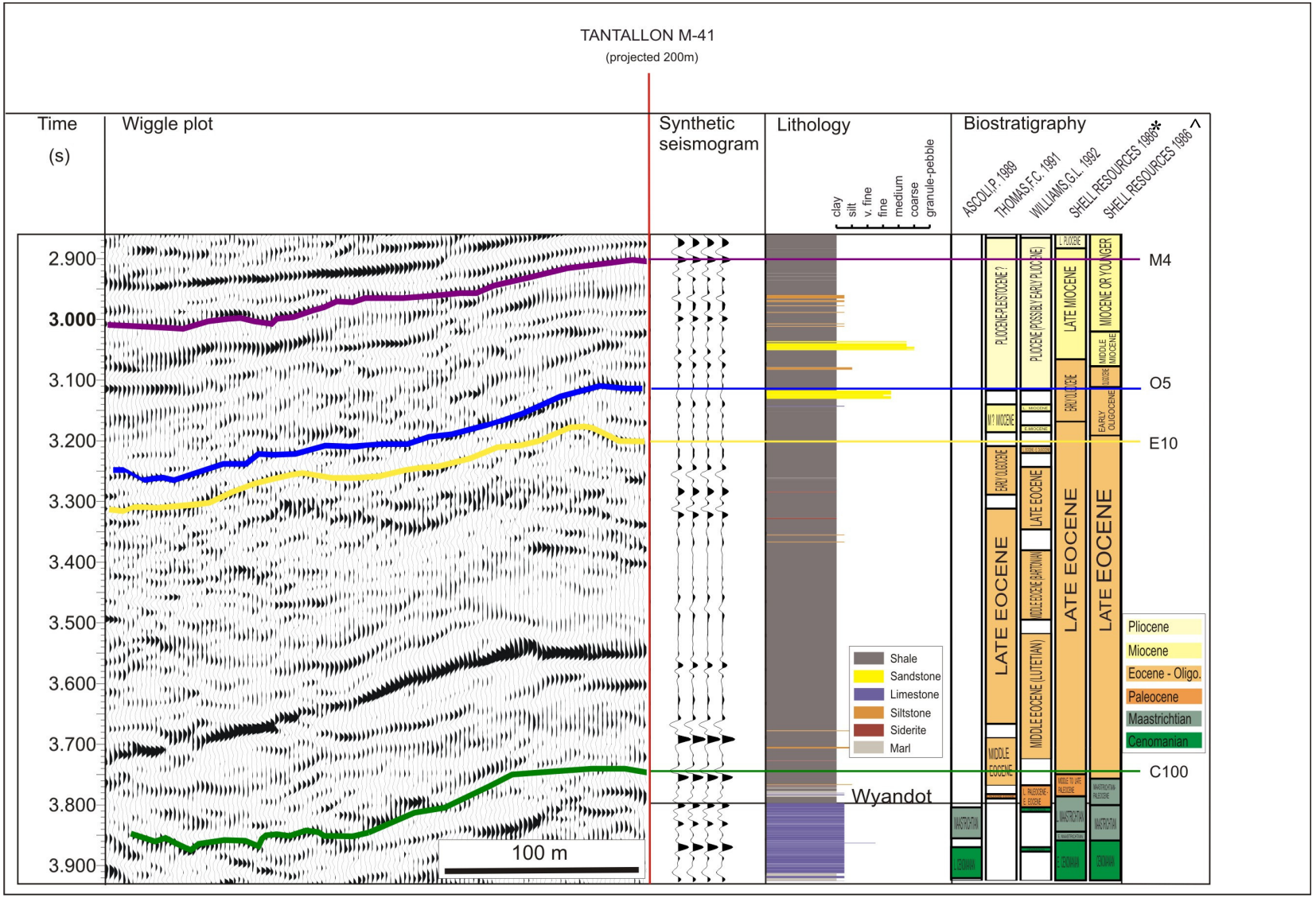

Figure 3.17: Age control diagram for Tantallon M-41 well. Comparison of the wiggle plot, synthetic seismogram, lithology and available biostratigraphy determine age ranges of reflections. The projected well location is represented as a vertical red line.

Several key reflections identified within the Cenozoic section of the Stonehouse dataset are correlated along strike to the Tantallon well, including reflections C100, E10, O5, and M4. The Tantallon well was dated by several studies with differing results. A range of ages is therefore provided for each reflection horizon.

Age constraints for the C100 reflection range from Middle to Late Paleocene (Shell Canada Resources 1986*) through to Middle Eocene (Ascoli 1989). The most recent study places the C100 reflection as a hiatus between Late Paleocene-Early Eocene (Williams 1992). The reflection is therefore inferred to be of Late Paleocene age based on the most recent age date and the C100 correlation at the Sachem well.

The E10 reflection is dated as Late Eocene (Shell Canada Resources1986^) and also represents a hiatus between Late Eocene-Early Oligocene and Early Miocene (Williams 1992). Reflection E10 is tentatively referred to as Late Eocene- Early Oligocene in age.

The age of reflection O5 ranges from Early Oligocene (Shell Canada Resources 1986*^) and also represents a hiatus between Late Miocene to Pliocene (Williams 1992). Given the large distribution of age dates, and the confidence in the correlation to the Sachem well, the O5 reflection is referred to as Middle Oligocene in age.

Age constraints for reflection M4 range from Late Miocene (Shell Canada Resources 1986*) through to probable Pliocene-Pleistocene (?) (Ascoli 1989, Thomas 1991). The M4 reflection is therefore refered to as Late Miocene to Pliocene in age.

Chapter 4. O5 Canyons

As indicated at the outset, it is the intent of this thesis to understand shelf to slope sedimentation processes as influenced by canyon development, particularly with respect to an Oligocene canyon system on the eastern Scotian Slope. The O5 surface shows a single large canyon that erodes underlying stratigraphy and extends downdip across the Stonehouse 3D volume. It is in excess of 30 km long, 9 km across and 800 m deep and appears to be the major sediment pathway in this region during the Oligocene period. This canyon system and its infill will be described in detail from the 3D volume, but to understand the regional context, it is necessary to study regional 2D seismic reflection profiles to trace its lateral extent and morphology.

4.1 Mapping of the O5 canyon system beyond 3D seismic limits

Interpretations from the Stonehouse volume were extended toward the eastern Scotian Slope and seaward using a network of 2D seismic reflection data from TGS-NOPEC and the Parex Group in order to map the extent of the E7 to O5 canyon. The canyon system measures >150 km in length, 6 to15 km in width and incises to a depth of 1 km. Overall very little change in canyon orientation is observed with the exception of a slight deflection to the west approximately 7 km downslope of the 3D data volume (Fig. 4.1). The cause of canyon deflection is not directly observed, yet the canyon continues along a relatively linear trend even after the offset.

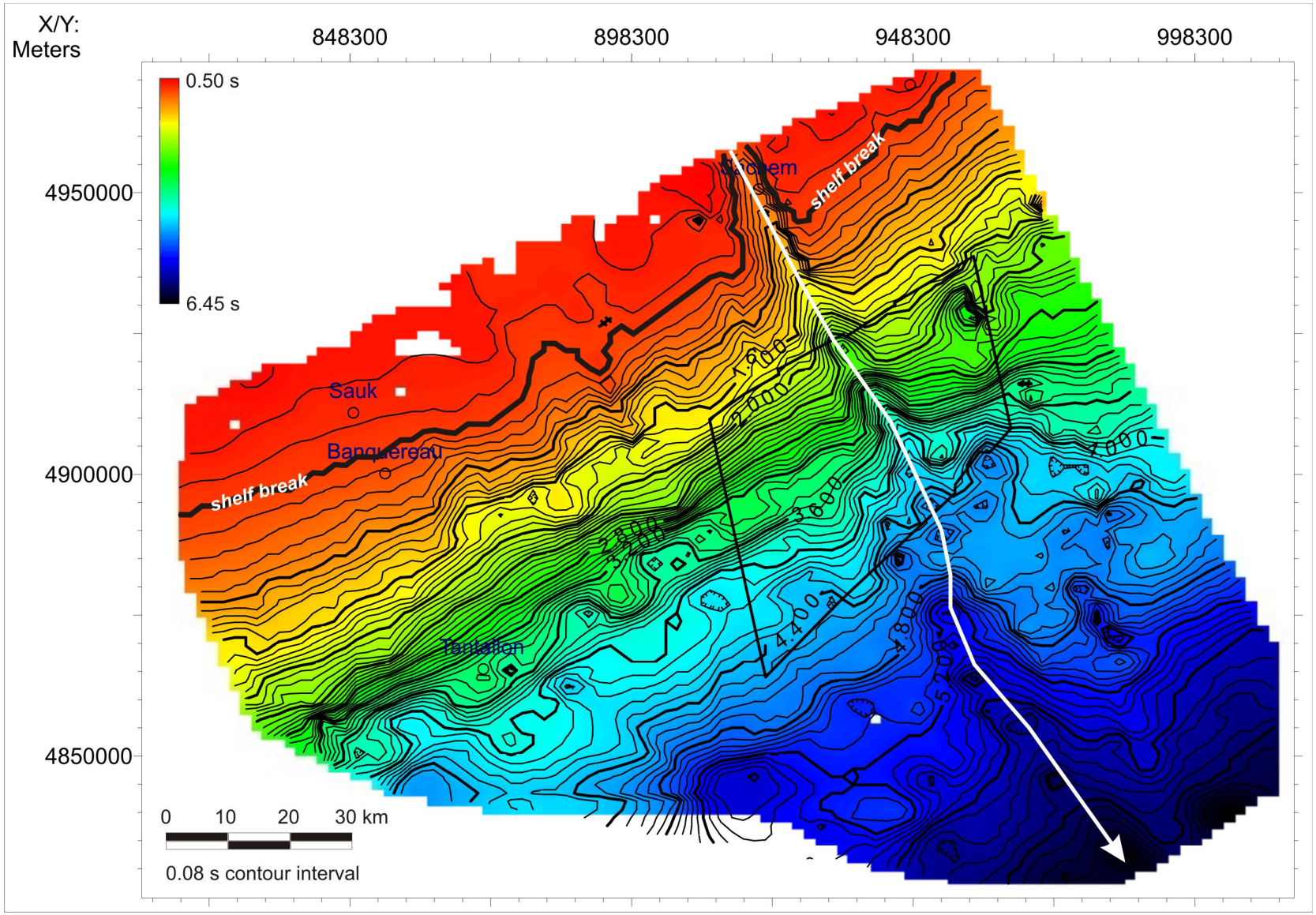

Figure 4.1: Regional correlation of the O5 canyon surface in two-way travel time (TWTT) below the modern seasurface displaying a slight deflection in canyon orientation on the slope. The Oligocene shelf break is interpreted at 0.08 s (TWTT). The boxed area indicates the location of the Stonehouse 3D seismic volume.

4.2 Major phases of canyon erosion

Investigation of the Cenozoic stratigraphy of the eastern Scotian Shelf and Slope has led to the identification of three regional unconformities that incise the stratigraphy of the Cenozoic section: C90, E7 and O5. Shelf parallel trending seismic lines provide an image of cross-sectional geometries of the E7-O5 canyon system (Fig. 4.2).

The oldest and first of the Cenozoic unconformities (1), C90, is best observed in the most upslope region of the dataset where the unconformity incises Units I and II, cutting through the C100 reflection. Morphology of the surface is irregular with variable amounts of erosion.

The second of the regional unconformities (2), E7, represents a localized sub-regional unconformity and marks the oldest of the stacked canyon thalwegs, thereby approximating the onset of canyon incision. The E7 unconformity denotes a major phase of canyon erosion that incises Units I and II, cutting reflections E55 and E10. The V-shaped incision appears to have eroded as much as 1.2 km of section, cutting through the C90 unconformity in the upslope region. Depth of incision varies from the shelfward extent of the dataset through to the base of slope where evidence of incision is removed due to subsequent re-incision.

Unconformity 3, represented as reflection O5, is the youngest and final phase of re-incision prior to the complete infill of the canyon system. The O5 reflection denotes a widespread regional surface with a broad U-shaped incision, wider than the initial E7

incision. The O5 unconformity incised the high amplitude chaotic fill above reflection E7 (Unit IIb) and cuts through Unit III. The unconformity locally merges with the E7 surface representing a correlative conformity on the flanks of the canyon.

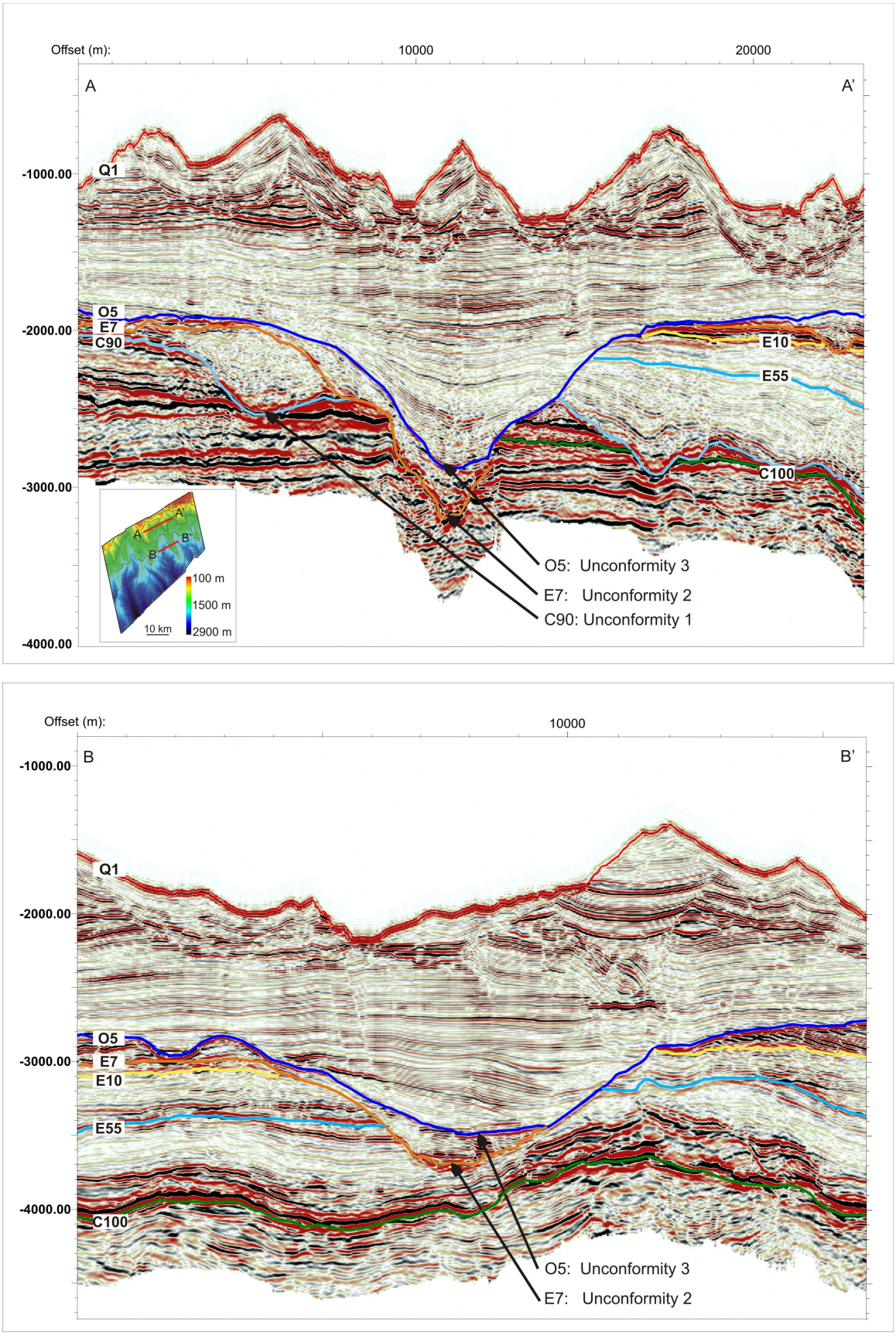

Figure 4.2: Episodes of canyon incision within the Stonehouse dataset. The upper profile 'A' displays the incision of the canyon through the base of the Cenozoic interval, which occurs only in the updip area of the Stonehouse dataset. The lower profile 'B' is typical of the canyon system, displaying the E7 and O5 incision above the base Cenozoic interval.

The E7 unconformity is mapped throughout the 3D dataset for a down-slope distance of ~20 km. In plan view, the surface displays a variety of amplitudes giving it a braided appearance with a series of meander loops that are high in amplitude (Fig. 4.3).

Similar to incision E7, the surface morphology of the O5 canyon incision is relatively flat with a slightly sinuous pattern (Fig. 4.4). The east canyon wall appears steeper and stepped compared to the western wall. The O5 thalweg has high amplitude lineaments similar to the high amplitude loops of E7, oriented parallel to the canyon axis.

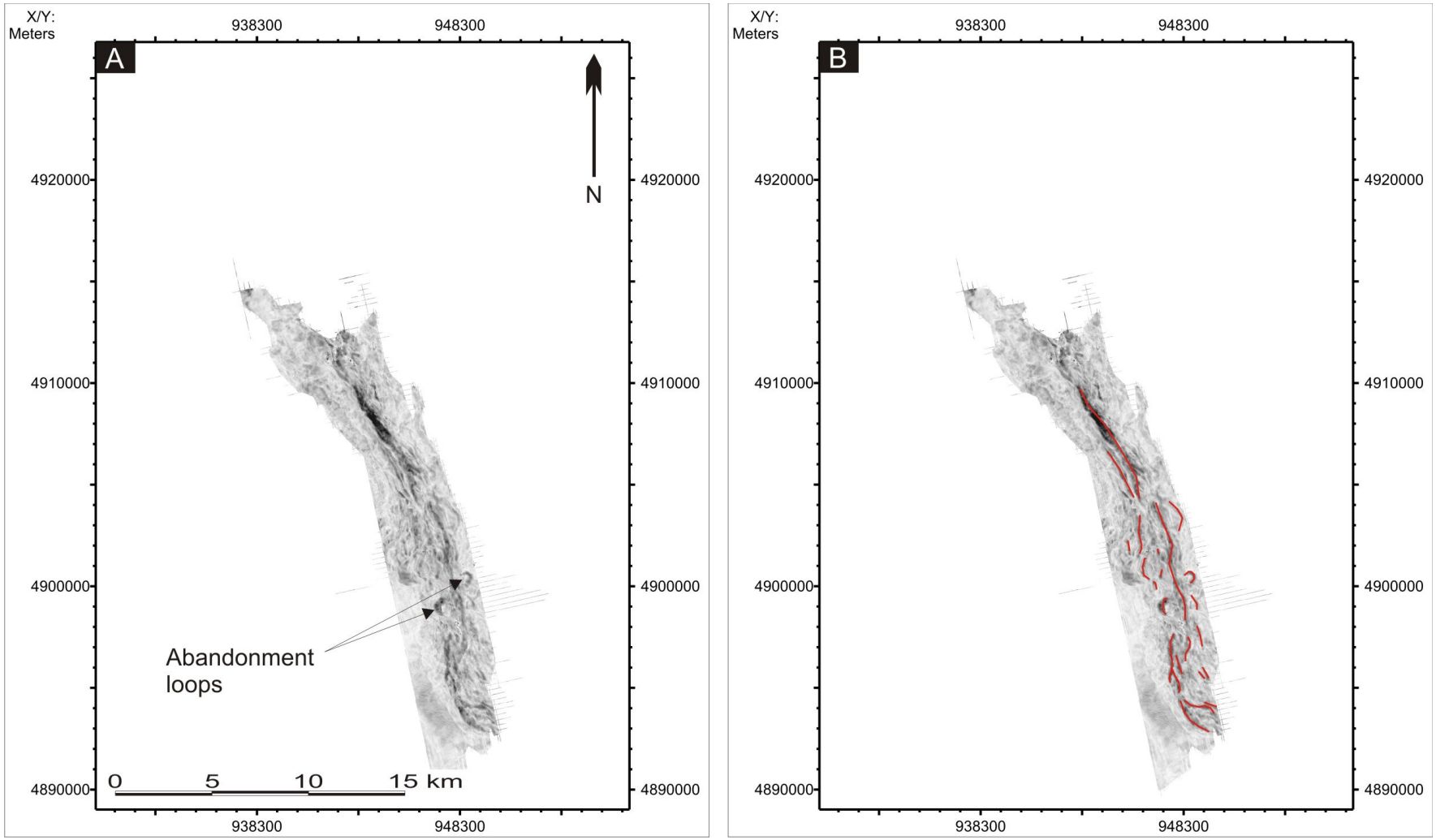

Figure 4.3: Amplitude extraction of the deepest canyon incision E7. A) Uninterpreted E7 surface displaying a braided, or cross-cutting channel morphology with high amplitude meander loops. B) Interpreted E7 surface with meander loops highlighted in red.

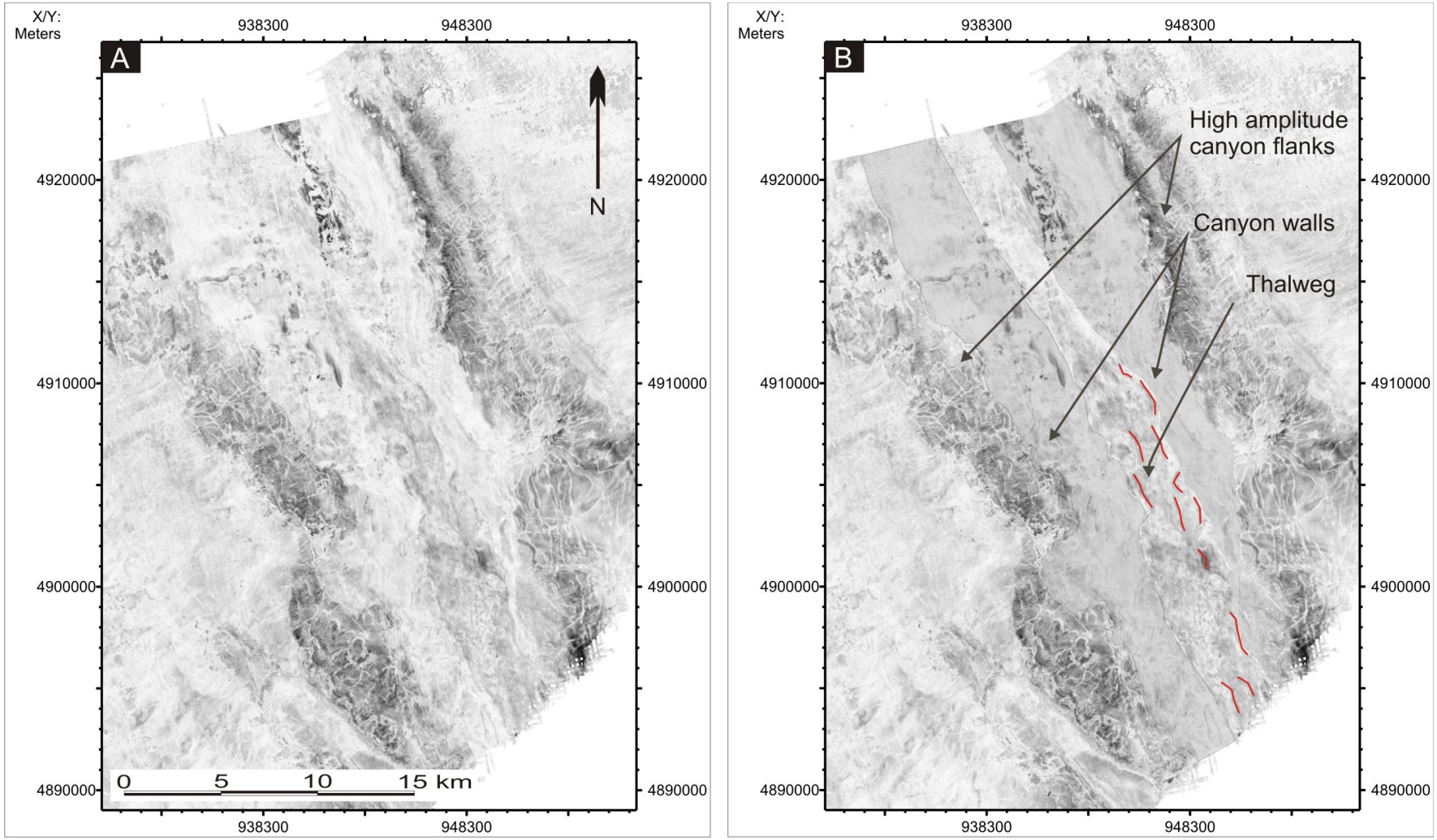

Figure 4.4: Amplitude extraction of O5 surface. A) Uninterpreted O5 canyon surface displaying a range of amplitudes; the highest of which are noted along the flanks of the canyon. B) Interpreted O5 canyon image denoting the high amplitude flanks, low amplitude canyon walls and moderate amplitude thalweg with minor braiding.

Close inspection of seismic profiles down-axes of the O5 and E7 thalwegs indicate the two phases of incision are located in approximately the same position with a southeast trending orientation despite their differences in morphology and fill patterns (Fig.4.5).

Seismic reflection profiles down the axis of the E7 thalweg indicate incision of a low amplitude facies consisting of semi-continuous sub-parallel to parallel reflections. In comparison, the facies located directly above the E7 horizon consists of low to high amplitude reflections with moderate continuity. This upper facies represents the fill that occurs between the O5 and E7 incisions.

The seismic reflection profile down-axes of the O5 thalweg indicates that the O5 canyon incised the low to high amplitude facies with moderate continuity, representing an erosional remnant of early fill. Seismic facies located directly above the O5 horizon consist of low amplitude continuous parallel reflections that onlap the O5 surface.

Minor, small-scale erosive surfaces are identified between reflections within the canyon fill yet the overall sequence is void of other large-scale phases of incision until the modern network of seafloor canyons; thereby making the O5 surface the final phase of canyon incision prior to complete infill of the canyon.

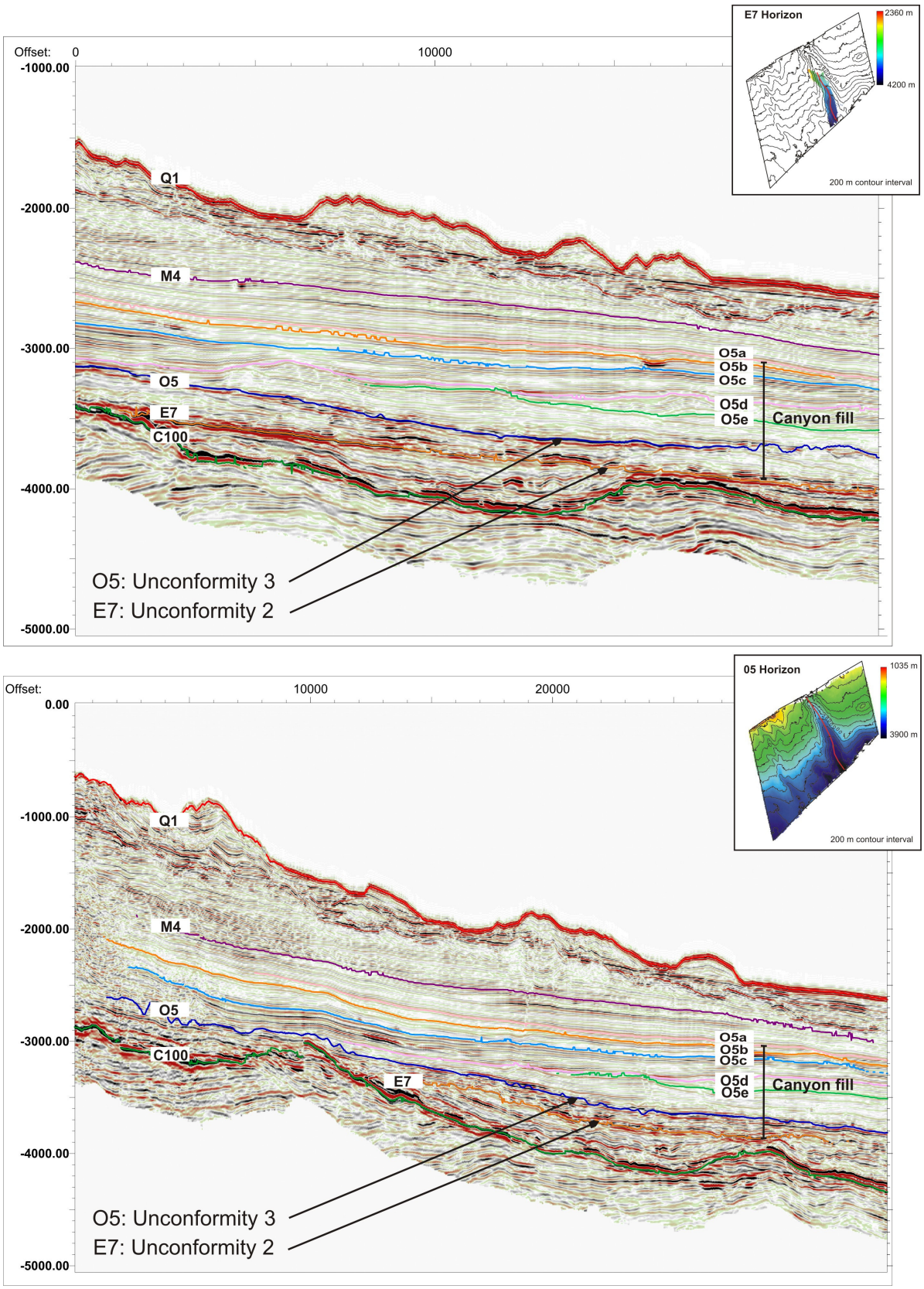

Figure 4.5: Dip profiles down the axes of the E7 and O5 incisions. The E7 incision (upper image) is limited in its extent while the O5 incision (lower image) is present across the entire dataset.

4.3 Major period of canyon fill

The E7 to O5 canyon system filled through a series of depositional sequences post O5 incision. The fill sequences are located within Unit IV between the O5 and M4 surfaces, preferentially accumulating at least initially in the deeper section and on the western wall of the canyon (Fig. 4.6).

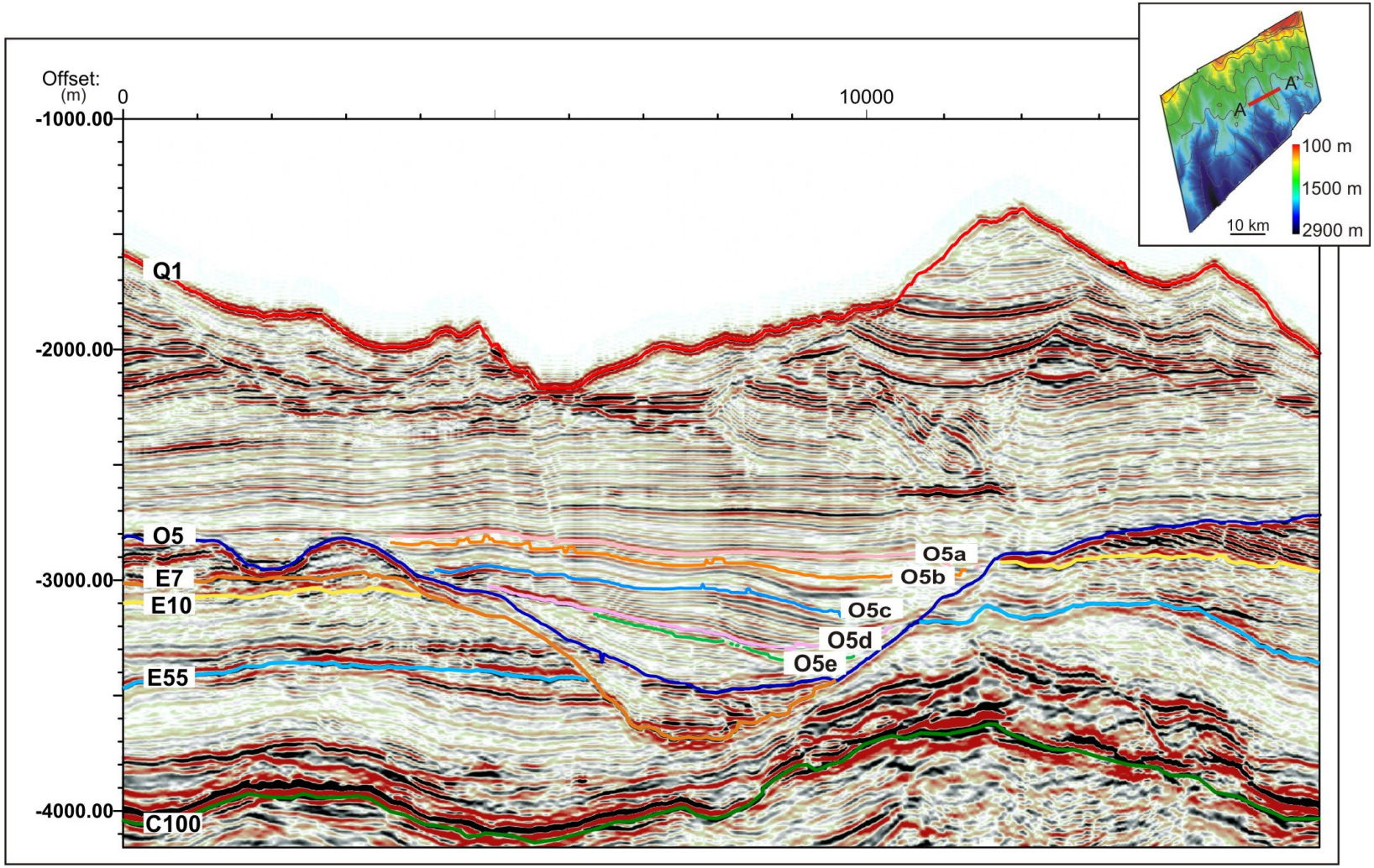

Figure 4.6: Reflections O5e to O5a separate fill sequences within the canyon system after the final phase of canyon incision.

Reflections separating fill sequences are described from oldest (deepest) to youngest (shallowest): the deepest reflection, **O5e,** (low to moderate amplitude, continuous) is confined to the deep-water section of the dataset (Fig. 4.7). In plan view, the surface morphology indicates deposition central to the lowermost part of the canyon as well as deposition along the western canyon wall.

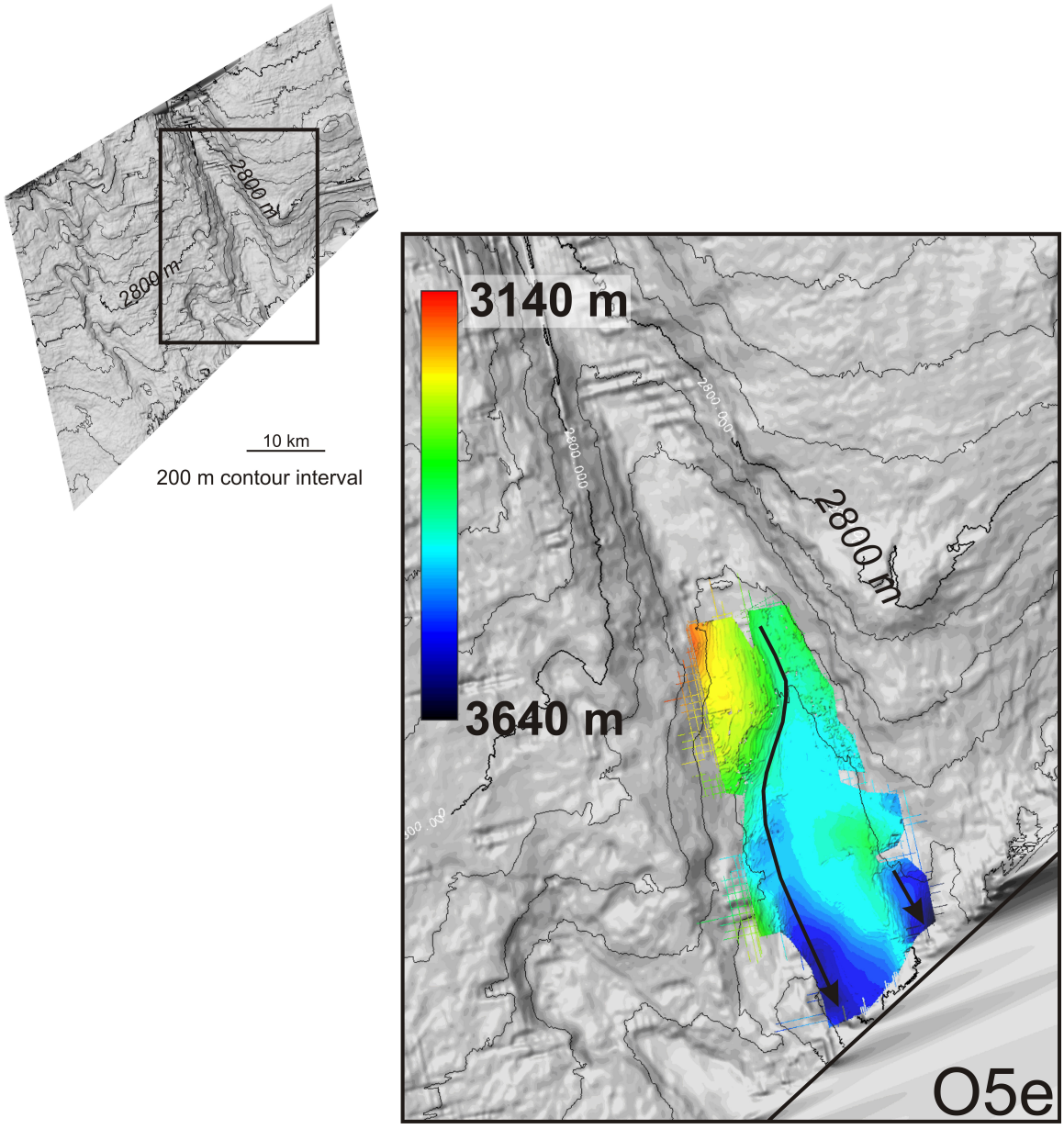

Figure 4.7: The lowest horizon of the final canyon fill package, O5e, indicates deposition in the lowermost part of the canyon system with a shift in canyon axes orientation. Color bar indicates metres below modern sealevel.

Thickness of the lowermost fill sequence ranges from 100 to 290 m. The greatest thickness occurs in the most seaward section and along the western canyon wall ranging from 220 to 290 m. Thickness of the remainder of the sequence is on the order of 100 to 220 m (Fig. 4.12A).

Reflection **O5d** (low amplitude, fairly continuous) is also confined to the deeper section and extends toward the canyon walls (more widespread than O5e) (Fig. 4.8). Similar to O5e, channels diverge around a mound located central to the lowermost part of the canyon.

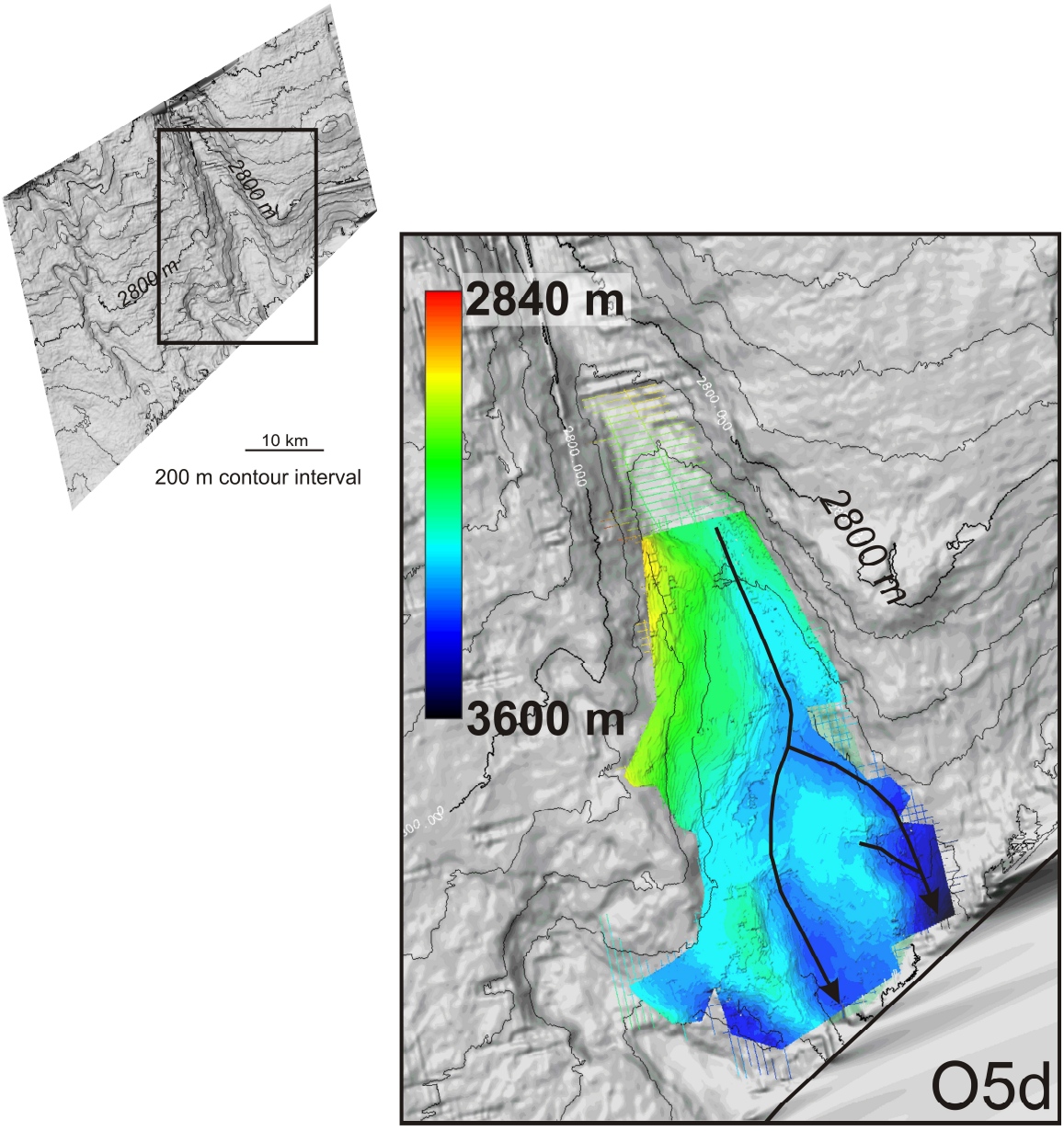

Figure 4.8: Horizon O5d is more widespread than the lower fill horizon with the development of a second branch as flow diverges around a centrally located mound. Color bar indicates metres below modern sealevel.

Distribution of fill between O5e and O5d horizons (Fig. 4.12B) indicate that the greatest thickness occurs in the most seaward section, ranging from 100 to 200 m thick. Distribution of the sequence thins landward to 8 m.

Reflection **O5c** (high to moderate amplitude, fairly continuous, subject to moderate faulting) onlaps the west canyon wall extending into the headless canyon located to the west (Fig 4.9). The main channel orientation is maintained with an additional channel occurring in the headless canyon region.

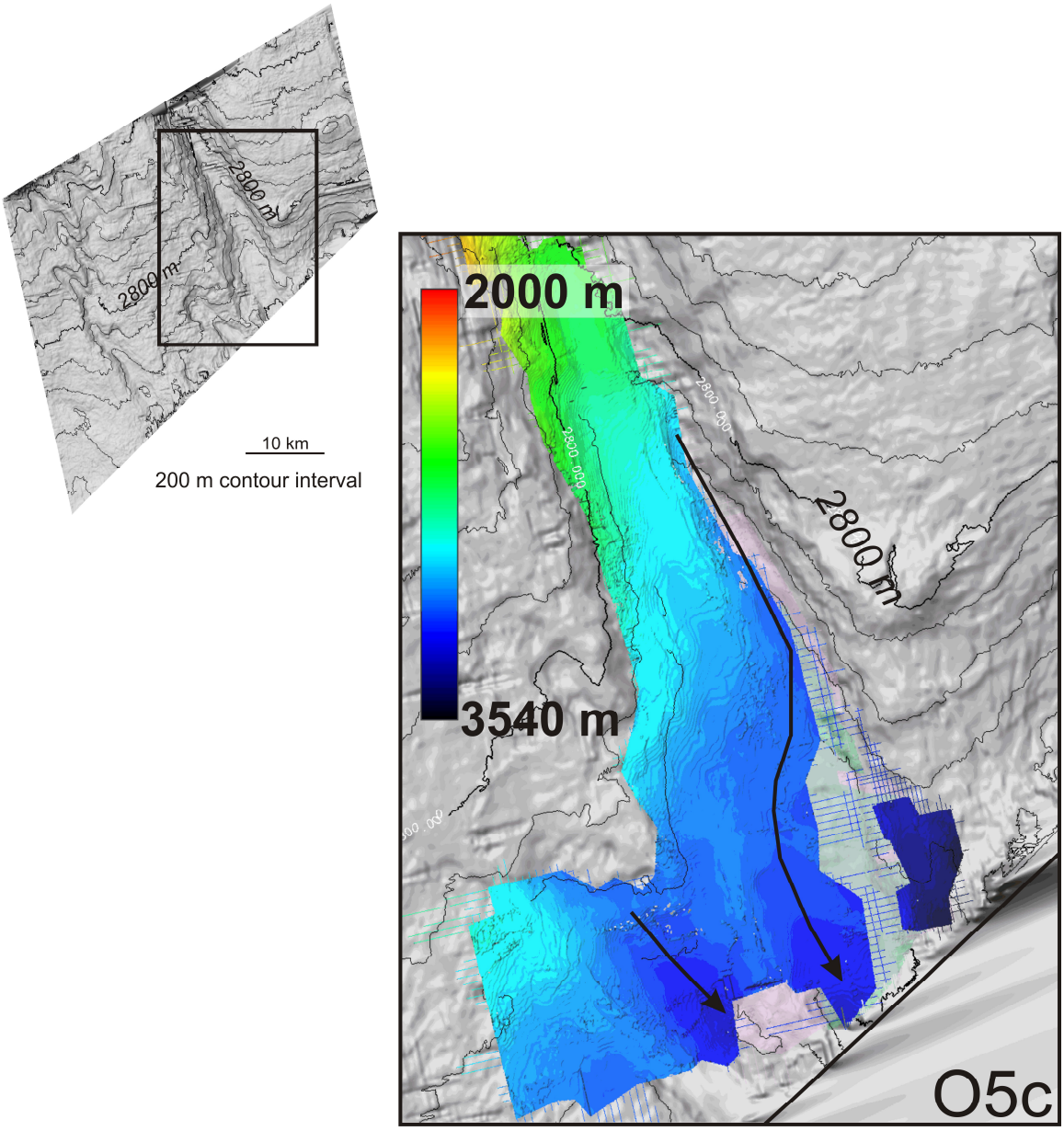

Figure 4.9: Horizon morphology of fill surface O5c indicates that fill was distributed in the main canyon axes as well as a nearby headward eroding canyon. Color bar indicates metres below modern sealevel.

Thickness of the O5d and O5c interval ranges from 80 to 260 m (Fig. 4.12C). The thickest interval occurs along the western flank of the canyon ranging from 170 to 260 m. Elsewhere the sequence ranges from 80 to 170 m thick.

Nearing the top of the fill sequence, the **O5b** reflection (moderate amplitude, continuous, some fault offsets) is widespread across the canyon (Fig. 4.10). Minor chaneling occurs along the top of the surface, yet overall evidence of the lower channel system is absent.

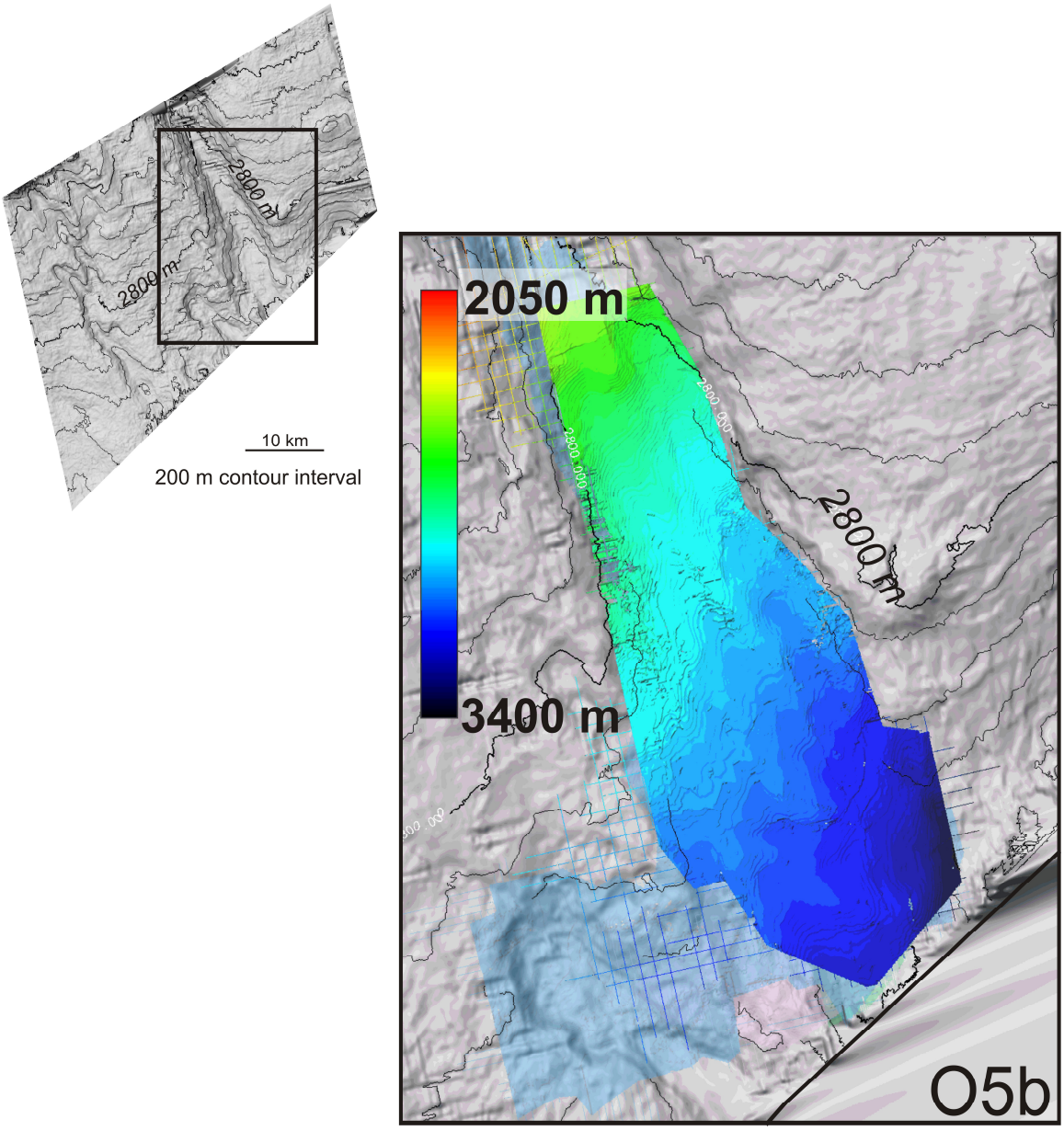

Figure 4.10: Fill horizon O5b is uniform and void of channelling lower in the sequence. The location of the lower fill is displayed as a semi-transparent solid color beneath the O5b horizon. Color bar indicates metres below modern sealevel.

The thickness of the interval between reflections O5c and O5b ranges from 40 to 230 m (Fig. 4.12D). The thickest part of the sequence is in the updip regions along the eastern flank of the canyon, ranging from 100 to 230 m. Accumulation between O5c and O5b in the most seaward section ranges from 40 to 100 m in thickness.

O5a (moderate amplitude, continuous, some fault influence) marks the top of the canyon fill sequence (Fig. 4.11). Overall the surface has a smooth morphology with minor channelling. Evidence of the earlier canyon and channel incision is not observed.

Thickness distribution of the O5a to O5b interval ranges from 20-170 m (Fig. 4.12E). The greatest thickness occurs along the eastern side of the canyon, thinning seaward, with nearly uniform thickness distribution in the remainder of the canyon. Along the eastern flank, thickness ranges from 75 to 170 m, whereas in the remainder of the canyon, thicknesses are 20 to 60m.

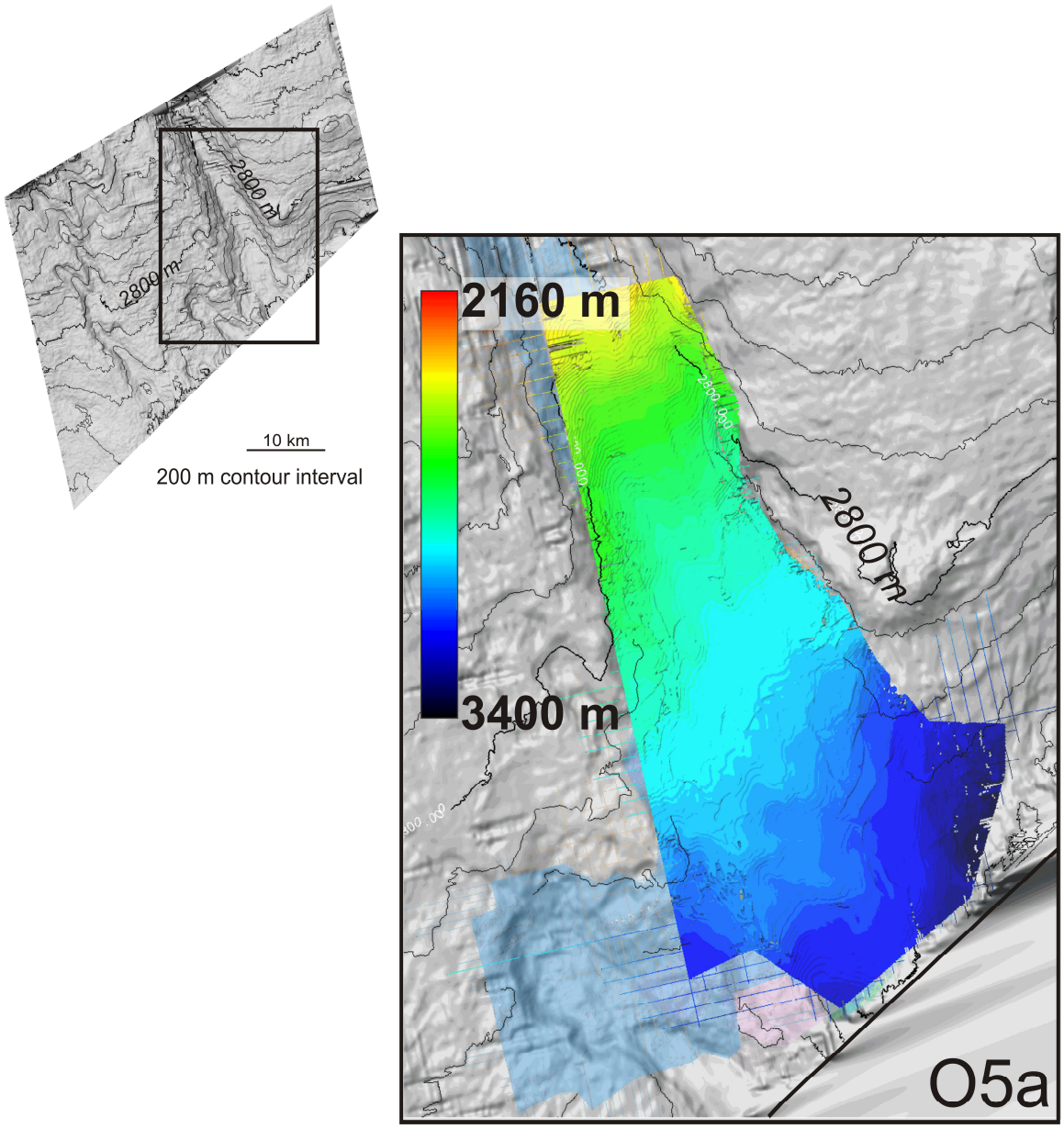

Figure 4.11: Distribution of fill horizon 05a demonstrates a uniform reflection distribution void of evidence for incision or impedance to flow. Color bar indicates metres below modern sealevel.

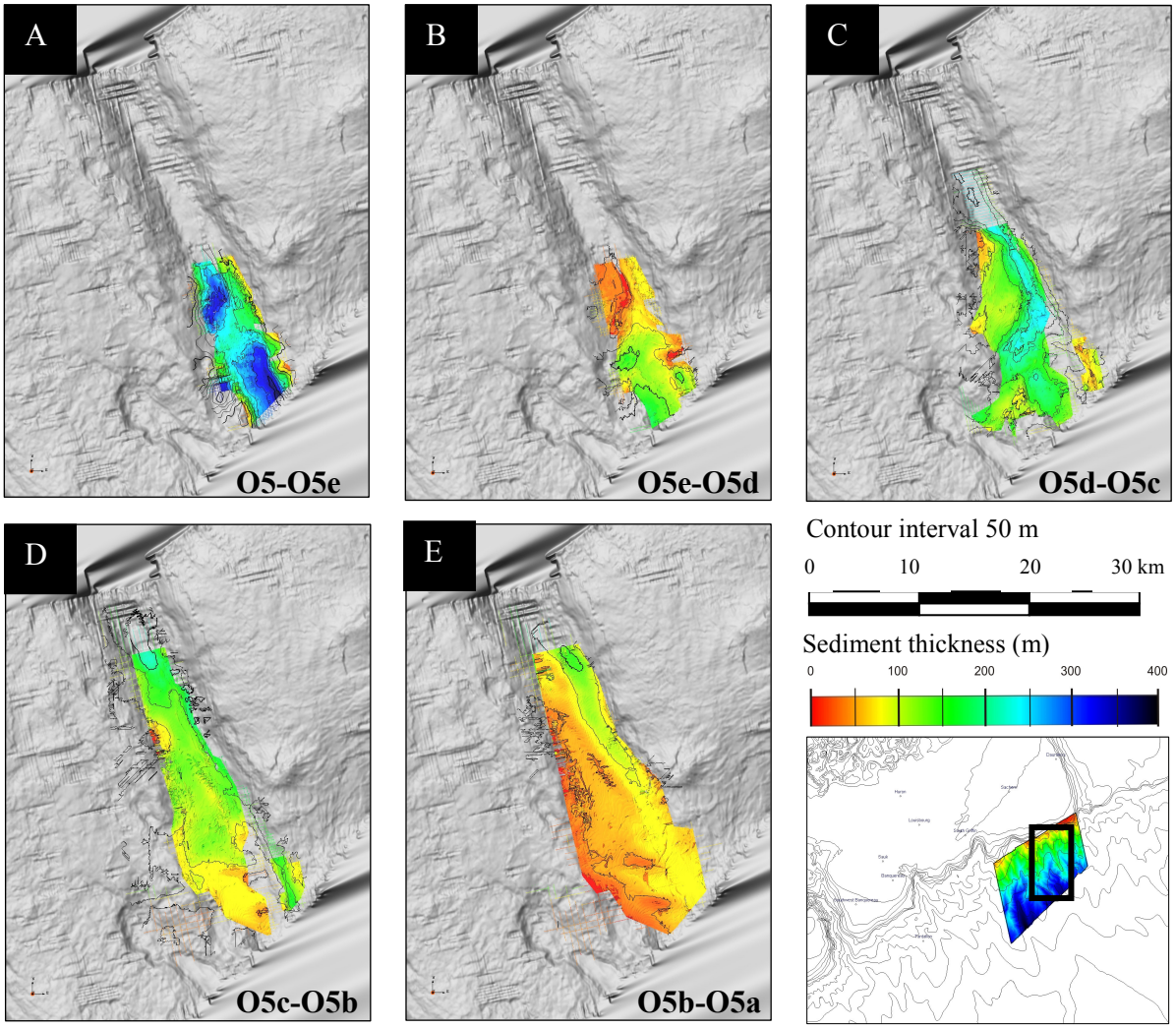

Figure 4.12: Thickness distribution maps of sediment infill sequences, as displayed over the O5 canyon surface. A) Thickness between surfaces **O5** and **O5e**, concentrated mainly in 2 adjacent deposits. B) Thickness between surfaces **O5e** and **O5d**, located mainly in the deeper section. C) Thickness between surfaces **O5d** and **O5c,** is concentrated mainly along the western canyon wall. D) Thickness between surfaces **O5c** and **O5b**, concentrated in the upslope area. E) Thickness between surfaces **O5b** and **O5a** is mainly located along the eastern canyon flank.

In order to study the down-slope evolution of the E7-O7 canyon system, a series of shelf to basin cross sections of the canyon system are described. The first set of canyon cross-sections are profiles A through C (Fig. 4.13), located nearest the shelf. Profile A on Figure 4.13 marks the most headward evidence of canyon incision based on evidence from the 2D seismic lines. The canyon cut is symmetrical, displaying a V-shaped morphology and denoting multiple phases of incision with asymmetric infill sequences. Seaward of profile A, profile B reflects a widening of the now U-shaped symmetric canyon with symmetric fill. Profile C is located within the limits of the Stonehouse dataset, yet is interpreted from a 2D seismic line for consistency. The U-shaped canyon is symmetric and has increased in depth with little change in width.

Canyon profiles D through E (Fig. 4.14), located seaward of the Stonehouse study area, vary greatly from profiles A through C. Profile D displays the presence of the U-shaped canyon yet also displays levee geometries. Profile E, like profile D, displays levee deposits, yet deposits on profile E are more symmetric and smaller than the previous. The most seaward profile, profile F, displays only minor effects of canyon incision, reflected in the presence of a single symmetric channel.

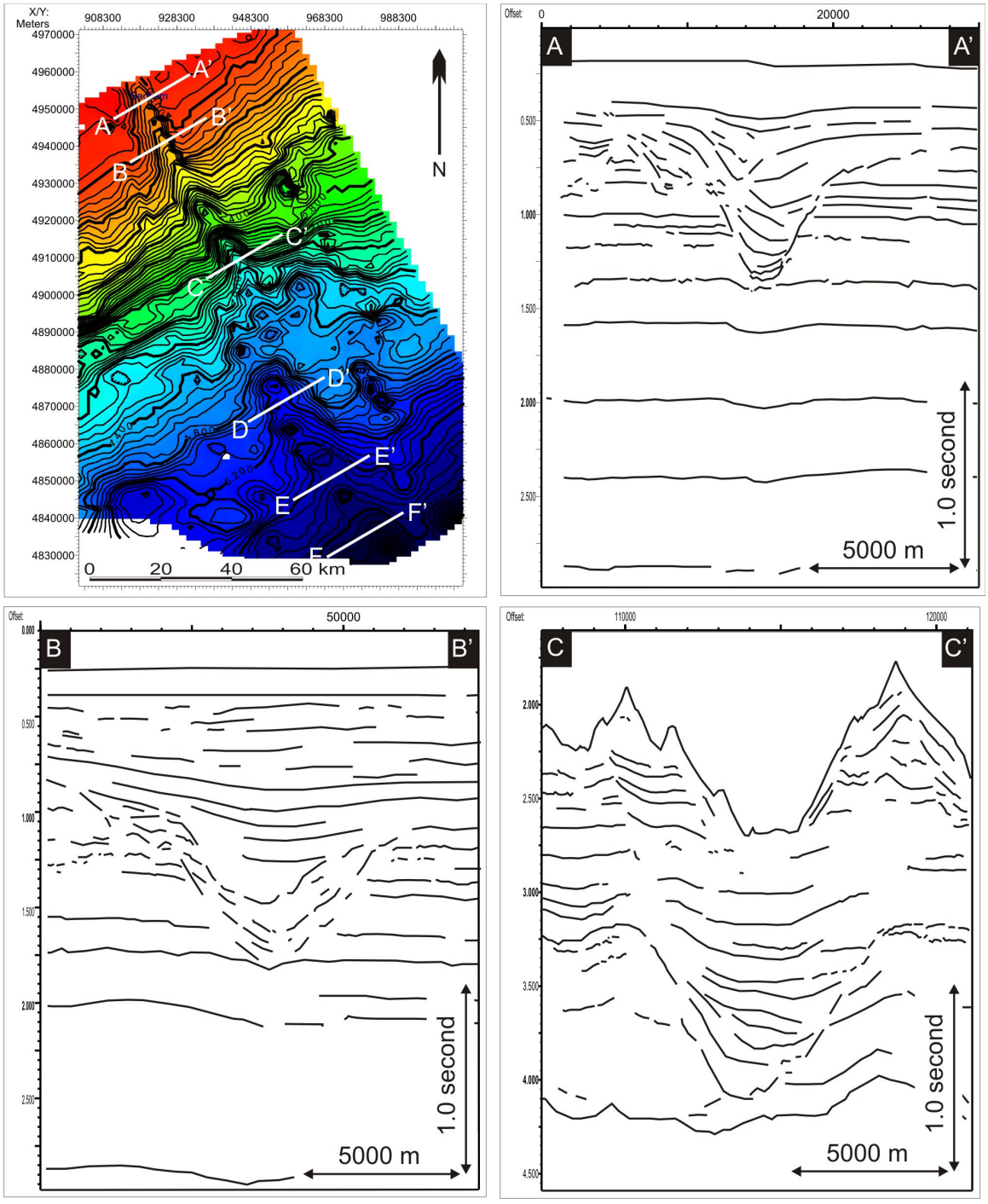

Figure 4.13: Schematic interpretation of 2D seismic lines across the canyon system. Profiles A and B are part of the Parex dataset, while profile C is a TGS-NOPEC line. Parex data are released and are publicly available, whereas TGS data are released August 2009. **(A)** Most shelfward profile, displaying V-shaped canyon morphology. **(B)** The symmetric canyon system shows multiple phases of incision and infill. **(C)** The widening U-shaped canyon displays asymmetry of infill deposits.

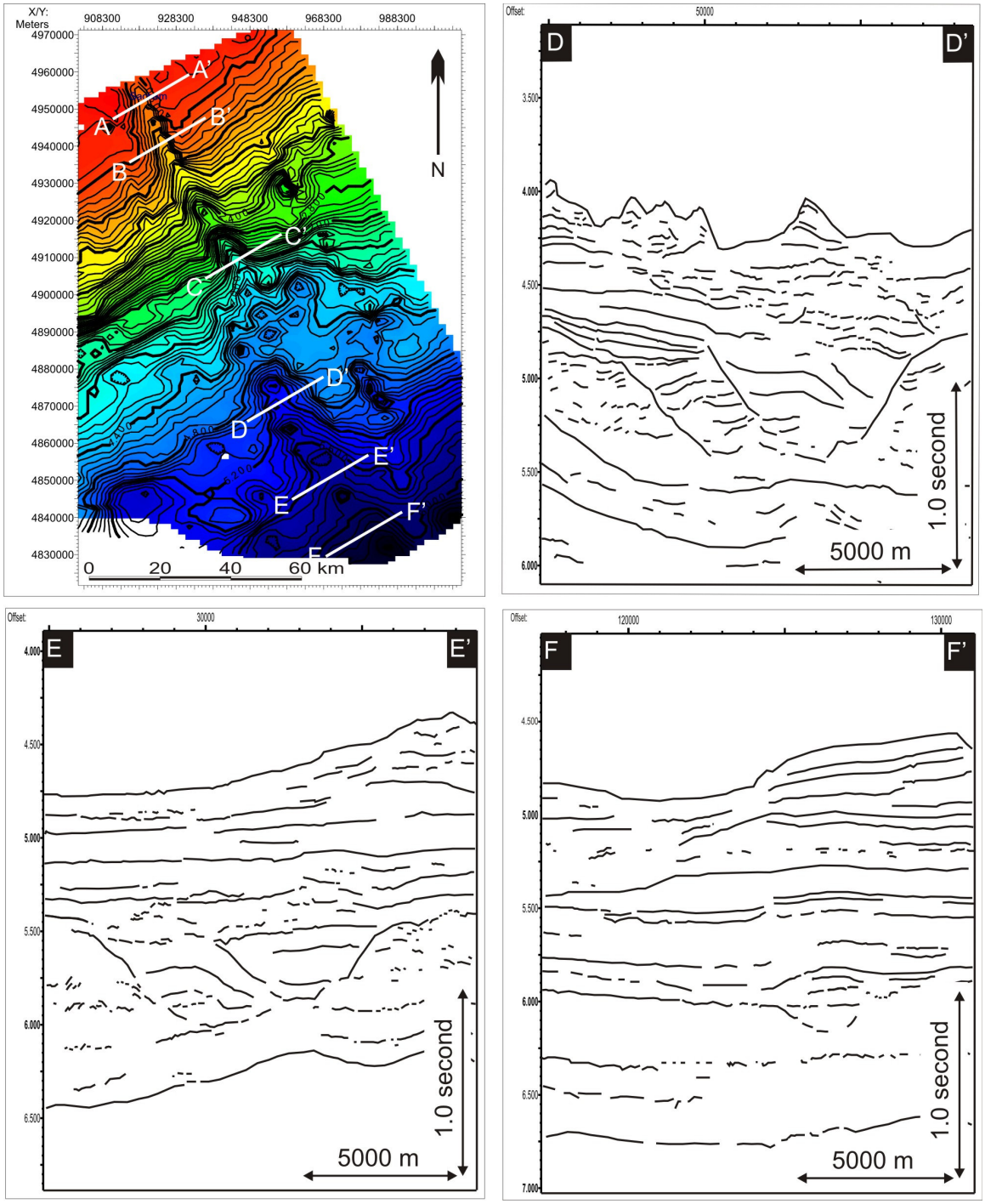

Figure 4.14: Schematic interpretation of 2D seismic lines across the canyon system from the TGS-NOPEC dataset extending interpretations from the Stonehouse dataset into deep water. (D) Levee deposits of the canyon system. (E) Levee deposits become more symmetric moving into the deep water. (F) The canyon system is no longer evident at its most basinward profile.

Chapter 5. Discussion

5.1 Cenozoic stratigraphy

Investigation of seismic units within the dataset and their shelf and along-slope extensions provides evidence for sea level and sediment input changes influencing both erosion and deposition along the eastern Scotian margin.

The lowermost unit of the Cenozoic sequence, Unit I, consists of the Paleocene and older interval below the C100 reflection (Fig. 3.8-3.10). Following deposition of the C100 reflection and the onset Unit II deposition, the Late Paleocene and older sequence was eroded by a regional unconformity, C90 (Fig. 4.2), in the updip region of the 3D seismic volume, creating a series of broad gullies (Fig. 3.2). Following the regional unconformity, deposition of Unit II continued into the Late Eocene-Early Oligocene (E10) and smoothed the morphology of the C90 surface. At the base of the interval, a series of high to moderate amplitude parallel reflections are truncated giving the base of the sequence a mounded morphology. At the top of this sequence, reflections are parallel and continuous with little change in amplitude, suggesting widely distributed and uniform sedimentation (Fig. 3.8-3.10). Thickness of the unit ranges from 66-1500 m; being thicker in the northeast (Fig 3.8). Channeling occurs at the top of the unit on the E10 surface (Fig. 3.4).

The Late Paleocene (C100) to Late Eocene-Early Oligocene (E10) interval (Unit II) is incised by the E7 unconformity, inferred to be of Early Oligocene age, marking the onset

of canyon incision (Fig. 3.8-3.9). The Early Oligocene unconformity incises Units I and II and is limited in extent due to subsequent re-incision.

Unit III, the Late Eocene /Early Oligocene (E10) to Oligocene (O5) interval consists of a high amplitude faulted but continuous seismic facies interrupted by channels and episodic erosion (Fig. 3.8-3.10). The unit is absent across part of the study area due to later erosion, yet given the consistent reflection character was likely a widespread continuous sequence. The top of the sequence is the O5 surface; a widespread erosional unconformity (Fig. 3.5).

The Oligocene (O5) to Late Miocene-Pliocene (M4) interval, Unit IV is characterized by low amplitude continuous parallel to sub-parallel reflections suggesting uniform sedimentation and lithology. The interval fills the underlying Oligocene canyon system and smoothes regional topography (Fig. 3.8 –3.9).

The remainder of the Cenozoic sequence consists of the Late Miocene/Pliocene (M4) to modern sequence (Q1) (Fig. 3.8-3.10). The interval consists of moderate to high amplitude semi-continuous reflections interpreted as deposition under variable or episodic energy conditions. The interval is incised by a dense network of dendritic sinuous canyons that breach the shelf break and extend to the base of slope. The sequence displays faults with minor offset that parallel canyon walls, indicating potential failure planes that would broaden these submarine canyons.

5.2 Sea-level variation and associated depositional sequences

Eustatic sea-level is controlled by ocean-basin volume and ocean-water volume. Eustatic changes are measured between the sea surface and a fixed datum (usually the center of the Earth). Relative sea-level, on the other hand, is measured locally and controlled by subsidence, uplift, compaction, sediment supply and eustatic sea level. Distinguishing between eustatic and relative sea levels, therefore, is a mechanism to understand local geologic changes such as uplift, subsidence and sedimentation.

Determining paleoshelf break positions and correlation from the shelf through to the slope on shelf-perpendicular (dip-line) profiles is essential for determining the overall evolution of stratigraphic sequences, from which the relative importance of sediment input, sea level fluctuations and tectonic controls may be possible to constrain. Investigation of the shelf to slope transition zone throughout the Cenozoic in the study area indicates significant migration of the paleo-shelf break (Fig.5.1), in particular between the Paleocene, Oligocene and modern positions.

The position of the Paleocene shelf break (reflection C100) approximates the modern shelf break position. The position of the paleo-shelf break migrated ~20 km landward between the Paleocene and Middle Oligocene (O5). The landward movement of the paleo-shelf break indicates that relative sea level outpaced sediment supply at the shoreline causing transgression. The absence of a highstand systems tract above the transgressive succession indicates a rapid drop in sealevel or forced regression following the landward migration.

Following the widespread Oligocene unconformity Miocene sequences prograded seaward during an apparent regression as sediment supply outpaced relative sea level. Progradation continued throughout the Miocene and into the Pliocence with the shelf break advancing seaward. From the Pliocene to recent, sediment supply and sea level rise must have balanced resulting in aggraddation of the shelf break position.

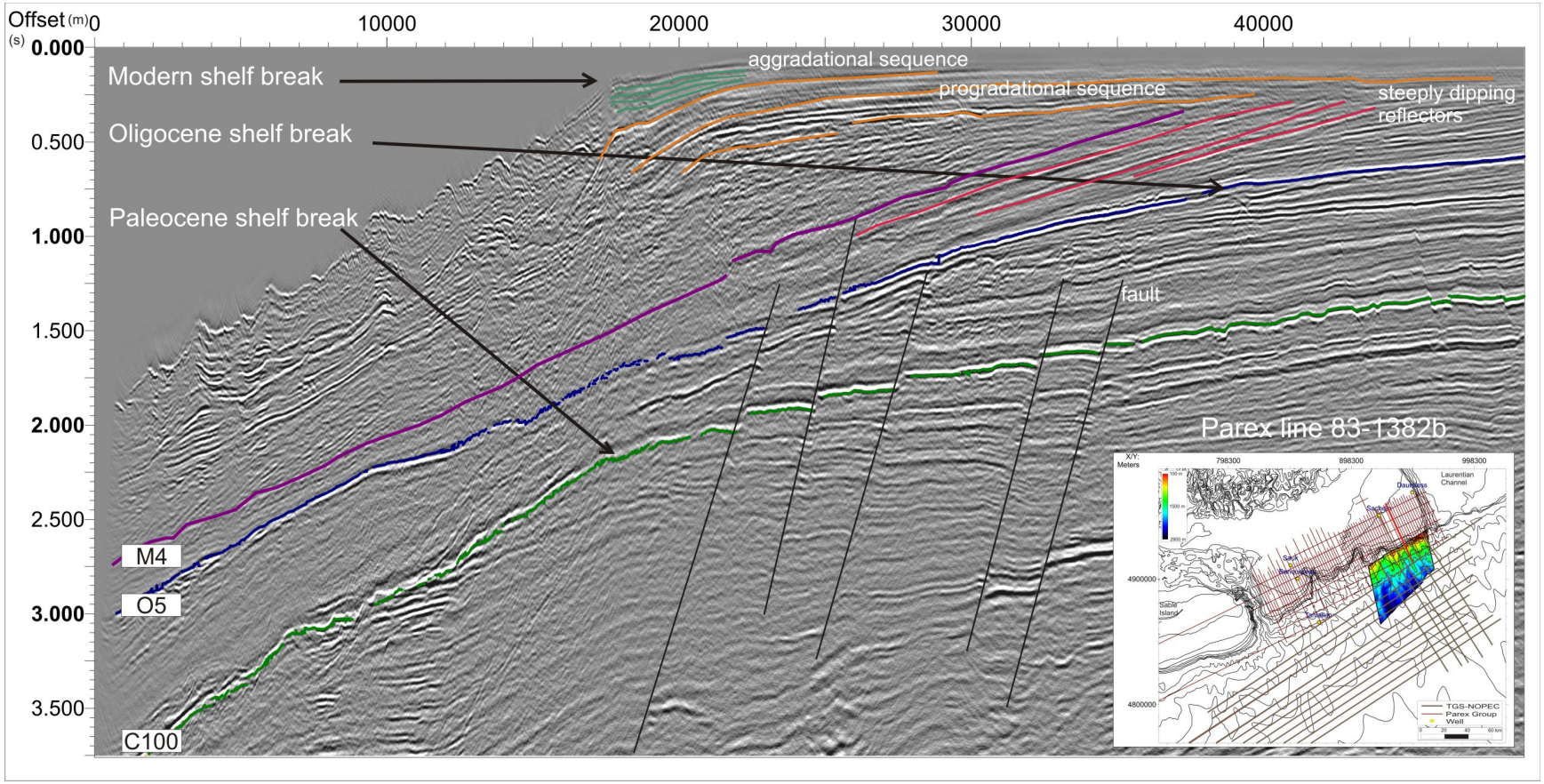

Figure 5.1: 2D dip line on the eastern Scotian Shelf noting paleo-shelf break and reflection geometry changes. Changes in reflection geometry are generated as the shelf break migrated to keep pace with changing sea level.

5.3 Canyon Formation

Numerous theories are proposed for initial canyon formation, yet determining the onset of channel and canyon systems is problematic given that incision and subsequent loss of strata remove any record of its initial formation.

Relative sea level lowering, creating drainage systems on the shelf and upper slope and a dynamic shelf break environment may initiate canyon formation. Lower relative sea level reduces sediment accommodation space on the shelf, resulting in sediment delivery more directly to the slope. Downslope erosive processes such as hyperpycnal flows and turbidity currents are far more vigorous at these times (Parker 1982; Kneller and Buckee 2000; Mulder et al., 2003). Slope failure is another causative mechanism for submarine canyon formation which may or may not be related to changes in relative sea-level or sediment supply. Slope failure surfaces or scars resulting from localized failure can retrogress up the continental slope evolving into a headward eroding canyon system. Over time, many submarine canyons evolve from repeated erosional events, presumably of varying magnitude and multiple causes (Pratson 2007).

The canyons correlated distance on the shelf, as well as partial fill and re-incision suggest the canyon system formed due to a fluctuation in sea level causing possible subarial or shallow water exposure causing offshelf processes to prevail. Reflection E7 marks the initial erosive phase and onset of the E7-O5 canyon system, It is is inferred to represent an Early Oligocene eustatic highstand (Fig.5.2). A relative sea level control such as tectonic uplift would likely therefore be required in order for incision to occur. Evidence

of forced regression at the Oligocene paleo-shelf break may be indicative of a pulse of uplift while sea level was rising causing a landward shift in the shelf-break position to be overlain by a major unconformity and the final phase of incision (O5). Unfortunately, due to lack of available well control, the timing of such an uplift cannot be further constrained.

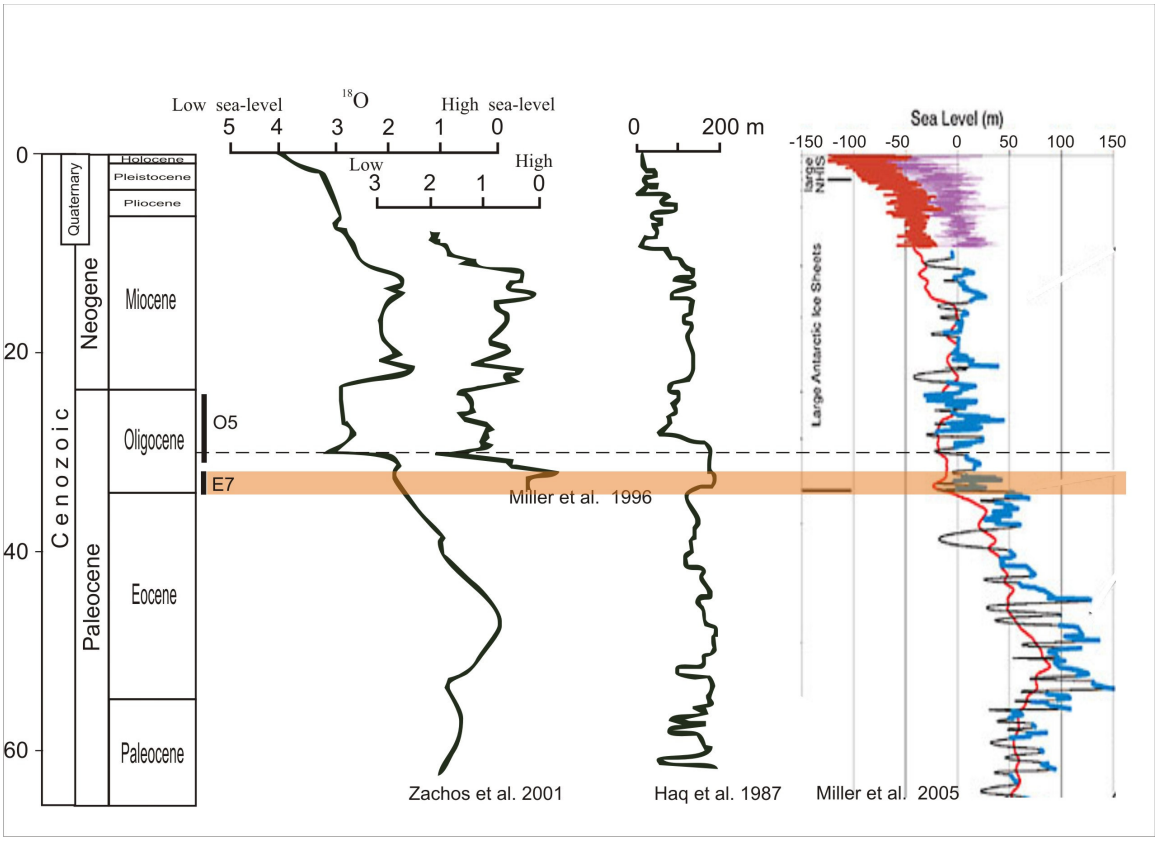

Figure 5.2: Comparison of global eustatic curves of Zachos et al. 2001; Miller et al. 1996; Haq et al. 1987 and Miller et al.2005 (image modified from MacDonald 2006). The age ranges for the E7 and O5 surfaces are indicated by the black bars.

Tectonic uplift was proposed for the Scotian margin based on apatite fission track thermochronology studies. Zentilli (2007) suggested that inversion of the margin and erosion of ~1 km of post-Albian cover onland and offshore likely occurred in the Eocene-Oligocene (Zentilli 2007).

The narrowest and shallowest submarine canyons begin on the middle to lower continental slope and are U-shaped in cross section. Canyons that begin on the shelf and upper slope are often larger, and have V-shaped or U-shaped cross-sections (Mountain 1987). The largest submarine canyons are those that incise the shelf break, particularly those that are or at one time were directly connected to a river (Twichell and Roberts 1982; Farre et al 1983); these canyons are predominantly V-shaped in cross-section (Pratson et al 2007).

Preservation of multiple stacked channel thalwegs indicate that the Oligocene (E7 to O5) canyon system formed through multiple phases of incision. The morphology of incisional phases changes throughout evolution of the canyon. In cross-section, the initial incision exhibits a V-shaped morphology where the E7 unconformity incised as much as 1.2 km into Units I and II. In comparison, the final phase of canyon re-incision, O5, exhibits a broad U-shaped canyon morphology that locally merges with the E7 surface on the flanks of the canyon representing a correlative conformity.

Changes in morphology of the incision surfaces indicate changes to the canyon's evolution over time. The V-shaped incision is related to the processes that initially

carved the canyon which is a function of the volume of material, or cross sectional area of the flow. The U-shaped morphology of the final incision utilizes of the path of earlier incision where the lower fill is less consolidated than surrounding substrate and is easier to erode. The erosive flows then broaden the canyon walls giving the later incision a U-shaped morphology.

The Oligocene canyon investigated within this study documents the largest buried canyon system between the Gully and the Laurentian Channel. Given that the axis of the canyon system incises up to 1 km depth, extends >150 km and is up to 10 km in width, as much as 3000 km^3 has been removed and deposited further seaward on the abyssal plain. The size of this system suggests that it must have acted as a major erosional conduit in the Oligocene on the eastern Scotian Slope. The amount of material moved down the canyon cannot be accounted for.

The amount of erosion in terms of both magnitude and extent combined with the the V-shaped morphology of the initital phase of canyon incision has led to speculation of a possible connection to fluvial processes on the adjacent emergent shelf. On mid-latitude shelves, canyons are usually linked to lowstand fluvial sources (Shepard and Dill 1966, Pratson 2007). Studies by Wade et al. (Atlantic Geoscience Society, 2001) indicate a possible 30 Ma river system in the area of the modern Gully. There is a lack of seismic reflection data proximally on the shelf to determine whether the E7-O5 canyon is linked to fluvial processes.

5.4 Canyons and sediment delivery

Deposition within a canyon system is a function of sediment supply and the energy of flow. Debris can be deposited within a canyon only to be later reworked by flow of greater magnitude, on a variety of time scales.

Canyon fill generally consists of stacked parallel reflectors that indicate an overall ponded fill sequence, perhaps separated by small scale erosive events or periods of non-deposition. The presence of ponded fill and overall uniform reflection geometry suggests the infill of the canyon system occurred under quiescent conditions. Lack of debris in the form of mounds, blocks, or other chaotic deposits disrupting the passive sequence suggests that the canyon system became inactive causing it to backfill starting in its downslope extent. Several factors could have caused the canyon system to become inactive, the most obvious being a rise in relative sea level. A rise in relative sea level would drown the canyon system cutting it off from shelf and shelf-edge hydrologic systems.

The fill of an Oligocene-aged canyon on the Scotian Shelf was sampled by sidewall cores at the Wenonah J-75 well where benthic foraminifer assemblages suggest unique hydrological factors were involved during canyon infill (Thomas 2005). Infill sediments contained low paleo-biodiversity assemblages, suggesting that high sedimentation rates diluted microfossil assemblages and/or sudden changes in sediment load either buried or eliminated benthic communities (Thomas 2005).

Chapter 6. Conclusions

The Cenozoic evolution of a portion of the eastern Scotian margin was examined through a series of key reflections that demonstrate periods of erosion and incision linked to relative sea level and sediment input control. The key reflections are readily recognized throughout the study area on both 2D and 3D reflection seismic data and were correlated to biostratigraphic control at the Sachem D-76 and Tantallon M-41 wells. Biostratigraphic ties provide age constraints for the last 65 Ma, dating the key reflections as (C100) Late Paleocene, (E55) Eocene, (E10) Late Eocene-Early Oligocene, (O5) Oligocene, (M4) Late Miocene-Pliocene. The reflections are placed into seismic-stratigraphic sequences based on reflection configuration, continuity and boundary relationships, related to the position of relative sea level. Through the application of seismic stratigraphic concepts, the key reflections were used to define a seismic stratigraphic framework for the Cenozoic section on the eastern Scotian Slope. Principal among these surfaces and the focus of this study was a major Oligocene erosional unconformity that generated a major canyon system comparable in size to the modern day Gully of the central Scotian Slope.

Shelf edge stratigraphy demonstrates migration of the paleo-shelf break position linked to transgressional and regressional phases. The landward movement in paleo-shelf break position between the Late Paleocene and Middle Oligocene indicates that relative sea level outpaced sediment supply resulting in transgression. The absence of a highstand systems tract above the transgressive sequence indicates a fall in base level and resultant forced regression. Following the Oligocene unconformity, Miocene sequences prograded

seaward during normal regression which continued into the Pliocene advancing the shelf break position. During the Pliocene through to recent the shelf break has been aggradational indicating a balance between sea level and sediment supply.

On the slope, major unconformitites (picked horizons) and interval units show multiple periods of regional erosion resulting in variable thickness. In particular the upslope portions of the dataset demonstrate the most severe incision and the greatest variability in unit thickness. Downslope there is less erosion with relatively uniform distribution. The fact that erosion is more severe in the shallower water suggests erosion occurred due to low sea level stand causing offshelf processes to prevail.

The Oligocene canyon system formed during a period of presumed high eustatic sea level (Miller et al. 2005), yet the above evidence and correlation of the canyon beneath the modern shelf, suggests that canyon incision likely started from the shelf, related to low sea level stand that may have resulted in subaerial or shallow water exposure. To account for this discrepancy, it is suggested that there must have been major local tectonic effects (Pe-Piper and Piper 2004; Zentilli 2007). Unfortunately, age controls are insufficient to be more precise about sea level positions.

The canyon infilled (at least partially), and was subsequently re-incised, further suggesting a fluctuation in sea level. Incision of the two phases is different based on mapping of the thalwegs. The initial phase presents a cross-cutting system, whereas the older phase does not, suggesting the later phase may have been more energetic, perhaps

linked to a sea level lowstand and consequent higher sediment input and coarser grain sizes.

Ultimate infill of the canyon system from Middle to Late Miocene suggests a high sea level stand and sediment ponding within the accommodation space of the canyon. The canyon infilled by ponding processes from deep to shallow suggesting sea level rise gradually isolated the system. Minor evidence of sedimentary processes such as channelling and infill from the west are apparent in the lower fill.

Modern slope canyon systems are observed around the globe, not just on glaciated margins where glacial ice streams are believed to be responsible. Slope canyon systems are clearly a fundamental slope processes, the inception of which is not fully understood. These systems play a role in shelf to slope sediment delivery, not just in modern times but in the past as well. The presence of the 150 km long E7 to O5 canyon system indicates the removal of at least 3000 km^3 of sediment, representing significant slope bypass and sediment delivery to deep water. Not only was a significant amount of sediment removed to the deep basin during the sculpting of the canyon, but it then acted as a sediment conduit throughout the Oligocene providing a pathway for sediment delivery to deep water.

In terms of an exploration model, the canyon thalweg and levee deposits may provide significant sand with reservoir potential. Because of this canyon, the principal exploration target is likely in ultra deep water, suggesting on any margin, periods of low

sea level and canyon development likely mean reservoir material is in the ultra deep water.

References:

Ascoli, P. 1989. Report on the biostratigraphy (Foraminifera and Ostracoda) and depositional environments of the Shell *et al.* Tantallon M-41 well, Scotian Shelf, from 3135 to 5600 m (T.D. 5602 m). Report No. BAS-PAL.5-89PA, 7 p.

Atlantic Geoscience Society. 2001. The Last Billion Years. Nimbus Publishing, Halifax, p 141.

Balkwill, H.R., and McMillan, N.J. 1990. Mesozoic-Cenozoic geology of the Labrador shelf, Baffin Bay, and Davis Straight. In, M.J. Keen and G.L. Williams (Eds.), Geology of the continental margin of Eastern Canada, Geological Survey of Canada, Geology of Canada, No.2: pp. 295-314.

Berggren, W.A., and Hollister, C.D. 1974. Paleogeography, paleobiogeography, and the history of circulation in the Atlantic Ocean. In, W. Hay (Ed.), Studies in paleo-oceanography: Society of Economic Paleontologists Mineralogists. Special Publication, No. 20, p. 126-186.

Brown, A.R. 2003. Interpretation of three-dimensional seismic data. AAPG Memoir 42, SEG Investigations in Geophysics, No, 9: pp. 20-42.

Campbell, D.C., Shimeld, J.W., Mosher, D.C. and Piper, D.J.W. 2004. Relationships between sediment mass-failure modes and magnitudes in the evolution of the Scotian Slope, offshore Nova Scotia. Offshore Technology Conference, Houston Texas, U.S.A., 3-6 May 2004, paper number OTC 16743.

Canada Nova Scotia Offshore Petroleum Board. 2008. Call for bids 2008-2009, NS08-2. CD-ROM.

Catuneanu, O. 2002. Geological Society of Africa Presidential Review No. 1: Sequence stratigraphy of clastic systems: concepts, merits, and pitfalls. Journal of African Earth Sciences, **35**: 1-43.

Christie-Blink, N. 1991. Onlap, offlap, and the origin of unconformity-bounded depositional sequences. Marine Geology, **97**: 35-56

Christie-Blick, N., Austin, J.A., Jr., and Shipboard Scientific Party. 1998. Introduction: Oligocene to Pleistocene eustatic change at the New Jersey Continental Margin – A test of sequence stratigraphy. In, J.A. Austin, Jr., N., Christie-Blick., M.J., Malone et al., (Eds.), Proceedings of the Ocean Drilling Program, Initial reports, vol 174A. p. 5-16.

Cloetingh, S., Gradstein, F.M., Kooi, H., Grant, A.C., Kaminski, M., 1990. Plate reorganization: a cause of rapid late Neogene subsidence and sedimentation around the North Atlantic. Journal of the Geological Society, London **147**, 495–506.

DeConto, R.M., Pollard, D., Wilson, P.A., Palike, H., Lear, C.H. and Pagani, M. 2008. Thresholds for Cenozoic bipolar glaciation. Nature, **455** (2): 652-657.

Deptuck, M. E. 2003. Post-rift geology of The Jeanne D'Arc Basin, with a focus on the architecture and evolution of early Paleogene submarine fans, and insights from modern deep-water systems: Unpublished. PhD thesis, Dalhousie University 369 p.

Doré, A.G., Lundin, E.R., Jensen, L.N., Birkeland, Ø., Eliassen, P.E., Fichler, C. 1999. Principal tectonic events in the evolution of the northwest European Atlantic margin. In, A.J., Fleet, S.A.R., Boldy, (Eds.), Petroleum Geology of Northwest Europe: Proceedings of the 5th Conference. Geological Society, London, pp. 41–61.

Doré, A.G., Cartwright, J.A., Stoker, M.S., Turner, J.P., White, N.J. 2002. Exhumation of the North Atlantic margin: introduction and background. In: A.G., Doré, J., Cartwright, M.S., Stoker, J.P.,Turner, N., White, (Eds.), Exhumation of the North Atlantic Margin: Timing, Mechanisms and Implications for Petroleum Exploration. Geological Society, London, Special Publications **196**, 1–12.

Eliuk, L.S. 1978. The Abenaki Formation, Nova Scotia Shelf, Canada – a depositional and diagenetic model for a Mesozoic carbonate platform. Bulletin of Canadian Petroleum Geology, **26**: 424-514.

Elliott, G.M., Shannon, P.M., Haughton, P.D.W., Praeg, D. and O'Reilly, B.O. 2006. Mid-to Late Cenozoic canyon development on the eastern margin of the Rockall Trough, offshore Ireland. Marine Geology, **229**: 113-132.

Ewing, J.I. and Hollister, C.D. 1972. Regional aspects of deep-sea drilling in the western North Atlantic. Initial Reports on Deep Sea Drilling Project, v. 11, p. 951-973.

Farre, J. A., McGregor, B. A., Ryan, W. B. F., and Robb, J. M. 1983. Breaching the shelfbreak; Passage from youthful to mature phase in submarine canyon evolution. In, Stanley, D. J., and Moore, G. T., (Eds.), The shelfbreak: Critical interface on continental margins: Society of Economic Paleontologists and Mineralogists Special Publication No. 33, p. 25–39.

Fensome, R.A., Crux, J.A., Gard, I.G., MacRae, R.A., Williams, G.L., Thomas, F.C., Fiorini, F. and Wach, G. 2008. The last 100 million years on the Scotian Margin, offshore eastern Canada: an event-stratigraphic scheme emphasizing biostratigraphic data. Atlantic Geology, **44**: 93-126.

Flynn, R.F.J. 2000. Tunnel valleys under the southeastern Scotian Shelf: B/Sc. (hon.) thesis, Saint Mary's University, Halifax, Nova Scotia, 52 p.

Fulthorpe, C.S. and Austin, J.A., Jr. 1998. Anatomy of rapid margin progradation: three-dimensional geometries of Miocene clinoforms, New Jersey Margin. American Association of Petroleum Geologists Bulletin, **82** (2): 251-273.

Fulthorpe, C.S., Austin, J.A., Jr. and Mountain, G.S. 1999. Buried fluvial channels off New Jersey: Did sea-level lowstands expose the entire shelf during the Miocene? Geology, **27** (3): 203-206.

Galloway, W.E. 1989. Genetic stratigraphic sequences in basin analysis, I. Architecture and genesis of flooding-surface bounded depositional units. American Association of Petroleum Geologists Bulletin, **73**:125-142.

Given, M.M. 1977. Mesozoic and early Cenozoic geology of offshore Nova Scotia. Bulletin of Canadian Petroleum Geology, **25**: 63-91.

Goodwin, R. H., and Prior, D. B. 1989. Geometry and depositional sequences of the Mississippi Canyon, Gulf of Mexico, Journal of Sedimentary Petrology, **59**: 318–329.

Gradstein F.M., Jansa L.F., Srivastava S.P., Williamson, M.A., Bonham Carter G. & Stam B. 1990. Chapter 8: Aspects of North Atlantic Paleooceanography. In, M.J. Keen, and G.L. Williams, (Eds.), Geology of the continental margin off eastern Canada, Geological Survey of Canada, Geology of Canada no. 2, (also Geological Society of America, The Geology of North America I-1), 351-389.

Gradstein, F.M., Ogg, J.G., and Smith, A.G. 2004. A geologic time scale 2004. Cambridge University Press, Cambridge, 585p.

Greenlee, S.M., Devlin, W.J, Miller, K.G., Mountain, G.S. and Flemings, P.B. 1992. Integrated sequence stratigraphy of Neogene deposits, New Jersey continental shelf and slope: Comparison with the Exxon model. Geological Society of America Bulletin, **104**: 1403-1411.

Haq, B.U., Hardenbol, J., and Vail, P.R. 1987. Chronology of fluctuating sea levels since the Triassic. Science, **253**: 1156-1167.

Ings, S.J., and Shimeld, J.W. 2006. A new conceptual model for the structural evolution of a regional salt detachment on the northeast Scotian margin, offshore eastern Canada. AAPG Bulletin, **90** (9): 1407-1423.

Ivany, L.C., Besbitt, E.A., and Prothero, D.R. 2003. The marine Eocene-Oligocene transition; a synthesis. In D.R. Prothero, L.C. Ivany, E.A. Nesbitt (Eds.), From greenhouse to icehouse; the marine Eocene-Oligocene transition, pp. 522-534.

Jansa, L.F., and Wade, J.A. 1975. Geology of the continental margin off Nova Scotia and Newfoundland. In, W.J.M. van der Linden and J.A. Wade (Eds.), Offshore Geology of eastern Canada, Volume 2, Regional Geology. Geological Survey of Canada, Paper 74-30, v. 2: 51-106.

Japsen, P., Chalmers, J.A. 2000. Neogene uplift and tectonics around the North Atlantic: overview. Global and Planetary Change **24**: 165–173.

Kearey, P, and Brooks, M. 1991. An Introduction to Geophysical Exploration, 2nd edition. Geoscience Texts. Blackwell Scientific Publisher, Oxford, 254p.

Keen, C.E. and Beaumont, C. 1990. Geodynamics of rifted continental margins. In, M.J. Keen and G.L. Williams (Eds.). Geology of the continental margin of Eastern Canada, Geological Survey of Canada, Geology of Canada, No.2: pp.391-472.

Kennard, L. Schafer, C., and Carter, L. 1990. Geology of the continental margin off eastern Canada. Geological Survey of Canada, Geology of Canada no. 2, 855.

Kidston, A., Brown, D., Altheim, B., and Smith, B. 2002. Hydrocarbon Potential of the Deep-Water Scotian Slope. Canada Nova Scotia Offshore Petroleum Board, Halifax, Nova Scotia, 111p.

Kidston, A.G., Smith, B.M., Brown, D.E., Makrides, C. and Altheim, B. 2007. Nova Scotia Deepwater post-drill analysis 1982-2004. Canada Nova Scotia Offshore Petroleum Board, Halifax, Nova Scotia, 181p.

Kneller, B.C. and Buckee, C. 2000. The structure and fluid mechanics of turbidity currents: a review of some recent studies and their geological implications. Sedimentology, 47: 62–94.

Louden, K. 2002. Tectonic evolution of the east coast of Canada. CSEG Recorder: 37-48.

MacDonald, A. W. 2006. Cenozoic seismic stratigraphy of the central Nova Scotian continental margin: The interplay of erosion, deposition and salt tectonics. Unpublished MSc thesis, Saint Marys University 152 p.

MacLean, B., and Wade, J., 1993, Seismic Markers and Stratigraphic picks in the Scotian Basin wells: East Coast Basin Atlas: Dartmouth, Geological Survey of Canada.

McIver, N.L. 1972. Mesozoic and Cenozoic stratigraphy of the Nova Scotia Shelf. Canadian Journal of Earth Sciences, **9**: 54-70.

Miller, K.G., Kent, D.V., Brower, A.N., Bybell, L.M., Feigenson, M.D., Olsson, R.K., and Poore, R.Z. 1990. Eocene-Oligocene sea-level changes on the New Jersey coastal plain linked to the deep-sea record. Geological Society of America Bulletin, **102**: 331-339.

Miller, K.G., Kominz, M.A., Browning, J.V., Wright, J.D., Mountain, G.S., Katz, M.E., Sugarman, P.J., Cramer, B.S., Christie-Blick, N. and Pekar, S.F. 2005. The Phanerozoic record of global sea-level change. Science, **310**: 1293-1298.

Miller, K.G., and Mountain, G.S. 1996. Drilling and dating New Jersey Oligocene-Miocene sequences: Ice volume, global sea level, and Exxon records. Science, New Series, **271** (5252): 1092-1095.

Miller, K.G., Mountain, G.S., and Tucholke, B.E. 1985. Oligocene glacio-eustasy and erosion on the margins of the North Atlantic. Geology, **13**: 10-13.

Miller, K.G., Rufolo, S., Sugarman, P.J., Pekar, S.F., Browning, J.V., Gwynn, D.W. 1997. Early to middle Miocene sequences, systems tracts, and benthic foraminiferal biofacies. Proceedings of the Ocean Drilling Program, Scientific Results, 150X, pp. 169–186.

Mitchum, R.M., Vail, P.R., and Thompson, S. 1977a. Seismic stratigraphy and global changes of sea-level, part 2: The depositional sequence as a basic unit for stratigraphic analysis. In, C.E. Payton (Ed.), Seismic Stratigraphy – Applications to Hydrocarbon Exploration. American Association of Petroleum Geologists Memoir 26, pp. 53-62.

Mitchum, R.M., Vail, P.R., and Sangree, J.B. 1977b. Seismic stratigraphy and global changes of sea level, Part 6: Stratigraphic interpretation of seismic reflection patterns in depositional sequences. In, C.E. Payton (Ed.), Seismic Stratigraphy – Applications to Hydrocarbon Exploration. American Association of Petroleum Geologists Memoir 26, pp. 117-133.

Mobil-Texaco, 1976, Sachem D-76, Well history report. Canada Nova Scotia Offshore Petroleum Board, Dartmouth, Nova Scotia, unpublished report.

Mosher, D.C., Bigg, S., and LaPierre, A. 2006. 3D seismic versus multibeam sonar seafloor surface renderings for geohazard assessment: Case examples from the central Scotian Slope. The Leading Edge, **25** (12): 1484-1494.

Mosher, D.C., Moran, K, and Hiscott, R.N. 1994. Late Quaternary sediment, sediment mass-flow processes and slope stability on the Scotian Slope. Sedimentology, **41**: 1039-1061.

Mosher, D.C., Piper, D.J.W., Campbell, D.C., and Jenner, K.A. 2004. Near surface geology and sediment-failure geohazards of the central Scotian Slope. American Association of Petroleum Geologists Bulletin, **88**: 705-723.

Mosher, D.C., Piper, D.J.W., Vilks, G., Aksu, A.E., Fader, G.B. 1989. Evidence for Wisconsinan glaciations in the Verrill Canyon area, Scotian Slope. Quaternary Research **31**, 27–40.

Mountain, G.S. 1987. Cenozoic margin construction and destruction offshore New Jersey. In, C. Ross and D. Haman (Eds.), Timing and depositional history of eustatic

sequences: constraints on seismic stratigraphy. Cushman Foundation for Foraminiferal Research, Special Publication, 24, p. 57-83.

Mountain, G.S., Burger, R.L., Delius, H., Fulthorpe, C.S., Austin, J.A., Goldberg, D.S., Steckler, M.S., McHugh, C.M., Miller, K.G., Monteverde, D.H., Orange, D.L., and Pratson, L.F. 2007. The long-term stratigraphic record on continental margins. In, C.A. Nittrouer, J.A. Austin, M.E. Field, J.H., Kravitz, J.P.M., Syvitski, P.L. Wiberg (Eds.), Continental margin sedimentation: from sediment transport to sequence stratigraphy. Special publication 37 of the IAS, pp. 381-458.

Mountain, G.S., Damuth, J.E., McHugh, C.M., Lorenzo, J.M., and Fulthorpe, C.S. 1996. Origin, re-burial and significance of a mid-Miocene canyon, New Jersey continental slope. In, G.S. Mountain, K.G. Miller, P. Blum, C.W. Poag and D.C. Twichell (Eds.), Proceedings of the Ocean Drilling Program, Scientific Results, 150: College Station, Texas, Ocean Drilling Program, p. 283-292.

Mountain, G.S., and Tucholke, B.E. 1985. Mesozoic and Cenozoic geology of the U.S. Atlantic continental slope and rise. In, C.W. Poag (Ed.), Geologic Evolution of the United States Atlantic Margin. Van Nostrand Reinhold, New York, p. 293-341.

Mulder, T., Syvitski, J.P.M., Migeon, S., Faugères, J.C., and Savoye, B., 2003. Marine hyperpycnal flows: initiation, behavior and related deposits. A review. Marine and Petroleum Geology **20**: 861–882.

Myers, R.A. and Piper, D.J.W. 1988. Seismic stratigraphy of late Cenozoic sediments in the northern Labrador Sea: a history of bottom circulation and glaciation. Canadian Journal of Earth Sciences, **22**: 2059-207.

Owens, J.P., and Gohn, G.S. 1985. Depositional history of the Cretaceous series in the U.S. coastal plain: stratigraphy, paleoenvironments, and tectonic controls of sedimentation. In C.W. Poag, (Ed.), Geologic Evolution of the United States Atlantic Margin, Van Nostrand Reinhold, New York, pp. 25–86.

Owens, J.P. and Sohl, N.F. 1969. Shelf and deltaic paleoenvironments in the Cretaceous-Tertiary formations of the New Jersey coastal plain. In, S. Subitzky (Ed.), Geology of selected areas in New Jersey and eastern Pennsylvania and guidebook of excursions, pp. 235-278.

Parker, G. 1982. Conditions for the ignition of catastrophical erosive turbidity currents. Marine Geology **46**: 307–327.

Pe-Piper, G, and Piper, D.J.W. 2004. The effects of strike-slip motion along the Cobequid – Chedabucto – southwest Grand Banks fault system on the Cretaceous-Tertiary evolution of Atlantic Canada. Canadian Journal of Earth Sciences, **41**: 799-808.

Piper, D.J.W. 2005. Late Cenozoic evolution of the continental margin of eastern Canada. Norwegian journal of geology, **85**: 305-318.

Piper, D.J.W., and DeWolfe, M. 2003. Petrographic evidence from the eastern Canadian margin of shelf-crossing glaciations. Quaternary International, **99-100**: 99-113.

Piper, D.J.W., Normark, W.R., and Sparkes, R. 1987. Late Cenozoic stratigraphy of the central Scotian Slope, eastern Canada. Bulletin of Canadian Petroleum Geology, **35**: 1-11.

Piper, D.J.W., Shaw, J., and Skene, K.I. 2007. Stratigraphic and sedimentological evidence for late Wisconsinan sub-glacial outburst floods to Laurentian Fan. Palaeogeography, Palaeoclimatology, Palaeoecology, **246**: 101-119.

Poag, C.W. 1985. Cenozoic and Upper Cretaceous sedimentary facies and depositional systems of the New Jersey slope and rise. In, C.W., Poag (Ed.), Geological evolution of the United States Atlantic Margin, Van Nostrand and Reinhold, New York, pp. 217-264.

Poag, C.W. and Mountain, G.S. 1987. Late Cretaceous and Cenozoic evolution of the New Jersey continental slope and upper rise: an integration of borehole data with seismic reflection profiles. In Poag, C.W., Watts, A.B., et al., Initial Reports, Deep Sea Drilling Program, 95: Washington (U.S. Govt. Printing Office), pp. 673-724.

Poag, C.W., and Sevon, W.D., 1989. A record of Appalachian denudation in postrift Mesozoic and Cenozoic sedimentary deposits of the U.S. middle Atlantic continental margin. Geomorphology, **2**:119–157.

Praeg, D., Stoker, M.S., Shannon, P.M., Ceramicola, S., Hjelstuen, B., Laberg, J.S. and Mathiesen, A. 2005. Episodic Cenozoic tectonism and the development of the NW European 'passive' continental margin. Marine and Petroleum Geology, **22**: 1007-1030.

Pratson, L.F., Nittrouer, C.A., Wilberg, P.L., Steckler, M.S., Swenson, J.B., Cacchione, D.A., Karson, J.A., Murray, B., Wolinsky, M.A., Gerber, T.P., Mullenbach, B.L., Spinelli, G.A., Fulthorpe, C.S., O'Grady, D.B., Parker, G., Driscoll, N.W., Burger, R.L., Paola, C., Orange, D.L., Field, M.E., Friedrichs, C.T., Fedele, J.J. 2007. Seascape evolution on clastic continental shelves and slopes. In, C.A. Nittrouer, J.A. Austin, M.E. Field, J.H., Kravitz, J.P.M., Syvitski, P.L. Wiberg (Eds.), Continental margin sedimentation: from sediment transport to sequence stratigraphy. Special publication 37 of the IAS, pp.339-380.

Rohrman, M., van der Beek, P. 1996. Cenozoic postrift domal uplift of North Atlantic margins: an asthenospheric diapirism model. Geology, **24**: 901–904.

Ryan, W. B. F., Cia, M. B., Miller, E. L., Hanselman, D., Nesteroff, W. D., Hecker, B., and Nibbelink, M. 1978. Bedrock geology in New England submarine canyons: Oceanologica Acta, v. 1, p. 233–254.

Schenk, P.E. 1973. Nova Scotia, Morocco and continental drift. Earth Sciences Symposium on Offshore Eastern Canada, Geological Survey of Canada Paper 71-23: 219-222.

Schenk, P.E. 1981. The Meguma Zone of Nova Scotia- A remnant of Western Europe, South America, or Africa? In, J.W., Kerr, A.J. Fergusson, and L.C. Machan (Eds.). Geology of the North Atlantic borderlands. Canadian Society of Petroleum Geologists Memoir 7: 119-148.

Schenk, P.E. 1997. Sequence stratigraphy and provenance on Gondwana's margin: The Meguma Zone (Cambrian to Devonian) of Nova Scotia, Canada. Geological Society of America Bulletin, **109**(4): 395-409.

Shannon, P.M., Stoker, M.S., Praeg, D., van Weering, T.C.E., de Haas, H., Nielsen, T., Dahlgren, K.I.T. and Hjelstuen, B.O. 2005. Sequence stratigraphic analysis in deep-water, underfilled NW European passive margin basins. Marine and Petroleum Geology, **22**: 1185-1200.

Shaw, J., and Courtney, R. C. 2004. Postglacial coastlines of Atlantic Canada: digital images: Geological Survey of Canada Open File 4302, p. 13.

Shaw, J., Piper, D.J.W., Fader, G.B.J., King, E.L., Todd, B.J., Bell, T., Batterson, M.J., and Liverman, D.G.E. 2006. A conceptual model of the deglaciation of Atlantic Canada. Quaternary Science Reviews, **25**: 2059-2081.

Shell Canada Resources, 1986. Tantallon M-41, Well history report. Canada Nova Scotia Offshore Petroleum Board, Dartmouth, Nova Scotia, unpublished report.

Shepard, F. P. 1981. Submarine canyons; multiple causes and long-time persistence: American Association of Petroleum Geologists Bulletin, **65**: 1062–1077.

Shepard, F.P., and Dill, R.F. 1966. Submarine canyons and other sea valleys. Rand McNally, Chicago, 381 p.

Sheriff, R.E. 2002. Encyclopedic Dictionary of Exploration Geophysics, 4th edition. SEG, Tulsa, 376p.

Sheriff, R.E., and Geldart, L.P. 1995. Exploration Seismology. Cambridge University Press, Cambridge.

Sloss, L.L. 1963. Sequences in the cratonic interior of North America. Geological Society of America Bulletin, **74**: 93-113.

Stoker, M.S., Pheasant, J.B. and Josenhans, H. 1997. Seismic methods and interpretation. In T.A. Davies, T. Bell, A.K. Cooper, H. Josenhans, L. Polyak, A.

Solheim, M.S. Stoker, J.A. Stravers (Eds.), Glaciated Continental margins: An atlas of acoustic images, pp. 9-19.

Stoker, M.S., Praeg, D., Hjelstuen, B.O., Laberg, J.S., Nielsen, T. and Shannon, P.M. 2005. Neogene stratigraphy and the sedimentary and oceanographic development of the NW European Atlantic margin. Marine and Petroleum Geology, **22**: 977-1005.

Stoker, M.S., Hoult, R.J., Nielsen, T., Hjelstuen, B.O., Laberg, J.S., Shannon, P.M. 2005a. Sedimentary and oceanographic responses to Early Neogene compression on the NW European Margin. Marine and Petroleum Geology, **22**: 1031-1044.

Sugarman, P.J. and Miller, K.G. 1997. Correlation of Miocene sequences and hydrogeologic units, New Jersey Coastal Plain. Sedimentary Geology, **108**: 3-18.

Swift, S.A. 1987. Late Cretaceous-Cenozoic development of outer continental margin, southwestern Nova Scotia. American Association of Petroleum Geolgists Bulletin, **71** (6): 678-701.

Telford, W.M., Geldart, L.P. and Sheriff, R.E. 1990. Applied Geophysics. Cambridge University Press, Cambridge, 770p.

Thomas, F.C. 1991. Report on the Cenozoic biostratigraphy (Foraminifera) and depositional environments of the Shell *et al.* Tantallon M-41 well, Scotian Shelf, from 2265 to 3115 m (top of Cretaceous). Report No. BAS-PAL.4-91FCT, 6 p.

Thomas, F.C., 2005. Oligocene benthic foraminifera from the Paleogene Wenonah Canyon, Scotian Shelf – normal versus canyon assemblages. Atlantic Geology, **41**: 1-16.

Tucholke, B.E. 1981. Geologic significance of seismic reflectors in the deep western North Atlantic Basin. SEPM Special Publication, No. 32: 23-37.

Tucholke, B.E., and Miller, K.G. 1979. Relationships between acoustic stratigraphy and lithostratigraphy in the Western North Atlantic Basin. In, B.E., Tucholke, and P.R., Vogt (Eds.), Initial Reports of the Deep Sea Drilling Project, v. 43. U.S. Government Printing Office, Washington, D.C., pp. 827-843.

Tucholke, B.E., and Mountain, G.S. 1986. Tertiary paleoceanography of the western North Atlantic Ocean. In P.R. Vogt, and B.E., Tucholke, (Eds.), The Geology of North America, Volume M, The Western North Atlantic Region: Geological Society of America, pp. 631-650.

Tucholke, B.E., and Vogt, P.R. 1979. Western North Atlantic: Sedimentary evolution and aspects of tectonic history. Initial Reports, Deep Sea Drilling Project, v. 43, pp. 791-825.

Twichell, D. C., and Roberts, D. G. 1982. Morphology, distribution, and development of submarine canyons on the United States Atlantic continental slope between Hudson and Baltimore Canyons: Geology, v. 10, p. 408–412.

Uchupi, E., and Swift, S.A. 1991. Plio-Pleistocene slope construction off western Nova Scotia, Canada. Cuadernos de Geologia Iberica **15**: 15-35.

Vail, P.R. 1987. Seismic stratigraphy interpretation procedure. In, A.W. Bally (Ed.) Atlas of Seismic Stratigraphy. American Association of Petroleum Geologist Studies in Geology, **27**:1-10.

Vanneste, K., Henriet, J.-P., Posewang, J., Theilen, F. 1995. Seismic stratigraphy of the Bill Bailey and Lousy Bank area: implications for subsidence history. In, R.A., Scrutton, M.S., Stoker, G.B., Shimmield, A.W. Tudhope, A.W. (Eds.), The Tectonics, Sedimentation and Palaeoceanography of the North Atlantic Region. Geological Society, London, Special Publications **90**, 125–139.

Veeken, P.C.H. 2007. Seismic Stratigraphy, basin analysis and reservoir characterization. Handbook of geophysical exploration. K. Helbig and S. Treitel (Eds). v. 37, 487p.

Wade, J.A., Campbell, G.R., Procter, R.M., and Taylor, G.C. 1989. Petroleum resources of the Scotian Shelf. Geological Survey of Canada Paper 88-19, 26.

Wade, J.A., and MacLean, B.C. 1990. Aspects of the geology of the Scotian Basin from recent seismic and well data. In Geology of the continental margin off eastern Canada: Geological Survey of Canada, Geology of Canada, no. 2. p. 190-238.

Wade, J.A., MacLean, B.C. and Williams, G.L. 1995. Mesozoic and Cenozoic stratigraphy, eastern Scotian Shelf: new interpretations. Canadian Journal of Earth Sciences, **32**: 1462-1473.

Welsink, H.J., Dwyer, J.D., and Knight, R.J. 1990. Tectono-Stratigraphy of Passive Margin off Nova Scotia. In, A. J. Tankard and J. R. Balkwill (Eds.), Extensional Tectonics and Stratigraphy of the North Atlantic Margins. American Association of Petroleum Geologists Memoir 46, pp.215-231.

Williams, G.L. 1992. Palynological analysis of the interval 2265-3235 m in Shell Tantallon M-41, Scotian Shelf. Report No. BAS-PAL.1-92GLW, 6 p.

Yilmaz, O. 1987. Seismic Data Processing, Society of Exploration Geophysicists, Investigations in geophysics No. 2, Tulsa, Society of Exploration Geophysicists, 529p.

Yilmaz, O. 2001. Seismic Data Analysis, Volumes 1 and 2. Society of Exploration Geophysicists, Investigations in geophysics No. 10, Tulsa, Society of Exploration Geophysicists, 2027p.

Zachos, J., Pagani, M., Sloan, L., Thomas, E., and Billups, K. 2001. Trends, rhythms, and aberrations in global climate 65 Ma to present. Science, **292**: 686-693.

Zachos, J.C., Shackleton, N.J., Revenaugh, J.S., Palike, H., Flower, B.P. 2001. Climate response to orbital forcing across the Oligocene-Miocene boundary. Science, **292**: 274-278.

Zentilli, M. and Grist, A.M. 2007. Abstract: Thermochronology evidence for Tertiary inversion of the continental margin of Nova Scotia, Canada. The first MAPG international convention conference & exhibition. Marrakech, October 28-31, 2007.

Zoeppritz, K. 1919. On the reflection and propagation of seismic waves at discontinuities. Erdbebenwellen VIIB, Gottinger Nachrichten I, pp. 66-84.